THESIS

DYNAMIC MECHANICAL ANALYSIS FOR QUALITY EVALUATION OF ADDITIVELY

MANUFACTURED CONTINUOUS FIBER REINFORCED THERMOPLASTIC MATRIX

COMPOSITES SUBJECT TO MANUFACTURING DEFECTS

Submitted by

Patrick A. Rodriguez

Department of Mechanical Engineering

In partial fulfillment of the requirements

For the Degree of Master of Science

Colorado State University

Fort Collins, Colorado

Spring 2019

Masters Committee:

   Advisor: Donald W. Radford

   Kaka Ma
   Paul Heyliger

ABSTRACT

DYNAMIC MECHANICAL ANALYSIS FOR QUALITY EVALUATION OF ADDITIVELY

MANUFACTURED CONTINUOUS FIBER REINFORCED THERMOPLASTIC MATRIX

COMPOSITES SUBJECT TO MANUFACTURING DEFECTS

Continuous fiber reinforced polymers (CFRP) have become integral to modern

mechanical design as value-added alternatives to metallic, ceramic and neat polymeric

engineering materials. Despite the advantages of CFRP, current methods of preparing laminated

continuous fiber reinforced polymers are fundamentally limiting in that reinforcement is

typically applied only in the plane of the mold or tool. Additionally, key operations inherent to

all CFRP processing approaches require a variety of skilled labor as well as costly net-shape,

hard tooling. As such, additive manufacturing has risen to the forefront of manufacturing and

processing research and development in the CFRP arena.

Additive manufacture of continuous fiber reinforced thermoplastics (CFRTP) exhibits

the potential to relieve many of the constraints placed on the current design and manufacturing of

continuous fiber reinforced structures. At present, the additive manufacture of CFRTP has been

demonstrated successfully to varying extents; however, comprehensive dialogue regarding

manufacturing defects and quality of the processed continuous fiber reinforced thermoplastics

has been missing from the field. Considering the preliminary nature of additive manufacture of

CFRTP, exemplary processed composites are typically subject to various manufacturing defects,

namely excessive void content in the thermoplastic matrix. Generally, quality evaluation of

processed composites in the literature is limited to test methods that are largely influenced by the

properties of the continuous fiber reinforcement, and as such, defects in the thermoplastic matrix are usually less-impactful on the results and overlooked.

Hardware to facilitate additive manufacturing of CFRTP was developed and continuous fiber reinforced specimens, with high fiber volume fractions (~ 50 %), were successfully processed. Early efforts at evaluating the processed specimens using defect-sensitive Short-Beam Strength (SBS) analysis exhibited limited sensitivity to void content, coupled with destructive, inelastic failure modes. As a path forward, an expanded study of the effects of void content on the processed specimens was conducted by means of Dynamic Mechanical Analysis (DMA). Utilization of DMA allows for thermomechanical (i.e. highly matrix sensitive) evaluation of the composite specimens, specifically in terms of the measured elastic storage modulus (E'), viscous loss modulus (E"), damping factor (tan δ) and the glass transition temperature (Tg) of the processed composite specimens.

The results of this work have shown that DMA exhibits increased sensitivity, as compared to SBS, to the presence of void content in the additively manufactured CFRTP specimens. Within the relevant range of void content, non-destructive specimen evaluation by DMA resulted in a measured, frequency dependent, 5.5 – 5.8 % decrease in elastic storage modulus per 1 % increase in void content by volume. Additionally, quality evaluation by DMA realized a marked decrease in the maximum measured loss modulus in the additively manufactured composites, ranging from 7.0 – 8.2 % per 1 % increase in void content by volume. Effects of void content were also measured in both the damping factor and glass transition temperature, where an approximate 1.6 °C drop in Tg was recorded over the relevant range of void content. The results of this work indicate, firstly, that DMA is a superior evaluation method, as compared to SBS, in terms of sensitivity to void content in additively manufactured

CFRTP. Additionally, the results of this work provide a clear expansion of the current state of the literature regarding additive manufacture of CFRTP materials in that the effects of prominent manufacturing defects have been assessed with regard to thermomechanical material performance. Furthermore, and finally, the results of this work establish a direct path forward to characterize long-term effects of manufacturing defects, by means of DMA, on the creep-recovery and stress relaxation behavior of the relevant composite material system.

ACKNOWLEDGEMENTS

TABLE OF CONTENTS

LIST OF TABLES

LIST OF FIGURES

1 Introduction

Additive manufacture of continuous fiber reinforced thermoplastic matrix composites (CFRTP) from a continuous commingled precursor is presented, and evaluated, in terms of quasi-static mechanical analysis and Dynamic Mechanical Analysis, specifically with respect to the presence of manufacturing defects. Pertinence of the work is defined in the following sub-sections, in terms of consideration of the current processing of continuous fiber reinforced polymers (CFRP), generalized polymer additive manufacturing, the state of reinforced polymer additive manufacturing, metrics of quality evaluation for CFRP, and Dynamic Mechanical Analysis as a quality evaluation tool for CFRP. The chapter concludes with the thesis statement and a brief outline of the experimental work.

1.1 Continuous Fiber Reinforced Polymers – Processing & Limitations

Continuous fiber reinforced polymers (CFRP) have become integral to modern mechanical design as value-added alternatives to metallic, ceramic and neat polymeric engineering materials. Some examples of the design benefits allowed by continuous fiber reinforced polymers include, but are not limited to; superior specific strength and stiffness, corrosion resistance, creep resistance, improved fatigue life and tailorable thermal properties [1]. Differing from engineering design practice as applied to metallic, ceramic and neat polymeric engineering materials, where structure is commonly designed to accommodate the limitations of the material of choice, the design of a continuous fiber reinforced composite structure is performed in-sync with the design of the continuous fiber reinforced composite material. This practice allows for designers to take full advantage of the benefits, mostly in terms of material tailor-ability, provided by anisotropic composite materials. As such, it is critical for designers to

have a working understanding of the variety of CFRP processing approaches available, as well as the key operations inherit to all processes therein, as CFRP processing dictates the final material properties of the CFRP.

Barbero summarizes the key operations inherent to all CFRP processing, or unit operations as denoted in the text, as follows: fiber placement along the required orientations in a mold or tool, impregnation of the fibers with the polymeric resin, consolidation of the constituents to remove excess resin, air and volatiles, cure or solidification of the polymer, extraction from the mold or tool, and post-processing operations such as trimming [1]. These key operations, critical as they may be to achieving material properties predicted by micromechanics, also impose limitations on what exactly can be processed and how costly, in terms of both time and monetary expenditure, that processing will be.

Fiber placement along required orientations in a mold or tool requires some level of skilled labor or precision automation, both of which share an associated dollar expenditure and add time to material processing. It should be acknowledged that the difficulty, or requisite care, associated with placing different fiber reinforcement types varies from process to process and material to material. For example, reinforcement layup for a resin infusion using dry preforms requires minimal care from the relevant technician outside of placing the reinforcement plies in the specified orientation and stacking sequence. On the contrary, a layup of the same part using a continuous carbon fiber prepreg requires considerable manual intervention from the technician to ensure each ply is properly tacked and consolidated against the ply beneath it, sans wrinkles or other placement related defects. Mold complexity also contributes to the difficulty of placing continuous fiber reinforcement; however, it also imposes an additional, different set of restrictions on the designer. Hard tooling required for production of a continuous fiber

reinforced primary structure is often bulky, costly to machine, and serves as an inhibitor for designers when it is necessary to alter design parameters within a product cycle.

Moving forward, consolidation of the constituents to remove excess resin, air and volatiles prior to cure or solidification of the CFRP is of critical importance to the ultimate material performance of a CFRP. As such, great care is taken during the material processing to ensure the laminate is free of any included foreign phases, adding to process time. Often times consolidation is achieved by means of both vacuum bagging, to remove air from the laminate, and autoclaving, to apply additional pressure (in excess of atmospheric pressure from vacuum bagging) and also regulate temperature during polymer cure or solidification. Vacuum bagging requires a variety of consumables and a skilled technician to lay up the consumables appropriately, extending an already lengthy process. Additionally, as applied to thermosetting polymer matrix materials, cure cycle times for a typical part can add 60 – 90 minutes to the process, and even days for very large structures [2]. Thermosetting polymers, the most typical polymer type supplemented with continuous reinforcement, also contribute a variety of different limitations to processing of the composite, such as exotherm during polymerization and off-gassing of volatile-organic compounds. It is for these reasons that major entities within the aerospace and automotive sectors are pushing for research and development in continuous fiber reinforced thermoplastics (CFRTP).

Thermoplastic polymers, as compared to thermosetting polymers, offer a variety of processing advantages, including, but not limited to; no out-time considerations, no in-mold cure cycle or polymerization, melt processability, recyclability and both semi-crystalline and purely amorphous microstructures. To date, continuous fiber reinforced thermoplastics have been limited to low-volume production, mainly in the aerospace sector, as a result of a lack of

familiarity with thermoplastic processing and continuous fiber reinforced thermoplastic feedstocks [2]. Continuous fiber reinforced thermoplastic feedstocks tend to take the form of unidirectional tapes, which can then be oriented, stacked, and consolidated using heated platens in a compression molding or stamp forming like process. Flat laminates, or those with simple curvature, are possible with this approach if matched molds are used in place of planar platens. This type of processing approach greatly reduces process cycle times, as compared to thermosets, due to the lack of a temperature-controlled cure cycle. Despite the advantage of reduced process cycle times, this continuous fiber reinforced thermoplastic processing approach shares some of the same restrictions already discussed with regard to continuous fiber reinforced thermosets, in the need for net-shape hard tooling, as well as part size being limited by the size of the processing equipment.

Based on the above information, it is clear that traditional methods of continuous fiber reinforced polymer processing, using either thermosets or thermoplastics, are arduous and time consuming. Additionally, it is clear now that thermoplastic matrix materials are superior to thermosetting matrix materials in terms of reducing the time required for material processing. Separate from the processing approaches discussed thus far, a fully automated method of continuous fiber reinforced polymer processing, commonly known as Automated Fiber/ Tape Placement (AFP or ATP), has postured itself at the helm of continuous fiber reinforced thermoplastic manufacture. For means of comparison, ATP serves as the composite processing analog to CNC work-cells in the metalworking industry [3]. ATP is a particularly favorable approach for thermoplastic composite processing because it allows for in-situ consolidation of the material being placed by the payout system, in addition to other well-known advantages allowed by automated manufacture such as precision and repeatability in material placement. In-

situ consolidation, in this context, is defined by both void compaction and removal as well as fusion bonding between the thermoplastic composite tape and the tool or a previously placed tape. An example of a typical AFP work-cell is shown in Figure 1.
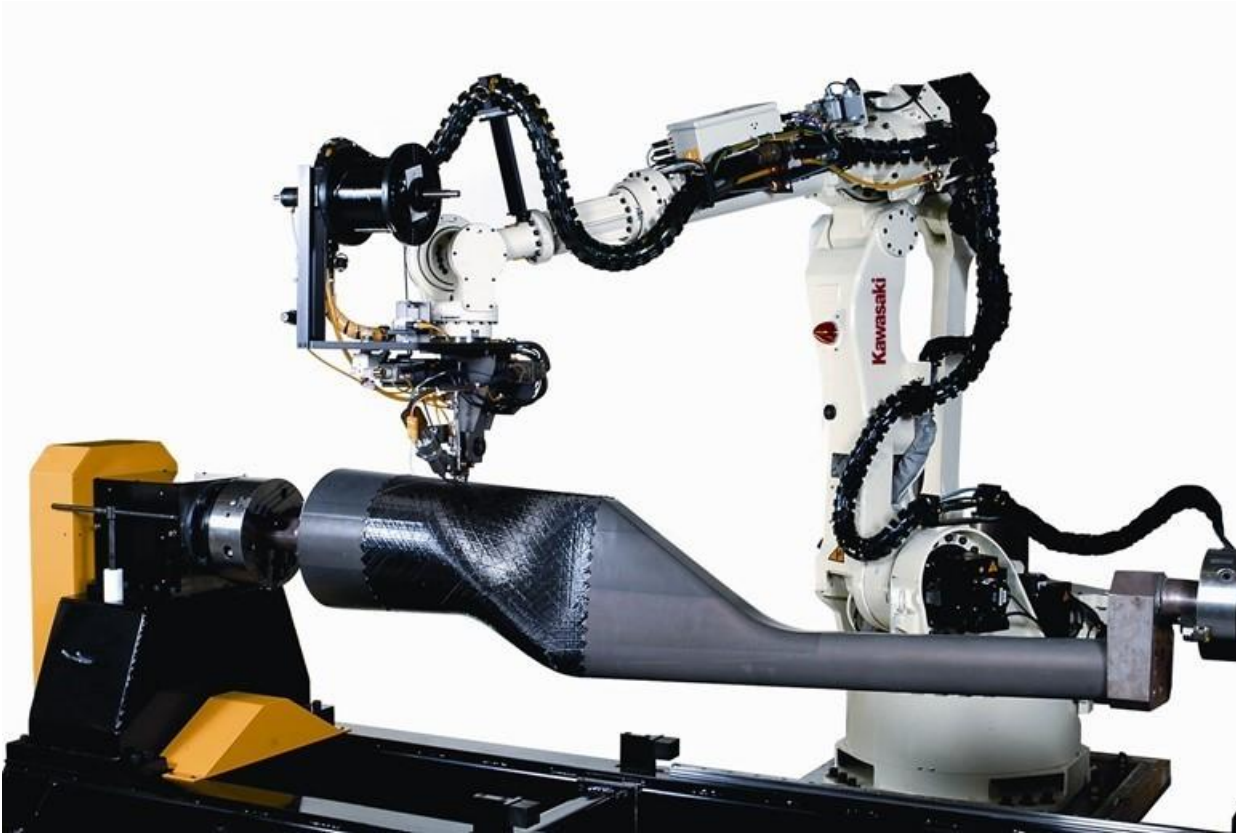
Figure 1: Automated tape placement (ATP) work-cell placing continuous fiber reinforced thermoplastic tape over complex tooling [4]

The ATP work-cell shown in Figure 1 is comprised of a robotic motion system, in this case integrating articulation of the tool and the placement head, a tool used to support material placement and provide the desired laminate geometry, and a material payout system. In terms of realizing in-situ consolidation of the reinforced thermoplastic tapes, the material payout system is of critical importance. In general, in-situ consolidation is facilitated through the application of some form of energetic stimulation as well as a normal compaction force during material placement [5]. Energy input, often to both the material and the substrate, is used to facilitate thermoplastic flow while the normal compaction force allows for the generation of intimate

contact between placed tapes as well as void compaction [5]. Despite intimate contact between tapes being initiated by the compaction force, tape surfaces are often rough and polymer healing, commonly referred to as autohesion, or the movement of polymer chains at the tape interface, is required to complete the consolidation process [5]. It should be noted that elevated temperature, not pressure, drives the healing process [5]. The healing process is predicted to occur wherever the in-situ temperature is in excess of the thermoplastic glass transition temperature [5]. This process is depicted schematically in Figure 2.
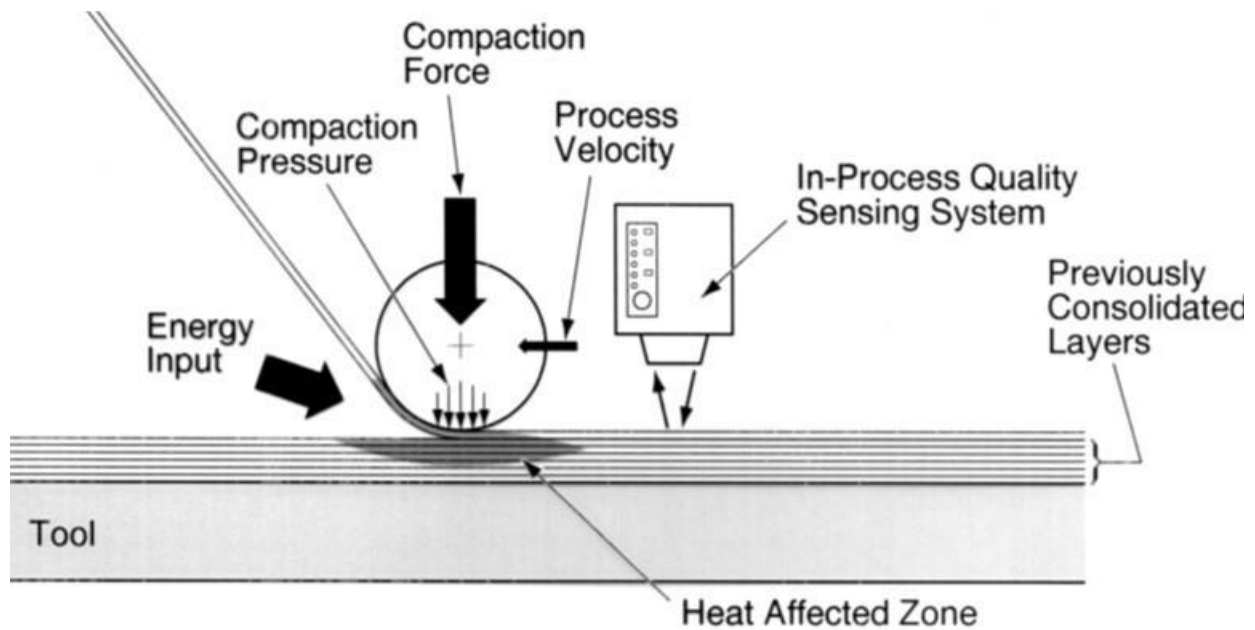
Figure 2: Representative schematic for in-situ consolidation of a generic reinforced thermoplastic tape [5]

In terms of competing with thermoset process times and material performance, in-situ consolidation is critical to the success of the thermoplastic ATP process. Evaluation of in-situ consolidation hinges on the microstructural changes enacted upon the material during processing which include, but are not limited to, melting, degradation, crystallization, intimate contact, autohesion, residual strains and void consolidation and growth [6]. In consideration of these microstructural changes, ATP process optimization, mechanical characterization, physical

characterization and quality assurance are of interest. Typical inputs in an ATP process optimization relate to energy delivery (hot gas temperature or laser power are exemplary), compaction force and compactor geometry, and material preheating parameters. Typical outputs include degree of tape bonding, void content, material degradation, degree of crystallinity, residual stresses and temperature distribution during processing [6].

Mechanical and physical characterization are typically utilized to evaluate the outputs of an ATP process optimization. For example, evaluation of tape bonding, an interlaminar shear dominated quality, can be accomplished quickly and qualitatively by the Short-Beam Strength test as outlined by ASTM D2344 [6,7]. This has been utilized extensively in the literature [6]. Other characterization techniques typically hinge on thermal analyses to identify small changes in the material microstructure. Such analyses include Differential Scanning Calorimetry (DSC), Dynamic Mechanical Analysis (DMA) and Thermogravimetric Analysis (TGA) [6]. Defects outside of the microstructural realm such as unwanted tape gaps/ overlaps, wrinkles, missing tows/ tapes, are also possible in the thermoplastic ATP process, and such they are a concern in terms of quality assurance [6]. It is typical for ATP payout heads to be equipped with online inspection systems in order to reduce the time required for defect inspection and improve process efficiency [6].

As shown in Figure 1, and supplemented by Figure 2, the material payout system in an ATP work-cell is often comprised of many integrated hardware elements that must operate in-sync to realize acceptable in-situ consolidation of the thermoplastic composite feedstock material. As such, payout systems are often complex, costly and very large relative to the material being placed, as well as the final laminate. Equipment cost is often a stumbling block for designers looking to manufacture laminates using ATP, and if hardware is not accessible,

design compromises must be made to facilitate laminate processing by more accessible methods. Despite the known processing benefits of thermoplastic ATP, equipment cost, hard tooling cost and the lack of an ability to place reinforcement out of the tooling plane inspire the aerospace and automotive sectors to look toward other processing technology outside of the composites realm for inspiration, direction and solutions to tomorrows engineering problems.

Currently there exists no single CFRP/ CFRTP manufacturing process that is all-encompassing in terms of creating net-shape, complex laminates free from the maladies associated with net-shape hard tooling. It is for this reason that composite processing incorporating concepts from additive manufacturing seems a logical next step in the progression of CFRP/ CFRTP processing. A discussion of relevant background information and literature related to the additive manufacture of unreinforced and reinforced polymers will be the subject of the following section.

1.2 Additive Manufacture – Unreinforced Polymers

Additive manufacturing, or more colloquially 3D printing, is a method of manufacture where a component is produced by the selective placement of material, usually layer-wise, to define both external and internal geometries as dictated by the relevant 3D CAD model. Generally, an additive manufacturing process, regardless of process type and the idiosyncrasies therein, follows a similar process chain composed of the following steps. The component of interest is developed into a three-dimensional model in a CAD package. The CAD model is then broken down into spatial data and processed into a control code specific to the method of additive manufacturing to be utilized. The control code, usually inclusive of motion, environment and material payout control, is then uploaded to the additive manufacturing platform and the process of creating the component is initiated. Upon completion of the additive

manufacturing process, the new component is removed from the additive manufacturing system for either delivery, or post-processing operations. The system can then be readied for further manufacturing. Some pertinent benefits of additive manufacturing, as compared to other conventional manufacturing methods such as casting, molding or machining, include more efficient material usage, fabrication of complex geometry without the need for net-shape tooling, an ability to vary design parameters in a product cycle and customer-wise part customization [8].

It should be acknowledged that polymers, metals, ceramics and biomaterials can be additively manufactured; however, only the additive manufacturing of polymers will be of interest moving forward. There are a variety of methods for the additive manufacture of polymers, both thermoplastic and thermoset, including, but not limited to, Fused Deposition Modeling (FDM), powder bed fusion, ink and binder jetting, stereolithography (SLA) and laminated object manufacturing (LOM). Fused Deposition Modeling, the most accessible of 3D printing methods, is characterized by the melt extrusion of thermoplastic filament layer by layer to produce net-shape components directly from a CAD model. Powder bed fusion accomplishes the same goal by utilizing either discrete binder placement or directed energy to fuse powder particles together along paths pre-determined from a CAD model. Fresh powder, in this case a thermoplastic, is spread over the previously processed material and the process is repeated in a layer-wise fashion until all relevant geometries have been generated. Ink and binder jetting share some similarities with powder bed fusion, with a distinguishing characteristic being the commonality of using multiple, in some cases hundreds or thousands, of material jetting nozzles. Stereolithography, one of the few common methods for processing thermosetting polymers, utilizes directed UV radiation to selectively initiate polymerization of the liquid resin, which is usually contained in a storage vat that makes up the available build volume. Finally, laminated

object manufacturing or LOM, differentiates itself from the previous processes by its inherent dependency on the cutting and lamination of sheets or rolls of material [8]. Either a form-then-bond, or the contrary bond-then-form, approach is used in processing, depending on the material being used for manufacture [8]. It is clear that LOM shares some inherent similarities with conventional composite manufacture; however, it cannot accommodate selective placement of reinforcing phases in the print process, a capability desirable from a CFRP view point and more realistic with respect to an FDM process.

It is generally accepted that polymeric components produced via additive manufacture, specifically FDM, exhibit some level of anisotropy as a result of the layer-wise material processing. During placement of the thermoplastic feedstock, intralayer bonding is driven through the autohesion process that was touched on earlier with regard to thermoplastic ATP in the composites industry. The quality of the intralayer bonding is dependent on molecular diffusion of polymer chains between adjacent paths to form a neck, as well as the randomization of the polymer chains across the interface [9]. A representation of this process is depicted in Figure 3.
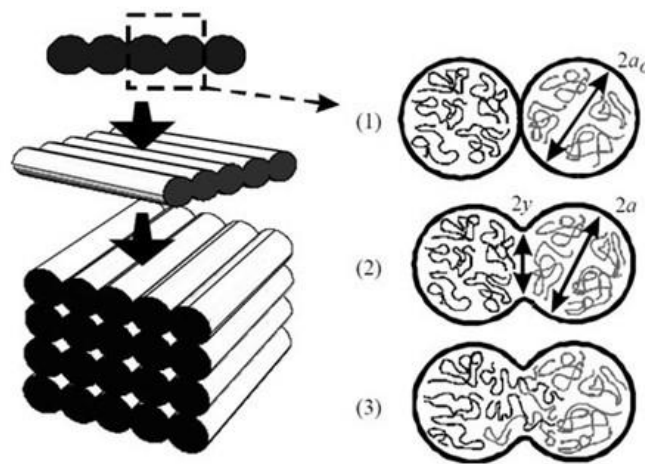
Figure 3: Bond formation process between adjacent filaments in the FDM process [9]

As illustrated by Figure 3, the necking process facilitates a fusion bond between the cylindrical thermoplastic extrusions that results in interstitial porosity and a reduced cross-sectional geometry in the necked region. Early studies on the anisotropic behavior of acrylonitrile butadiene styrene (ABS) as produced by FDM demonstrated a lower strength in the necked regions between the cylindrical extrusions as compared to the strength of bulk ABS [10]. Similarly, follow up works regarding the dependence of FDM components on the cross-sectional meso-structure of the printed coupon (meso-structure referring to interstitial void size and location in the cross-section) resulted in elastic moduli values ranging 11 to 37 percent lower, and failure strength values ranging 22 to 57 percent lower, than the ABS material feedstock [11]. An example of one of the cross-sectional meso-structures from [11] is shown in Figure 4, where the dark regions indicate interstitial porosity.
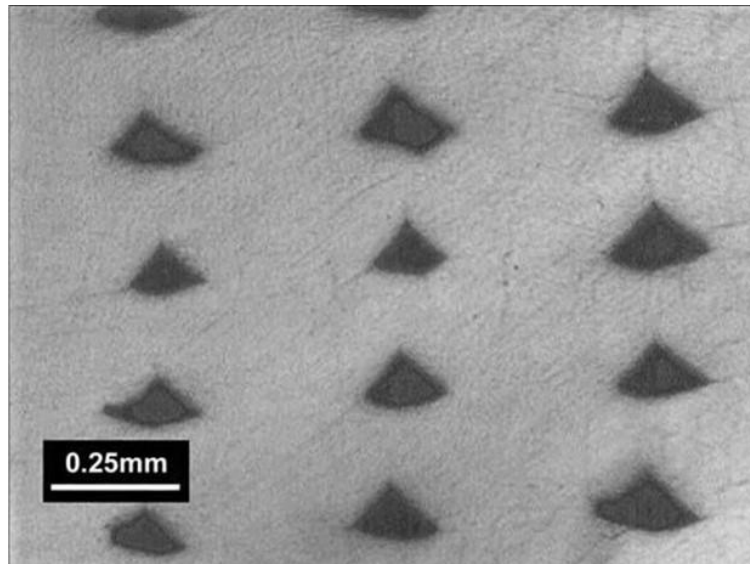
Figure 4: Cross-sectional meso-structure of a printed ABS part showing interstitial porosity and necked regions [11]

It is conceivable that the interstitial porosity, exemplified in Figure 4, can be reduced through manipulation of FDM process parameters such as extrusion, or road, spacing, print temperature and material throughput; however, modifying these parameters in such a way runs

the risk of compromising the geometric fidelity of the additively manufactured part, specifically in terms of surface roughness and geometric tolerancing. As such, efforts have been undertaken to improve the mechanical performance of 3D printed parts through the integration of fibrous reinforcement. These efforts span a broad spectrum, ranging from the improvement of 3D printed components all the way to the demonstration of additively manufacturing continuous fiber reinforced composite materials.

1.3 Additive Manufacture – Reinforced Polymers

There are many methods for processing fiber reinforced composites using additive manufacturing; however, many of these methods fail to realize the full potential of the design spectrum for advanced polymer matrix composites, specifically in terms of controlled fiber placement and high fiber volume fraction. Figure 5 gives a comprehensive overview of the variety of additive manufacturing processes currently available, some of which have already been discussed, as well as their potential to support the inclusion of either short or continuous fiber reinforcement in the build material.

As indicated by Figure 5, the ideal additive manufacturing platform for producing fiber reinforced polymer matrix composites with short, long and continuous fiber reinforcement is the FDM platform. This is directly attributed to certain key, inherent process characteristics relevant to the FDM platform. Short fiber reinforcement can be easily integrated into the FDM material feedstock due to the melt formed nature of the thermoplastic filament, using methods analogous to injection molding techniques with short fiber. The inclusion of continuous fiber is also feasible due to FDM being the only process listed in Figure 5 that utilizes both a moving print head and a line-based material deposition strategy [12]. It should be acknowledged that

utilization of a moving print head, as well as a line-based material deposition strategy, are critical to overcoming many of the aforementioned restrictions in conventional CFRP processing.

Technology	Abbr.	Physical effect	Geometry creation		Layer			Short fiber	Long fiber	Continuous fiber		
			Beam	Head	Point	Line	Layer			Roving	Tape	Fabric
Stereo lithography	SL	Photo polymerization	●	○	●	○	○	◑	○	○	○	○
Digital light processing	DLP	Photo polymerization	●	○	○	○	●	◑	○	○	○	○
Poly-jet modelling	PJM	Photo polymerization	○	●	●	○	○	○	○	○	○	○
Multi-jet modelling	MJ	Melting	○	●	●	○	○	○	○	○	○	○
Selective laser sintering	SLS	Sintering	●	○	●	○	○	●	○	○	○	○
Selective laser melting	SLM	Melting	●	○	●	○	○	◑	○	○	○	○
Electron-beam melting	EBM	Melting	●	○	●	○	○	◑	○	○	○	○
Fused deposition modelling	FDM	Melting	○	●	○	●	○	●	◑	●	○	○
Plaster-based 3D printing	3DP	Adhesive binding	○	●	●	○	○	◑	○	○	○	○
Laminated object manufacturing	LOM	Adhesive binding	●	○	○	○	●	◑	◑	○	●	●

○ impossible
◑ generally possible
● commercially available

Figure 5: Potential for fibrous reinforcement inclusion in various additive manufacturing processes [12]

Additionally, as indicated by Figure 5, the LOM process is also capable of facilitating the inclusion of continuous fiber reinforcement. The use of LOM to generate both ceramic and polymer matrix composites was explored early on in the literature [13]. In the LOM process, the layers that are placed atop one another are consolidated using either a sonotrode or a heated compaction device. Results showed that the LOM process was sufficient to physically bond the layers of constituent materials together; however, composite cure related post processing was required in the form of applied heat and mechanical pressure to achieve complete constituent cure and consolidation. It was found that fiber reinforced polymer matrix composites could not be fully consolidated or cured using the LOM process due to the finite amount of time the compaction device is in intimate contact with the relevant surface area of the LOM part [13]. Post-cured composites from the LOM process, based on glass fiber/ epoxy prepregs, exhibited comparable performance in tension, compression, flexure and Short-Beam Strength to material data from the prepreg supplier; however, without post cure, the compression strength of the LOM material was reduced to 30 % of manufacturer supplied value [13]. Data for LOM composites sans post cure with regard to tension, flexure and Short-Beam Strength was not

presented [13]. With regard to the work in [13], as well as the limited ability to selectively place reinforcement in LOM, FDM processes will be the main area of concern moving forward.

Numerous studies have been conducted in order to evaluate the feasibility, ease of integration, and subsequent mechanical properties of short fiber reinforced polymer matrix composites by FDM. Intuitively, adding a much stronger and stiffer reinforcing phase to a relatively compliant thermoplastic polymer will enhance the polymers mechanical and thermal performance; however, reinforcement content by weight, as well as reinforcement orientation, also have some effect on the processed material performance. The literature shows that as weight percentage of short fiber reinforcement is increased in a thermoplastic polymer filament for the FDM process, material model-based predictive difficulties arise in terms of determining fiber size and distribution through the deposited composite material, as well as in fiber/ fiber and fiber/ machine surface interactions [14]. In the FDM process, local short fiber interaction with other fibers, as well as machine surfaces, results in fiber damage in processing that leads to shorter than expected fibers in the final part and excessive abrasion on machine components [14]. Fiber breakage and subsequent fiber shortening was experimentally verified to increase as a function of fiber content by weight in both compression molded and FDM samples, with the most significant fiber shortening apparent in the FDM samples with the greatest fiber content [14]. The same work also found that incorporating short fiber content in the thermoplastic FDM feedstock resulted in significant void formation at the edge of, or around, the included fibers, which was not apparent in the compression molded samples. This local void formation, coupled with the shortened fiber lengths, was found to reduce the overall tensile strength of the FDM composite material, as compared to similar compression molded samples, through lack of intimate interfacial contact between the constituent materials [14].

14

Similarly, another contribution to the relevant literature explored the effect of adding various weight percentages of short reinforcement as well as various lengths of short reinforcement to ABS feedstock for the FDM process [15]. As compared to a neat ABS specimen, short fiber inclusion resulted in improvements in tensile strength and Young's modulus with a subsequent decrease in toughness, yield strength and ductility [15]. Specimens printed with 5 weight percent (wt %) reinforcement content exhibited the largest mean tensile strength, while those printed with 7.5 wt % reinforcement exhibited the largest mean Young's modulus, with relevant property increases ranging from $20 - 30$ % as compared to the neat specimen [15]. Conversely, specimens printed with 10 wt % and 15 wt % reinforcement exhibited mean tensile strengths and moduli more similar to the neat specimens, as well as significant drops in toughness, yield strength and ductility as compared to neat, 3 wt %, 5 wt % and 7.5 wt % printed samples [15]. Furthermore, printed specimens with 150 μm reinforcement length outperformed specimens with 100 μm reinforcement length in terms of tensile properties, while exhibiting an additional drop in toughness and ductility. Similar to [14], [15] also found that void content was largely exacerbated in the samples with the greatest short fiber content. Some of the aforementioned results from [15] are shown in Figure 6.

The examples discussed clearly demonstrate that the addition of short fiber to thermoplastic feedstocks for FDM can readily achieve the goal of improving certain aspects of the performance of 3D printed components; however, the impact of the addition of short fiber to the printing process has proved to be limited and ultimately results in composite material performance that is lacking in competitiveness with advanced, continuous fiber reinforced thermoplastics with high fiber volume fractions (reinforcement by volume as opposed to

reinforcement by weight, vernacular more common to continuous reinforcement). It is for this reason that the addition of continuous fiber to the 3D printing process has been investigated.

(a) Tensile strength

(b) Young's modulus

(c) Toughness

(d) Yield strength
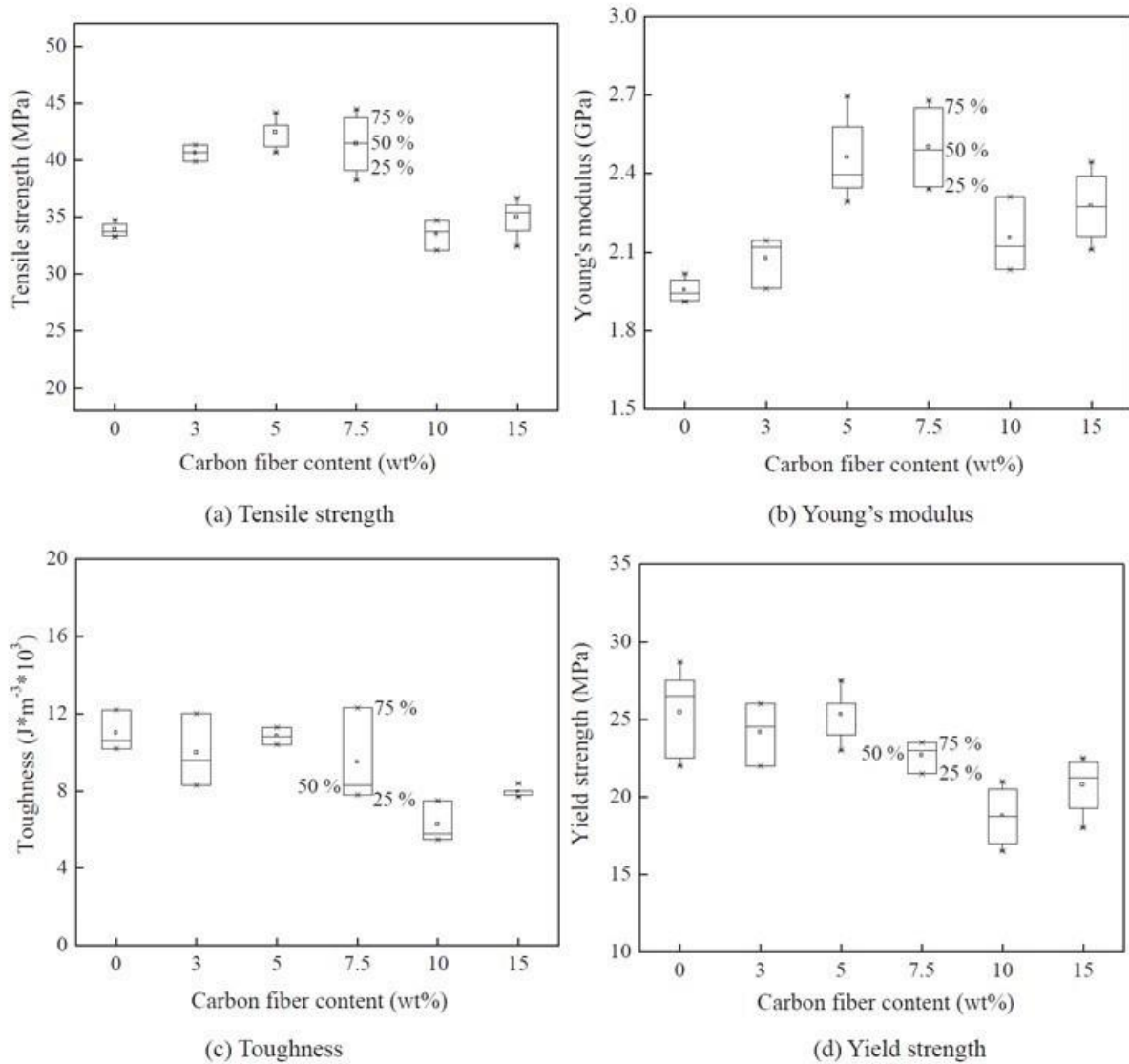
Figure 6: Mechanical performance of 3D printed specimens with varying short fiber content [15]

Current methods for the additive manufacture of continuous fiber reinforced thermoplastic matrix composite materials are most readily distinguished on the basis of how the constituent materials are brought together for the purpose of consolidation and placement. In general, the most common practices include, but are not limited to, combining constituents prior to the printing process as a pre-processed composite filament, combining constituents during the

16

printing process in a heated die, or combining the two material phases on the component or rigid

tool [12]. Each of these practices has been explored in the relevant literature to varying extents

and varying success.

In the case of combining the constituent material phases prior to the printing process, one

specific method that incorporates the use of a pre-processed composite filament has enjoyed

some success in the commercial arena. Relevant studies suggest that this platform is generally

confined to relatively low fiber volume fractions, ultimately limiting the structural performance

of the processed composite parts [16,17]. Continuous tows of approximately 1000 fibers, pre-

consolidated with thermoplastic, are placed using proprietary hardware and control code for the

purpose of reinforcing pre-placed layers of neat thermoplastic in an FDM processing approach

[16]. Presently, the construction of complex laminates seems to be out of reach for this platform,

as increasing the amount of fiber reinforcement in a given component results in uncontrollable

void formation between the placed pre-consolidated tows [16]. An example of increasing void

content with increasing fiber reinforcement, in terms of layers of the pre-processed composite

filaments, is shown in Figure 7.
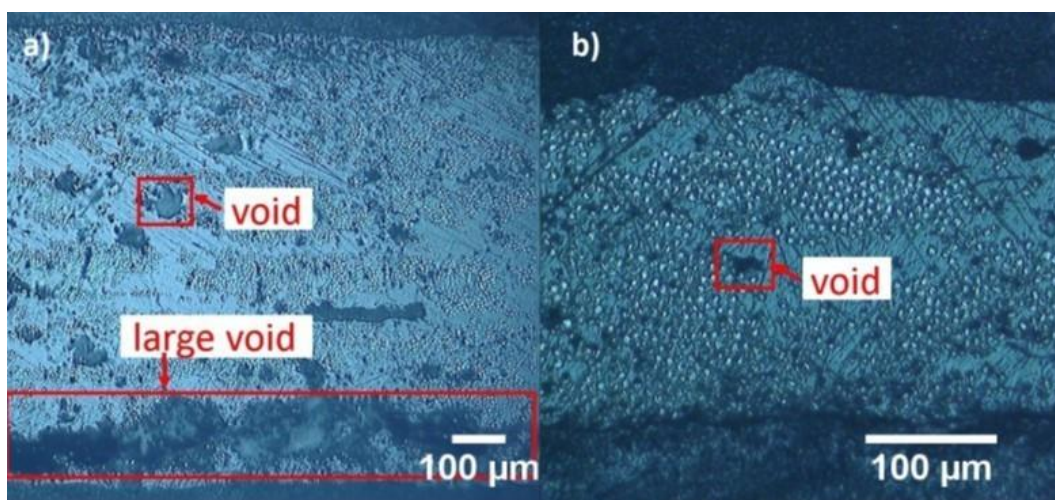
Figure 7: Cross-section of printed continuous fiber reinforced samples, a) cross-section with
six layers of fiber reinforcement sandwiched between two layers of neat polymer, and b) two
layers of reinforcement sandwiched between two layers of neat polymer [16]

In terms of combining the constituents during the printing process, a large body of work exists which explores different combinations of materials, hardware and process parameters. In general, the relevant body of work relies on pulling a dry, continuous tow (or roving) of fiber reinforcement into a heat affected zone using the controlled extrusion of thermoplastic through a slightly modified Fused Deposition Modeling style die [18–20]. Of particular interest to a majority of this work is the design of the heated die, where constituent integration tends to occur [19]. Recent efforts have explored the use of both straight and tapered internal die geometries, each yielding some relative success in terms of wetting the continuous fiber reinforcement with the high viscosity thermoplastic matrix [18,19]. Despite demonstrating an ability to wet continuous reinforcement, these methods still fall short in achieving idealized mechanical performance, in terms of being limited to relatively low fiber volume fractions (~ 8 – 35 %) [18–20]. An example of the process of combining the constituent materials during the printing process is shown in Figure 8.
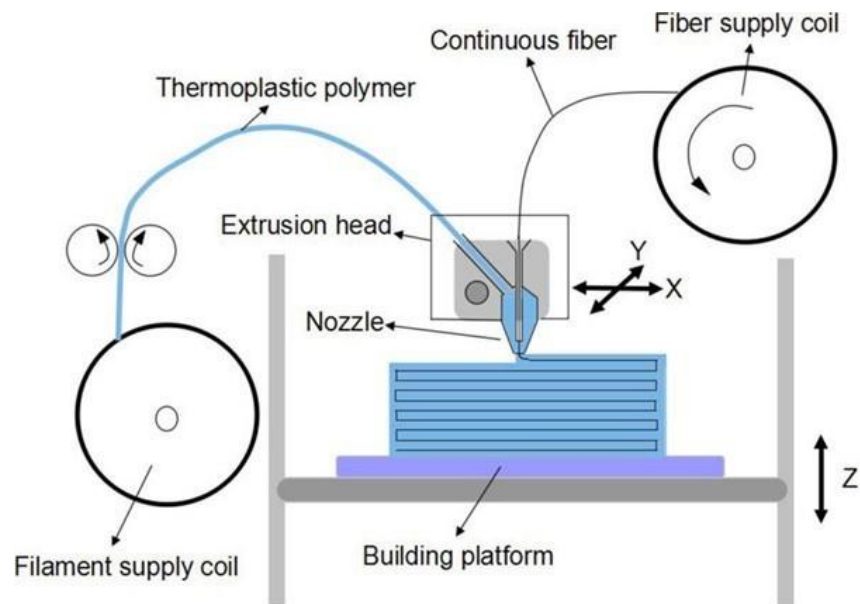
Figure 8: Schematic of constituent combination during the printing process in a heated die [18]

In contrast to the assortment of literature regarding constituent mixing during the printing process, there exists a much smaller body of work concerning mixing the constituent materials on the component or on a rigid tool. Research regarding the deposition of neat polyethylene terephthalate (PET) thermoplastic ahead of continuous glass fiber reinforcement under tension onto a rotating mandrel has demonstrated the feasibility of such a method [21]. In addition to exploring the placement of distinct constituents onto the rigid substrate, the relevant work also explored the use of a continuous commingled glass/ thermoplastic roving as a potential feedstock for the additive manufacture of continuous fiber reinforced thermoplastic composite materials [21]. Upon heating of the commingled precursor, the viscosity of the thermoplastic polymer is lowered to such a point that the simple application of mechanical pressure allows for matrix flow and subsequent fiber wetting, made easier by having the continuous reinforcement and matrix material already intimately intertwined in the "dry" state. Axisymmetric rings were processed on the mandrel, using both the distinct constituents, as well as the commingled roving, under applied mechanical pressure via a heated pressure foot, and mechanical properties were compared via ASTM D2344 for Short-Beam Strength [7]. Although the mechanical performance of the rings made from separate constituents was superior, this effort successfully demonstrated that a fourth option for fiber and matrix combination exists, that being in the use of continuous commingled feedstocks. Additionally, this effort successfully demonstrated the additive manufacture of continuous fiber reinforced thermoplastic matrix composite materials with fiber volume fractions in the more desirable range of 50 – 60 % [21].

Further efforts have been made in processing commingled continuous reinforcement and thermoplastic on both a rotating mandrel as well as a flat-plate substrate [22,23]. In the case of the more recent research on the rotating mandrel, the commingled feedstock was processed via a

standard FDM hot-end with a slightly altered die, or nozzle, for the purpose of material

throughput and consolidation in both conventional filament winding patterns as well as non-

conventional longitudinal paths [22]. Mechanical pressure was applied to the commingled

material in processing using displacement control against the rigid mandrel, dictated by the

machine control code, as well as the inherent tension present in filament winding [22]. Results

of consolidation by means of heated pultrusion through the hot-end and the application of

pressure via displacement control indicated some success, but not without the presence of voids

in the processed composite [22]. The methods for melt processing and application of

consolidation pressure that were applied in [22] were similarly applied in [23]. Although

material was successfully placed on the flat-plate substrate, or print bed, void content limited the

mechanical performance of the processed composite material as compared to the manufacturers

specifications for the continuous commingled precursor [23]. An exemplary cross-section from

[23] is shown in Figure 9. In reference to Figure 9, note that the lightest grey phase represents

the continuous fiber reinforcement, the dark grey phase represents the thermoplastic matrix

material and the black phase represents included void content.
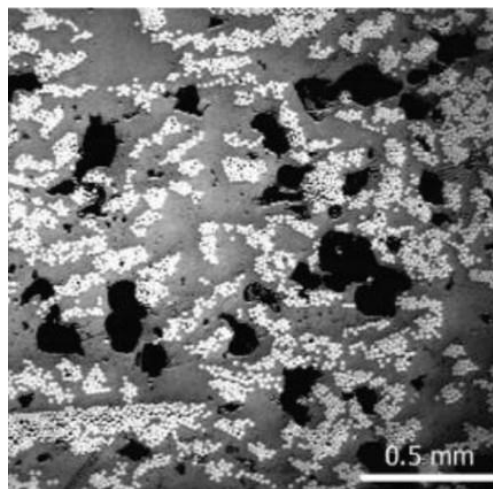
Figure 9: Cross-section of an additively manufacture 3-pt bend specimen processed from a
continuous commingled precursor showing both constituent phases as well as void content
[23]

In consideration of the efforts discussed, it is apparent that the utilization of continuous commingled reinforcement as a feedstock for the additive manufacture of continuous fiber reinforced thermoplastic matrix composites not only allows for the melt processability required by the FDM 3D printing process, but also an ease of processability at attractive fiber volume fractions in the range of 50 – 60% [21]. Placement of this high fiber volume fraction feedstock has been shown to be readily facilitated in the plane of the tool, colloquially referred to as the print bed [21–23]. To elaborate, commingled material was placed on a rotating mandrel, in layers moving radially outward from the mandrel in [21,22] and layers moving upward and away from the flat-plate substrate in [23]. In addition to the in-plane placement already discussed, several successful out-of-plane placement, or printing, operations have been documented in the literature as well [24–26]. An example of out-of-plane material placement can be seen in Figure 10, where a commingled precursor including stretch broken carbon fibers and polyamide 12 thermoplastic was printed in varied in-plane and out-of-plane configurations.
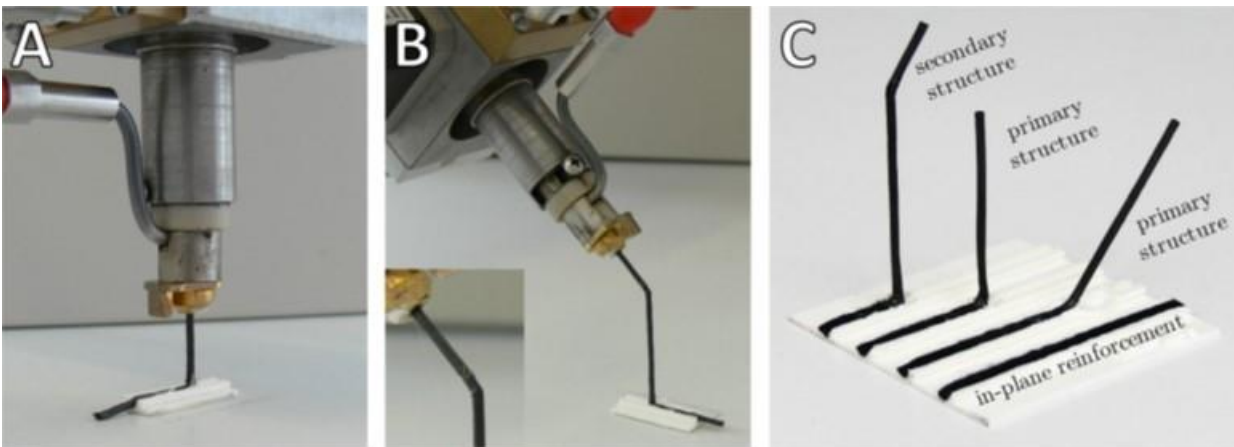
Figure 10: Example of in-plane and out-of-plane material placement using a continuous commingled precursor for additive manufacturing [25]

In the three examples of out-of-plane material placement that have been presented, as well as the earlier examples of in-plane material placement, a general inability to achieve complete consolidation of the constituent reinforcement and matrix materials is evident to

varying degrees [22–26]. As such, quality evaluation of printed continuous fiber reinforced thermoplastic matrix composite materials is of interest to the literature. Various methods employed for the purpose of evaluating the quality of printed continuous fiber reinforced thermoplastic matrix composite materials will be discussed in the next sub-section in order to provide scope for the quality evaluation methods that are employed in this work.

1.4 Quality Evaluation of Printed Continuous Fiber Reinforced Thermoplastics

Consistent with the variety of methods employed in the literature to additively manufacture continuous fiber reinforced thermoplastics, there exists a vast spectrum of processed composite material quality in the literature as well. As the relevant literature has yet to come to a substantive conclusion on what constitutes processed composite material quality, this work will discuss processed composite material quality, qualitatively and quantitatively, specifically in terms of reinforcement distribution in the thermoplastic matrix, reinforcement content by volume (fiber volume fraction) and void content by volume. Additionally, in cases where reinforcement surface modification is relevant, commentary on the performance of the composite interface/ interphase region will be included in the quality evaluation.

In order to compare and discuss the quality of additively manufactured continuous fiber reinforced thermoplastics, a baseline for processed material quality based on the aforementioned characteristics of quality is required. In consideration of the fact that automated thermoplastic tape placement remains the most advanced, accepted method of processing continuous fiber reinforced thermoplastics, a processed composite material example from the ATP arena will be considered and compared against moving forward. An example to serve as a visual baseline of processed composite material quality, coming from the ATP arena, is shown in Figure 11.
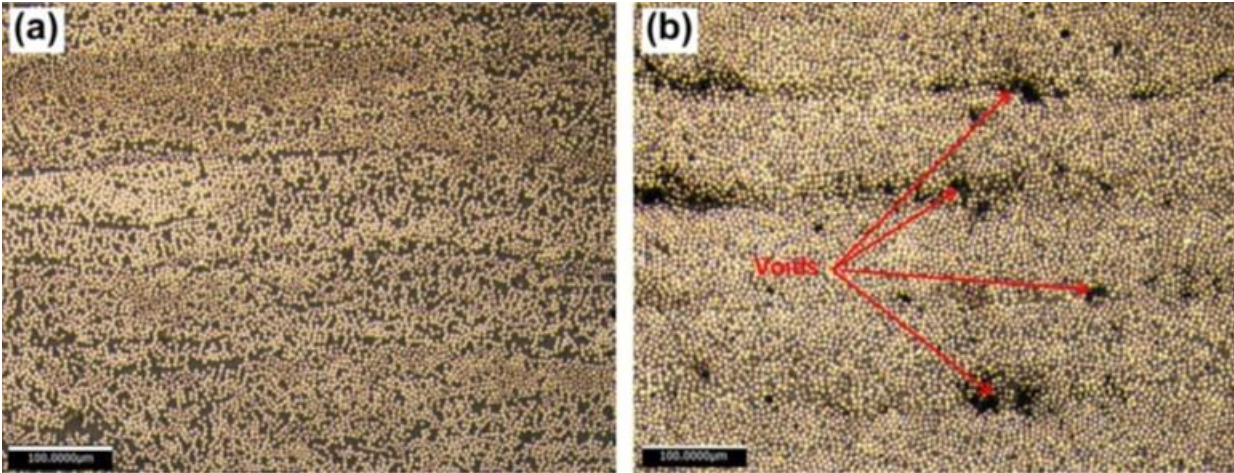
Figure 11: Cross-sectional micrographs (a) autoclave consolidated carbon fiber/ PEEK thermoplastic composite laminate (b) an ATP in-situ consolidated carbon fiber/ PEEK composite laminate [27]

Figure 11 shows two laminate cross-sections, both fabricated from carbon fiber/ polyether ether ketone (PEEK) thermoplastic tapes designed for the ATP process. Light grey regions in Figure 11, composed of small circular cross-sections, represent the carbon fiber reinforcement, while dark grey regions indicate the PEEK thermoplastic matrix and black regions indicate interlaminar void content. Note that black regions, representing void content, are only visually evident in the laminate produced under in-situ consolidation conditions, Figure 11 (b). Upon inspection of Figure 11, it should be clear that there is an almost homogeneous distribution of carbon reinforcement in the PEEK matrix, an indication of a nearly homogeneous reinforcement content by volume throughout the cross-section. For reference and scope, homogeneous reinforcement content by volume throughout the cross-section is required for accurate micromechanical predictions of material properties for a composite lamina, as well as macro-mechanical predictions of material properties for composite laminates. Additionally, it should be clear that both laminates in Figure 11 exhibit both an apparently high reinforcement content by volume, as well as a relatively low void content by volume. It is for these reasons that Figure 11 is considered an adequate comparative baseline to facilitate quality-based

23

discussion of other processed composite material examples from the continuous fiber reinforced thermoplastic additive manufacturing arena.

In contrast to Figure 11, which exhibits homogeneous reinforcement distribution, high reinforcement content and low void content, much of the literature relevant to continuous fiber reinforced additive manufacturing exhibits processed composite material characteristics at the opposite end of the spectrum with respect to the aforementioned ideal material characteristics. A cross-section from a fractured flexure coupon, additively manufactured using the method of combining constituents during the printing process, is shown below in Figure 12. Upon inspection of Figure 12, in comparison to Figure 11, many immediate differences in the processed material quality should be apparent, specifically in terms of reinforcement distribution, reinforcement by volume and voids by volume. As shown in Figure 12 a-f, discrete bundles of the continuous fiber reinforcement in the thermoplastic matrix are apparent, as opposed to the pseudo-homogeneous reinforcement distribution shown in Figure 11. This phenomenon is most closely associated with the method of combining the constituents during the printing process, which is also the most common method employed in the literature for the additive manufacture of continuous fiber reinforced thermoplastics.
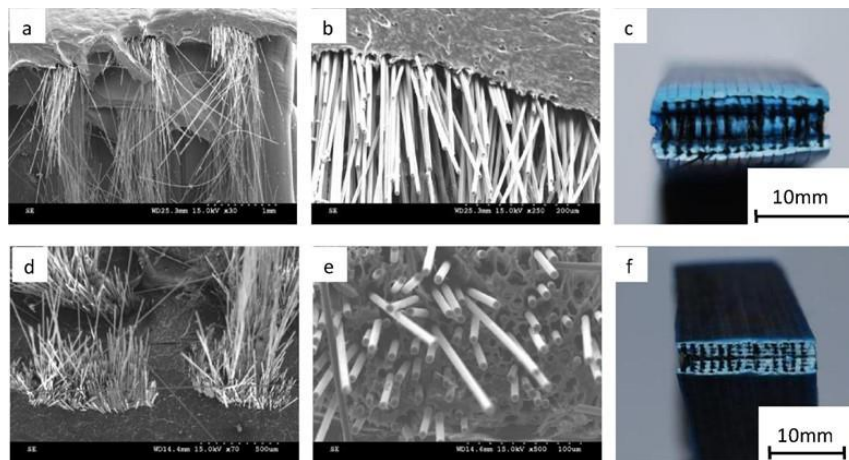
Figure 12: Microstructure of a fractured flexural test coupon printed from continuous carbon reinforcement and polylactic acid (PLA) thermoplastic [18]

Another notable implication of discrete fiber bundles in the process material, as opposed to near homogeneous reinforcement distribution, is the lack of wetting of the reinforcement within the bundles by the thermoplastic matrix. A lack of reinforcement wetting, in this context, ultimately results in unfilled gaps between the reinforcing fibers which translate to intralaminar voids in the processed composite material. Additionally, the discrete fiber bundles result in large interstitial matrix rich regions (with respect to the meso-structure) that correlate with a low fiber volume fraction in the processed composite material. A final notable takeaway from Figure 12, which is apparent in all images a-f, is the occurrence of fiber pullout in the failed coupon cross-section. This serves as an indication of poor interfacial bonding between the constituent materials, and ultimately poor load transfer from the thermoplastic matrix to the continuous reinforcement. To conclude, Figure 12 serves as a comparative example of a low-quality material that is typical in the literature, as compared to the high-quality material shown in Figure 11.

To serve as a final reference point for comparison of processed continuous fiber reinforced thermoplastic material quality from the literature Figure 13 has been included. Figure 13 exhibits a cross-section from an additively manufactured continuous fiber reinforced thermoplastic laminate from a continuous commingled precursor. In this case, the dark grey phase composed of small circular cross-sections represents continuous glass reinforcement, the light grey phase represents the polypropylene (PP) thermoplastic matrix and the red phase represents included void content. The included void content has been highlighted red by a digital thresholding technique that is common in the literature [23,24].
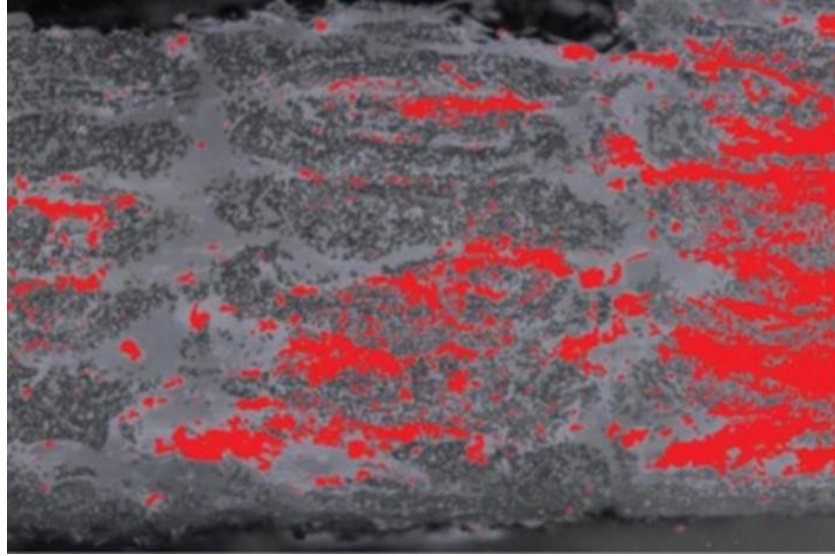
Figure 13: Cross-section of additively manufactured continuous fiber reinforced thermoplastic specimen from a commingled precursor, exemplary of reinforcement agglomeration, matrix-rich regions and void content [23]

Although Figure 13 does not depict the fracture surface of an additively manufactured continuous fiber reinforced thermoplastic from a continuous commingled feedstock, it does share a variety of similarities with Figure 12 that allow for comparative commentary on the processed composite material quality. As was evident to a greater extent in Figure 12, Figure 13 also shows continuous reinforcement agglomerates in the cross-section with matrix rich regions separating the reinforcement. Although the cross-section in Figure 13 exhibits a more even distribution of the reinforcement through the cross-section, it fails to match the pseudo-homogeneous reinforcement distribution evident in Figure 11. Additionally, Figure 13 exhibits both matrix rich regions and clearly visible void content, both of which ultimately lower the reinforcement content by volume of the processed composite material as well as the relative quality of the processed composite material.

After comparing Figure 12 and Figure 13 to the high-quality metric presented in Figure 11, and in consideration of the fact that Figure 12 and Figure 13 are representative of the processed material quality evident throughout the relevant literature, it should be clear that there

are readily apparent levels of processed composite material quality that vary significantly with respect to an ideal processed continuous fiber reinforced thermoplastic, see Figure 14. As such, it would seem logical that the literature would exhibit a variety of different quality evaluation techniques employed specifically to target and quantify the effects of quality variation in the processed composite material; however, as will be discussed shortly, this is not the case.
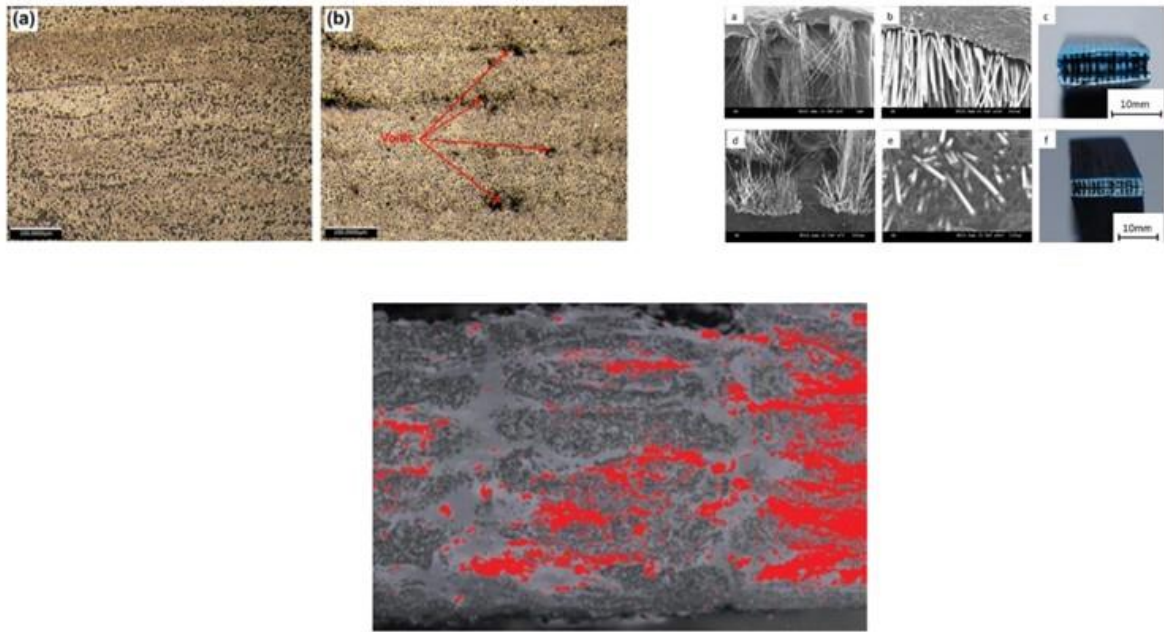
Figure 14: Comparative view of Figure 11, Figure 12 and Figure 13, refer to original figures for full size images [18,23,27]

The relevant literature concerning the additive manufacture of continuous fiber reinforced thermoplastics largely relies on tensile loading to failure as a quality evaluation tool [16,17,19,20,28–32]. This reliance on tensile loading to failure is apparent in the literature regardless of the method employed to bring the constituent materials together. Additionally, tensile loading to failure tends to be employed indiscriminately with regard to the relative quality of the processed composite material, specifically in terms of reinforcement distribution, fiber volume content or void volume content. For example, tensile loading to failure is apparent in a variety of works where fiber volume fractions range from as low as 1 % up to 40 %, where

27

discrete bundles of the continuous reinforcement are readily distinguishable and void content by

volume is either only qualitatively expressed or disregarded entirely [16,19,20,31].

Despite the fact that tensile loading until failure may allow for the empirical

determination of the ultimate tensile strength for additively manufactured continuous fiber

reinforced thermoplastics, the ultimate tensile strength is a fiber dominated property that has

been shown to, in carbon fiber/ epoxy laminates, be only moderately affected by gross void

content [33]. Figure 15 exhibits experimental data from [33] in support of this statement. Note

that a similar independence, or weak dependence at best, is noted in the compressive load at

failure for carbon fiber/ epoxy laminates processed under the same conditions.
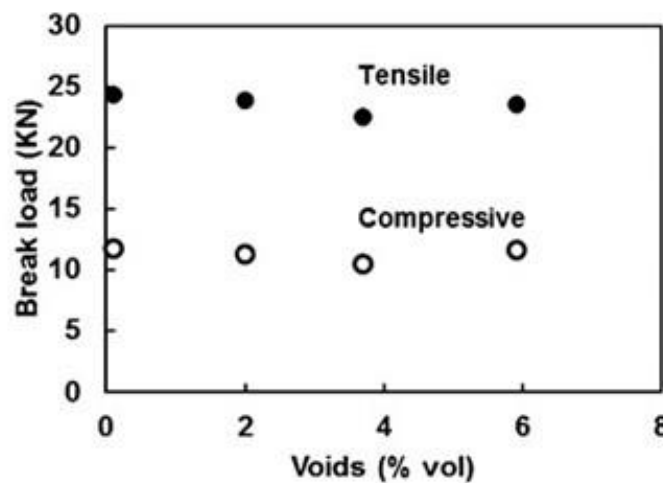
Figure 15: Tensile and compressive failure load as a function of gross void content for carbon
fiber/ epoxy laminates [33]

In addition to examining the dependence of tensile and compressive failure loads relative

to void content in carbon fiber/ epoxy laminates, [33] also examined the dependence of

interlaminar properties on gross void content. In contrast to the weak tensile and compressive

dependence on void content that was reported, a significant dependence of the composite

interlaminar properties on void content was observed [33]. Figure 16 shows the results of

interlaminar mechanical evaluation of carbon fiber/ epoxy laminates with varying void content,

in accordance with ASTM D2344 for Short-Beam Strength [7]. It should be noted that Figure 16 shows nearly a 25 % reduction in Short-Beam Strength with an approximate 6 % increase in void content.
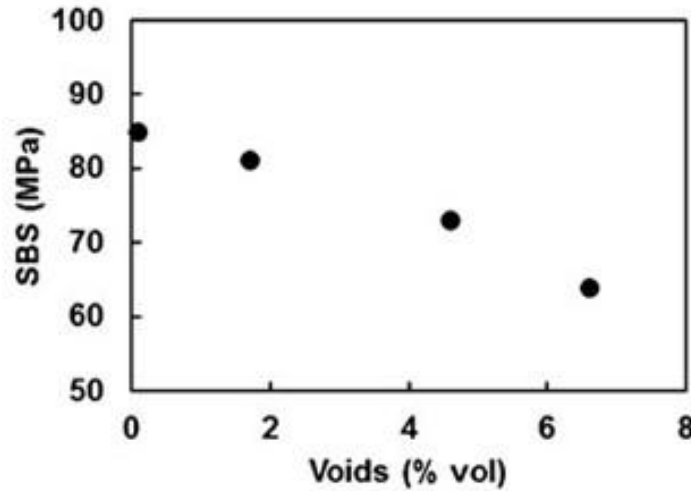
Figure 16: Short-Beam Strength (SBS) as a function of void content for carbon fiber/ epoxy laminates [33]

In consideration of the work reported in [33], it should be clear that tensile loading to failure is inadequate in terms of evaluating the quality of processed continuous fiber reinforced thermoplastics by additive manufacturing. This is stated specifically in reference to the limited sensitivity in tensile loading to failure to the aforementioned metrics of processed composite material quality, particularly reinforcement distribution and void content by volume. Other means of mechanical evaluation have been documented in the relevant literature, but to a lesser extent. Interlaminar mechanical evaluation, as well as flexural mechanical evaluation, have been employed in the literature; however, their use has been generally limited to the comparison of relative process parameter effects on the processed composite material and or comparison to neat polymer specimens [18,20,28–30,32]. In addition to interlaminar and flexural mechanical evaluation, specific works in the literature have employed other mechanical evaluation methods including Charpy impact, tensile and flexural fatigue to failure and quasi-static indentation

29

[29,30,32]. Again, it is emphasized that the primary use of these mechanical evaluation techniques has been exclusive of any quantitative commentary on either reinforcement distribution or void content, or more generally, manufacturing defects.

In contrast to the quasi-static mechanical testing that is common in the literature, with the exception of [30], the use of Dynamic Mechanical Analysis (DMA) has been employed in brief [19,20]. DMA can most readily be described as a thermomechanical analysis technique where a material specimen is cyclically loaded, in tension, compression, flexure, shear or torsion, while the specimen's viscoelastic response is tracked, often with regard to a temperature sweep or user defined temperature program. DMA is most useful in the analysis and evaluation of both neat polymers as well as polymer matrix composites as it is capable of providing both quantitative and qualitative information about the viscoelastic response of the material specimen, specifically with regard to the elastic response (storage modulus), viscous response (loss modulus) and loss tangent or damping factor (the ratio of the viscous and elastic responses, commonly tan δ). To serve as scope pertaining to the utility of DMA, DMA has successfully been employed as a method for investigating variations in the glass transition temperature of carbon fiber/ epoxy laminates with varying reinforcement angle and measurement criteria [34], studying the curing behavior of carbon fiber reinforced epoxies purposed for prepregging [35], and even as a method of evaluating fiber/ matrix interface effects on the measured glass transition temperature and damping factor of continuous fiber reinforced laminates as a function of varied fiber surface treatments [36].

Despite the clear utility of DMA as a thermomechanical evaluation tool for composite materials, it has primarily been utilized in the relevant literature for the purpose of quantifying the glass transition temperature of the additively manufactured continuous fiber reinforced

thermoplastics [19,20]. A notable exception in [20] should however be acknowledged. The

relevant investigation focused on assessing the effects of pre-process fiber surface modification,

specifically to facilitate the development of intimate fiber/ matrix contact and interface

generation, on the mechanical performance of additively manufactured continuous carbon fiber

reinforced polylactic acid (PLA) composites [20]. DMA scans were performed at 1 Hz using a

3-point bending fixture and a relevant temperature sweep on specimens with and without pre-

process fiber surface modification as well as on neat PLA specimens [20]. The effects of the

pre-process fiber surface modifications were reported in terms of specimen storage modulus, loss

tangent and glass transition temperature. It is most notable that the specimen group subjected to

pre-process fiber surface modification exhibited both the highest recorded storage modulus and

glass transition temperature, while also exhibiting the lowest recorded loss tangent [20]. Adding

to the impact of the pre-process fiber surface modifications was the reported storage modulus for

the additively manufactured composite specimens without fiber surface modification, exhibiting

a value well below that of the neat PLA specimen [20]. The relevant work attributed these

results to the enhanced interfacial bond, and subsequent load transfer, in the printed composites

utilizing the modified reinforcement, as well as the lack of interfacial bonding and the presence

of manufacturing defects, namely voids along the interface, in the untreated composite specimen

[20].

　　　Although DMA has only been minimally utilized as a quality evaluation tool with respect

to the additive manufacture of continuous fiber reinforced thermoplastics, the work in [20]

clearly illustrates that DMA is sensitive to process related quality variations in the sense of both

mechanical and thermal material performance. This attribute of DMA has been shown in other

arenas within the realm of continuous fiber reinforced polymer matrix composite processing, to

similar and differing extents. For the purpose of providing additional scope into the use of DMA in other arenas, it should be acknowledged that DMA has shown to be successful in tracking manufacturing defects, such as void content and fiber waviness, in carbon fiber/ epoxy laminates as demonstrated in [37] as well the effect of different reinforcement types and ply stacking sequences in [38]. Additionally, other work has shown that results from DMA, particularly with respect to the measured elastic response or storage modulus, can agree very well with more commonplace quasi-static mechanical evaluation methods [39]. In consideration of the proven utility of DMA as an evaluation tool for processed composite materials, as well as the clear gaps in the understanding of processed composite material quality with regard to additively manufactured continuous fiber reinforced thermoplastics, DMA seems to be a clear next step in the progression of quality evaluation of these materials as it relates manufacturing defects.

1.5 Experimental Motivation & Objectives

Current methods for preparing laminated continuous fiber reinforced composites, despite being well documented and reproducible, ultimately serve as limiting factors in the design and manufacturing of continuous fiber reinforced composite structures. Thermoplastic matrix materials offer a variety of processing benefits that ease certain limitations inherit to thermosetting matrix materials; however, processing of these materials tends to come at a significant cost in terms of the specific processing equipment required. Similarly, despite the clear benefits afforded by thermoplastic matrix materials, continuous fiber reinforced thermoplastics processed by conventional methods are still subject to the need for net-shape hard tooling, part size being limited by the size of processing equipment and an inability to include significant continuous reinforcement out of the laminate plane. The additive manufacture of continuous fiber reinforced thermoplastics exhibits the potential to relieve many of the

32

constraints placed upon the design and manufacturing of continuous fiber reinforced structures. As such, an in-depth understanding of additively manufactured continuous fiber reinforced thermoplastic matrix composite material quality and performance, as it relates to manufacturing defects, is requisite to furthering the generation of new knowledge and expanding upon the current state of the literature.

This work proposes a thermomechanical method of evaluating additively manufactured continuous fiber reinforced thermoplastic matrix composite material performance as it relates to the manufacturing defects that are notable in the literature and have yet to be substantively addressed. An additive manufacturing system was developed with the intent to process continuous fiber reinforced thermoplastic matrix composites by means of a continuous commingled precursor material. Processed CFRTP specimens were tailored to aid in developing an understanding of the effects of manufacturing defects, specifically included void content, on the quality of the processed composite material. To direct this effort, the scope of the investigation will be defined by the following hypothesis: *As compared to the relevant quasi-static methods, the use of Dynamic Mechanical Analysis will be more sensitive to the effects of manufacturing defects, specifically void content, on the thermal and mechanical quality of additively manufactured continuous fiber reinforced thermoplastics.*

To evaluate the proposed hypothesis, proof-of-concept studies were performed to verify the functionality of the additive manufacture system and approach. Subsequently, continuous fiber reinforced thermoplastic specimens with varying gross void content were additively manufactured and subjected to quality evaluation by means of Dynamic Mechanical Analysis methods. Gross void content for the relevant specimens is compared to the various outputs of the Dynamic Mechanical Analysis studies for the purpose of quantifying the impact of the

specific manufacturing defect mode on processed composite material quality. Further

comparisons of the relevant specimens are made using additional insights allowed by

metallographic techniques. Finally, the sensitivity of the proposed quality evaluation approach is

compared to the sensitivity of a common quasi-static test method.

2 Preliminary Studies – Hardware & Process Development

The following chapter presents early experimental efforts aimed at developing a working understanding of the hardware and processing parameters required for the additive manufacture of continuous fiber reinforced thermoplastics (CFRTP). Custom hardware was integrated with open-source firmware and software, from the Fused Deposition Modeling (FDM) arena, in order to effectively control process parameters and the requisite motion system for material payout. Quality evaluation of the processed continuous fiber reinforced thermoplastics is performed based on methods common to the literature. Results of the early experimental efforts are discussed, summarized and are presented as the groundwork for the major experimental effort, covered in the next chapter.

2.1 Experimentation with Processing of a Continuous Commingled Precursor

Preliminary experimentation with a fiber placement/ additive manufacturing (AM) system and a continuous commingled precursor material is outlined below. Content includes scope on the custom hardware required for experimentation, material specifics, path generation for the hardware, generation of process parameters, specimen preparation and test procedures. This is directly followed by results of the work, specifically in terms of visual evaluation, mechanical evaluation and metallographic evaluation. A short discussion is presented, followed by a summary of the preliminary experimental results.

2.1.1 Fiber Placement/ Additive Manufacturing System

The fiber placement/ AM processing system described in this work is a custom-designed, laboratory-scale platform based on architectures common to the FDM arena. The AM system utilizes stepper motor drives and associated control to facilitate the movement of two

independent 3-axis gantries which are capable of rapid travel and material payout throughout a three-dimensional build space. The geometry of the three-dimensional build space accessible by both gantries is defined by, in terms of X, Y and Z space, 762 mm x 381 mm x 152 mm (30" x 15" x 6"). Each gantry is configured to allow for the modular addition or subtraction of different material payout/ placement mechanisms, as end-effectors, with the current work utilizing one standard heated extrusion die (colloquially an FDM hot-end) for neat thermoplastic payout and a second modified FDM hot-end for payout of a continuous commingled E-Glass/ polypropylene (PP) precursor material. A custom brass nozzle was manufactured for the modified hot-end to facilitate adequate heat transfer and compaction application during placement of the continuous commingled precursor. The addition of an appropriately sized radius to the nozzle was performed to prevent reinforcement breakage upon exiting the nozzle, as well as to mitigate abrasion during processing. The two-gantry system is pictured on the left of Figure 17, while the modified FDM hot-end for the continuous commingled precursor placement is pictured on the right of Figure 17.
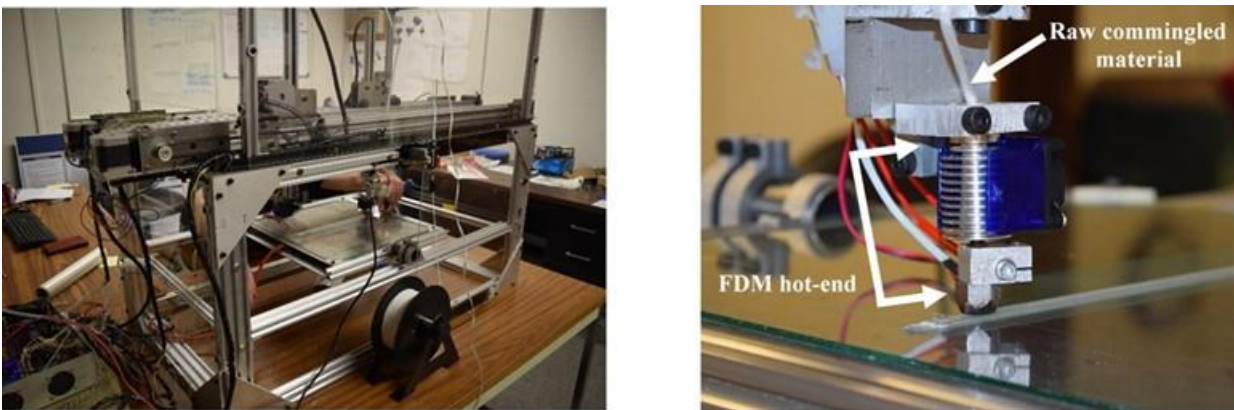
Figure 17: Two-gantry additive manufacturing system on left, modified FDM hot-end for placement of continuous commingled precursor on right

In the pictured state, the two-gantry additive manufacturing system utilizes 10 stepper motors to accomplish both dual-gantry movement and neat thermoplastic extrusion. Note that

neat thermoplastic extrusion is exclusive to the neat thermoplastic gantry. The stepper motors

are controlled using an Azteeg X3 Pro microcontroller, specifically chosen for its ability to

accommodate eight integrated stepper motor drivers, the most available at the time the system

was designed. To supplement the 3-axis capabilities of each gantry, additional degrees of

freedom are present within the machine, in terms of a manually orientable print substrate

(colloquially a print bed) as well as a manual wrist mounting platform for the modified hot-end

for continuous commingled precursor payout. These additional degrees of freedom allow for

material payout over conformable or angled surfaces, as well as placement of discrete out-of-

plane continuous fiber reinforcement. It should be noted that these additional degrees of

freedom are not relevant to the preliminary experimentation.

The print bed relevant to this work was designed in accordance with techniques common

to the FDM arena. To give the print bed shape and structure, two ~ 370 mm x 370 mm (14.5" x

14.5") aluminum plates are separated by steel hardware arranged corner-wise, in this case M5

bolts and nuts, to create a standoff distance of approximately 25 mm (1") between the plates.

The standoff is required to allow for accommodation of an adhesive-back silicon heating pad

affixed to the underside of the top aluminum plate, as well as to allow for leveling of the top

aluminum plate, by means of adjustment of the bolts, with respect to the hot-ends. The upper

aluminum plate is topped with an ~ 6 mm (0.25") thick glass plate to serve as an easily

replaceable, planar print substrate. Print bed temperature is controlled and regulated by means of

the silicon heating pad and a thermistor, common in FDM practices, which both interface

directly with the relevant FDM software. Another view of the machine, as well as the print bed

is shown in Figure 18.
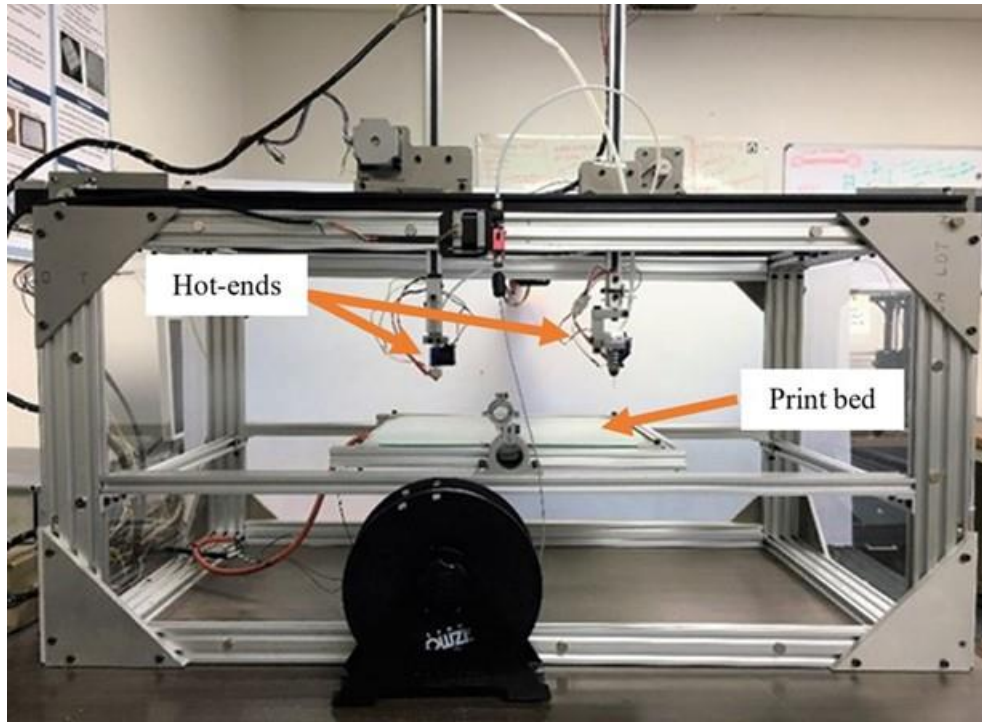
Figure 18: Additive manufacturing system with both hot-ends and print bed indicated

2.1.2 Materials

As mentioned in brief in the previous section, the material employed in this effort is a

continuous commingled precursor, supplied as a single roving wound around a bobbin. The

continuous commingled roving employed is composed, by weight, of 60 % E-Glass fiber and

40 % naturally colored, heat and UV stabilized polypropylene thermoplastic strands. Using

nominal densities, this translates to an approximate 35 % fiber volume fraction for the

commingled precursor. Typically, a single commingled roving is manufactured in such a way

that small agglomerates of fiber reinforcement are surrounded by larger diameter thermoplastic

strands, with this pattern repeating until the desired product tex (an expression of linear density,

grams per kilometer) is reached. An illustration of a representative cross-section of an un-

processed commingled roving is shown in Figure 19. In consideration of Figure 19, it should be

noted that the actual commingled roving does not exhibit a perfectly circular cross-section, but

rather that of a narrow quadrilateral. The cross-section of the un-processed commingled roving

is not critical to this work as during melt processing in the hot-end the commingled material re-

distributes itself to take the shape of the heated die.
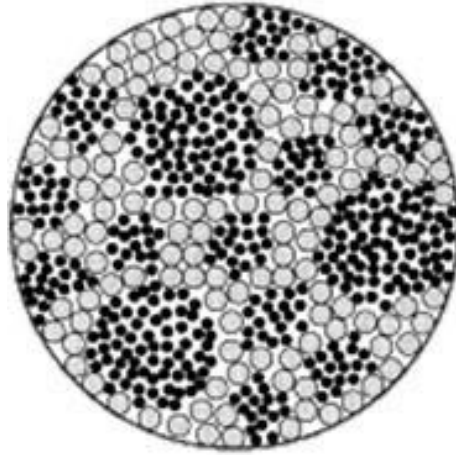
Figure 19: Representative cross-section of the commingled yarn [40]

A continuous commingled precursor was chosen for this work in consideration of both

material properties and ease of processability. First and foremost, continuous commingled

materials offer relatively high continuous fiber volume fractions in a readily melt processable

form, the latter being a demand of the FDM style processing approach. Additionally, continuous

commingled materials inherently bring both the thermoplastic matrix and continuous fiber

reinforcement into intimate contact in the raw material state, ultimately reducing the distance for

reinforcement wetting to a minimum while also preserving the handleability of a material

precursor in a textile form [24].

Additionally, it is noted that a polypropylene low-tack adhesive-back film was used as a

substrate for printing. The polypropylene film was placed directly onto the glass top of the print

bed to facilitate first layer adhesion of the E-Glass/ polypropylene composite material. The low-

tack adhesive back film, part number 7524T11, was purchased from McMaster Carr with a

specified nominal thickness of 0.002” (~ 0.05 mm) and was provided as a 12” tall roll.

2.1.3 Path Generation

Path generation by means of additive G-code was employed for both 3-axis gantries. Due to process discrepancies between typical thermoplastic payout in a standard FDM platform and placement of continuous commingled precursor materials, automated G-code generation by means of a standard FDM algorithm (colloquially a slicer) was not possible. Automated G-code generation by means of a slicer dictates discrete material placement in non-continuous paths by means of hot-end "travel moves" where the neat thermoplastic is retracted up into the nozzle and the hot-end is moved to a new location within the part geometry to continue the relevant build. Due to the lack of a cut and re-feed mechanism on the modified commingled hot-end, as well as the desire to maintain reinforcement continuity, all continuous fiber placement required G-code along a continuous, unbroken path. Additive G-code was written manually in a text editor in order to create various continuous fiber reinforced specimens for this preliminary work.

2.1.4 Process Parameters

Process parameters were determined based on prior experience with FDM with neat thermoplastics, in conjunction with qualitative analysis of early hardware testing with the commingled precursor. Typical print temperatures for polypropylene filament in an FDM environment (not a composite/ commingled system) fall within the range of 210 – 230 °C; however, during initial testing of the additive manufacturing system a process temperature of 270 °C was settled on as a baseline to take forward in experimentation. The baseline process temperature of 270 °C was chosen based on qualitative, visual evaluation of processed material consolidation (in terms of visible un-wetted glass fibers in the processed material) as well as the adhesion, or lack thereof, between adjacent layers of the commingled material.

Based on the qualitative information, specifically with regard to constituent consolidation and layer adhesion, that led to the development of the 270 °C baseline, process temperature was chosen as a reasonable parameter to vary in an experiment to quantitatively evaluate initial quality variation in printed composite samples from the commingled precursor. Three different temperatures, one of those being 270 °C, for processing the commingled material were used to prepare samples for Short-Beam Strength (SBS) testing. Short-Beam Strength testing was chosen in order to evaluate mechanical performance, specifically the composite interlaminar performance, in consideration of its sensitivity to manufacturing defects [21]. The lower bound for process temperature was determined from the earlier qualitative, visual evaluation which suggested that process temperatures below 250 °C resulted in subpar reinforcement wetting, analogous to processed material consolidation, with visible dry fiber in printed samples. The upper bound for process temperature, that being 290 °C, was dictated by the maximum processing temperature of the FDM hot-end in use, ~ 300 °C. In consideration of the lower and upper bounds on processing, the three temperatures used to prepare Short-Beam Strength samples were 250, 270 and 290 °C.

Other relevant process parameters include a print speed of 600 mm/ minute, a print speed commonly employed in the literature [18,28], a programmed layer height of 0.3 mm and a programmed layer width of 2 mm. Separately, in consideration of the polypropylene thermoplastic matrix, the print bed was heated to a temperature of 50 °C to mitigate warping of the placed layers of the commingled material. Warping of the placed composite material was encountered in early system testing with the print bed un-controlled, corresponding to a temperature somewhere between 20 – 25 °C. The observed warping was attributed to the interaction between the semi-crystalline microstructure of the polypropylene thermoplastic and

the uncontrolled temperature gradient between the relatively cold print bed and the relatively hot melt-processed commingled material. The chosen print bed temperature of 50 °C was determined to be an operational maximum due to the formation of bubbles between the print bed and the low-tack adhesive back polypropylene at temperatures of 50 °C or higher, likely due to the adhesive employed. Warping of the placed composite material was not entirely relieved with the print bed at 50 °C; however, it was mitigated to an acceptable level.

2.1.5 Specimen Preparation

Specimens for mechanical evaluation by means of Short-Beam Strength (SBS) were prepared using the aforementioned process parameters. A single unidirectional continuous fiber reinforced specimen, nominally 250 mm in length, was printed at each of the three specified process temperatures, those being 250, 270 and 290 °C. To ensure first layer adhesion, a strip of low-tack adhesive-back polypropylene film was applied to the glass print surface prior to print bed heating and sample printing. With the exception of the process temperature, all other process parameters were held constant for this effort. Print bed temperature was held at 50 °C, print speed used was 600 mm/ minute, programmed print layer height was 0.3 mm and programmed layer width was 2 mm. Due to the prototypical state of the additive manufacturing system, no cut and re-feed system for the continuous commingled material, or independent compaction device for consolidation was implemented.

In this work material compaction, or consolidation pressure, was applied in-situ during commingled material payout solely by means of displacement control of the modified FDM hot-end. With respect to this work, displacement control is defined as the practice of programming, via machine control code, a layer height in deficit of the thickness of a single layer of printed commingled material (printed with "no" consolidation pressure). Displacement control allows

for the application of consolidation pressure by means of the stiffness of the entire Z-axis of the relevant gantry, effectively using the machine as a pressure foot. The nominal thickness of the melt-processed commingled material without displacement control (i.e. the smallest amount of applicable consolidation pressure to ensure the printed material adhered to the print bed) was approximately 1.2 mm. The chosen layer height of 0.3 mm was the smallest programmable layer height achievable, and thus the greatest consolidation pressure achievable, due to Z-axis motor being over-torqued at programmed values in deficit of 0.3 mm. Layer width of 2 mm was chosen based on measurements taken from single layer samples of the commingled material processed with a programmed layer height of 0.3 mm.

All processed composite beams exhibit non-uniform fiber overlap as a result of the generated continuous fiber paths, where the manually written G-code specified extra deposition of the commingled material outside of the sample beam geometry to account for re-tacking of the commingled material. Re-tacking of the commingled material was required following requisite 180° turns in the control code at the length-wise beam extremities, limiting the presence of the non-uniform fiber overlap to the ends of sample beams. An example of a sample beam during printing can be seen in Figure 20. Note the fiber overlap at the 180° turns at the ends of the beam, as well as slight warping of the processed composite material. Warping of the printed composite beam is evident in Figure 20 and is distinguished by visible peel-up of the low-tack adhesive-back polypropylene film applied to the print surface.
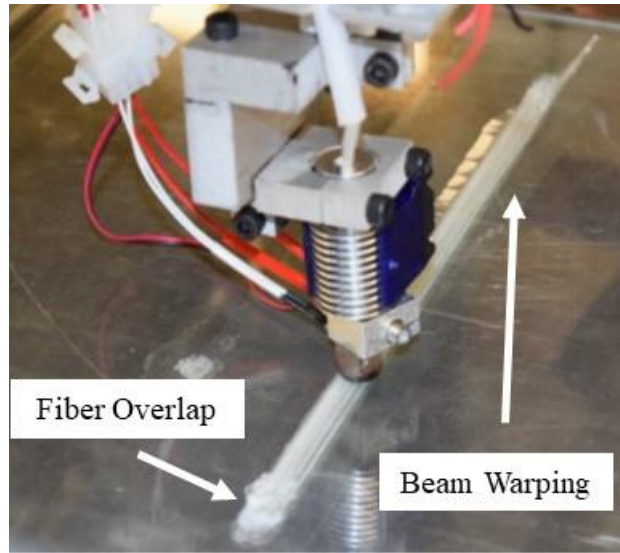
Figure 20: Continuous fiber reinforced polypropylene beam during printing

2.1.6 Test Procedures

Specimens for Short-Beam Strength evaluation were cut from the printed sample beams such that the continuous fiber reinforcement spanned the length of the specimen. The unidirectional glass fiber reinforced Short-Beam Strength samples were fabricated and tested in accordance with ASTM D2344 in order to investigate processed material quality variation with process temperature. Short-Beam Strength evaluation by means of ASTM D2344 is a common method to assess processed composite material quality as it relates to manufacturing defects, and has been shown to give reasonable information regarding both interlaminar properties and constituent material consolidation [21,41,42]. For flat specimens, as relevant to this work, the ASTM standard dictates the use of conventional loading pins, nominally 3.18 mm (0.125") in diameter, and loading nose, nominally 6.35 mm (0.25") in diameter. Short-Beam Strength specimen dimensions were nominally 18 mm long by 2.9 mm tall and 6.2 mm wide. The test span used for the determination of the Short-Beam Strength for the relevant specimens was 12 mm. The loading rate used was 0.05 inches per minute as specified by the relevant ASTM for the SAE machine employed (equivalent loading rate of 1 mm/ minute on a metric machine, note

44

this is not a direct conversion) [7]. Seven specimens from each print temperature group were evaluated.

2.1.7 Results

Specimens were produced by melt processing a continuous E-Glass/ polypropylene commingled roving using the purpose-built additive manufacturing system. As-printed sample beams were visually examined and then cut and sanded for geometric fidelity with respect to the ASTM standard for Short-Beam Strength. Post-processed Short-Beam Strength specimen were then tested in accordance with the relevant ASTM. Results from the Short-Beam Strength evaluation are supplemented with metallography of representative composite specimen cut from the as-printed sample beams.

2.1.8 Visual Evaluation

As-printed sample beams processed at temperatures of 250, 270 and 290 °C are shown in Figure 21. Samples exhibit an opaque nature due the "natural color" of the polypropylene strands in the continuous commingled roving. This opaque nature makes detailed visual analysis of specimen wetting characteristics difficult. Localized areas that are rich in neat thermoplastic can be seen at the edges of all three samples in Figure 21. These neat thermoplastic areas indicate, to some extent, that flow of the polypropylene matrix was achieved at all relevant process temperatures. Full melting, or viscous flow, of the polypropylene gives some qualitative indication that partial or full wet-out of the E-Glass reinforcement was achieved in all samples. Note the samples shown in Figure 21 are in the as-printed state, where the sample width was approximately 8 mm.
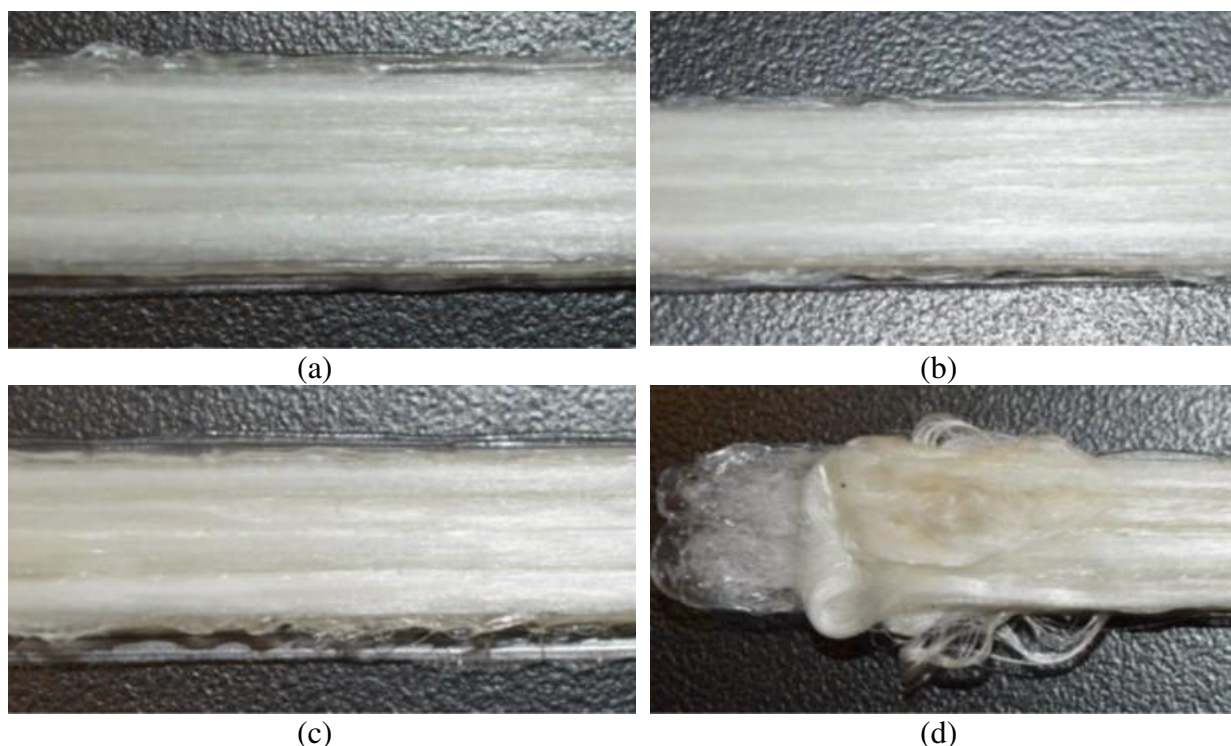
Figure 21: Visual comparison of as-printed sample beams (a) mid-span of 250 °C beam (b) mid-span of 270 °C beam (c) mid-span of 290 °C beam (d) fiber overlap at beam end

Figure 21 visually indicates that continuous glass fiber placement, with uniformity along the length of each as-printed beam, has been demonstrated. With the exception of the farthest ends of the sample beams, continuous fiber placement along the length of the specimen is consistent and repeatable. Figure 21 also indicates a lack of geometric fidelity in the processed sample beams. Areas of neat polypropylene at the lengthwise edges of each sample imply that some level of post processing is necessary to obtain as-printed samples of proper dimensions for mechanical testing. Additionally, as a result of the prototypical nature of the additive manufacturing system in its current state, the ends of the sample beams exhibit fiber overlap, or loss of alignment resulting from programmed 180° turns in the control code. Along the length of the beam, approaching the center of the specimen, fiber overlap is not present and proper layer adhesion with respect to the substrate and other printed layers of commingled material is achieved.

2.1.9 Mechanical Evaluation

Short-Beam Strength testing was used as a quantitative analysis tool to investigate composite quality variation with process condition. Short-Beam Strength testing, following ASTM D2344 [7], was chosen as the primary mechanical analysis tool for this work as it provides information related to both interlaminar properties and constituent material consolidation within a polymer matrix composite [21,41,42]. Interlaminar property investigation is useful to this work as it gives insight into the extent of the intimate contact generated between the constituent materials, in this case E-Glass and polypropylene, during melt processing in the hot-end, as well as the intimate contact generated between the printed layers of the relevant sample beams.

All Short-Beam Strength failures observed are classified as "inelastic", as depicted in the relevant ASTM [7] as well as Figure 22. Characteristics of this failure mode include, but are not limited to, significant deformation without fracture and no definitive or visible cracking or shear failure at the mid-plane of the test specimen. Tested specimens showed elastic behavior on the load/ displacement profile, followed by yielding (viscous flow), and either load plateauing or slight load increases over relatively long periods of time (30 seconds past yield or more). Peak load values (P_{max}) from the Short-Beam Strength tests were utilized to determine the mean Short-Beam Strength, Equation 2.1, for each of the three sample groups (A is cross-sectional area) as described in the ASTM standard for this form of failure. Results from the testing, in terms of the mean Short-Beam Strength and associated standard deviations, are shown in Table 1.

$$SBS = 0.75 \, (P_{max}/A) \tag{2.1}$$
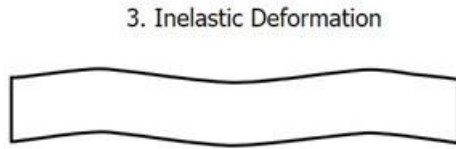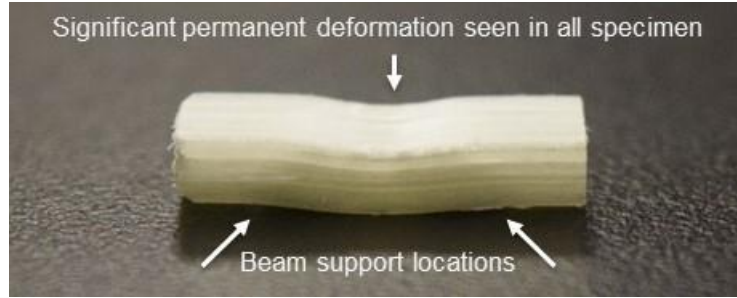
| (a) | (b) |

Figure 22: (a) Illustration of the inelastic failure mode [7] (b) SBS sample showing inelastic failure

Table 1: Properties comparison for printed SBS samples

Specimen	Short-Beam Strength (Mpa)
Commingled EG/PP – 250 °C	13.1 ± 1.15
Commingled EG/PP – 270 °C	14.1 ± 0.93
Commingled EG/PP – 290 °C	17.6 ± 1.00

The resulting Short-Beam Strength values show an increasing trend with increasing process temperature. Additionally, it should be noted that, although the magnitude of the standard deviation does not decrease with increasing process temperature, the percent standard deviation within each sample group decreases with increasing process temperature. Standard deviations relative to each sample group, expressed as a percentage of the mean, are approximately 8.8 %, 6.6 % and 5.7 %.

2.1.10 Metallographic Evaluation

Specimens were mounted and ground for microscopy. Representative micrographs of one specimen from each process temperature, 250, 270 and 290 °C are shown in Figure 23. Firstly, Figure 23 clearly depicts the polypropylene low-tack adhesive-back film applied to the build surface of the machine prior to printing, distinguished by the prominent white line running across the upper-most width of each cross-section. It should be noted that the relative thickness of the tape varies in the three cross-sections shown in Figure 23. This is due to the requisite post-processing, by means of sanding in this case, of the samples to the Short-Beam Strength

dimensions dictated by relevant ASTM standard. Figure 23 clearly shows the E-Glass reinforcement, the polypropylene matrix and areas where the constituent materials were not successfully consolidated and void content is prevalent. Figure 23 visually indicates that areas of poor wet-out, i.e. void content, decrease with increasing process temperature, most notably in comparison of (a) and (c). Additionally, Figure 23 visually indicates that reinforcement dispersion in the cross-section improves with increasing process temperature, again (a) to (c).

(a)

(b)

(c)
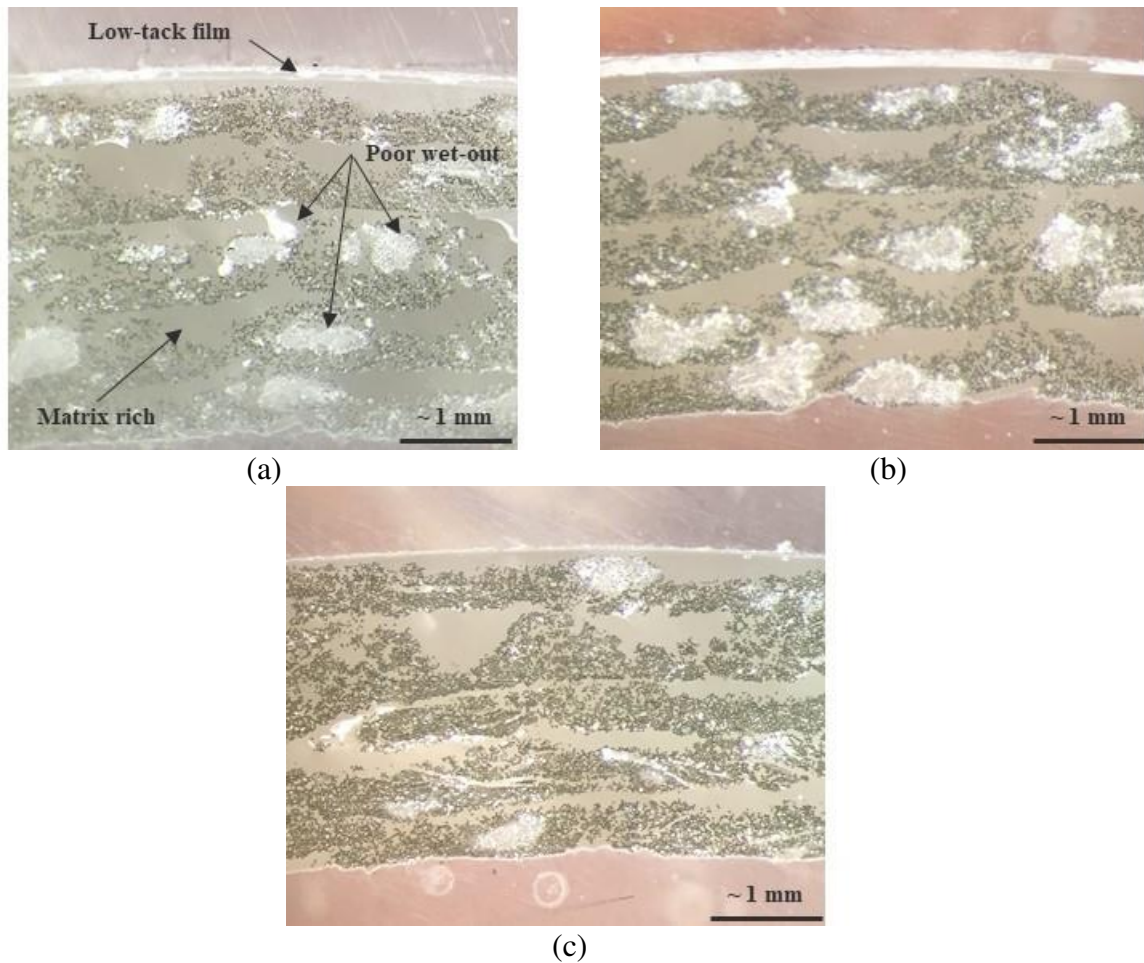
Figure 23: Metallographic comparison of representative beam cross-sections (a) 250 °C (b) 270 °C (c) 290 °C

In examining Figure 23, it should be noted that various matrix-rich regions exist in between the printed composite layers that make up all three of the representative specimens, (a) through (c). In addition to the matrix-rich regions, all cross-sections in Figure 23 exhibit varying

levels of reinforcement distribution across the width of the sample with some areas of reinforcement agglomeration, distinguishable by the wave-like shape of the layers of reinforcement through the sample thickness. Finally, although quantitative evaluation of fiber volume fraction was not performed, Figure 23 verifies a relatively high fiber volume fraction in all representative samples.

2.1.11 Discussion

The goal of this preliminary study was to demonstrate the capability of a continuous fiber reinforced composite processing system that combines aspects of automated fiber placement and Fused Deposition Modeling to realize the additive manufacture of high fiber volume fraction composites by means of a continuous commingled precursor material. The ability of this platform to serve as a process development system was evaluated in terms of qualitative information garnered through macroscopic visual analysis and metallographic techniques as well as quantitative information obtained through Short-Beam Strength testing. Data from the mechanical evaluation indicates both an increasing trend in Short-Beam Strength with increasing process temperature as well as a decrease in percent standard deviation with increasing process temperature. Both trends serve as an indication of improving interlaminar properties with increasing process temperature (i.e. reducing manufacturing defects), an intuitive conclusion in terms of improving constituent consolidation by means of lowering the thermoplastic viscosity in processing, as well as encouraging the autohesion process between the printed layers in the composite specimen.

In consideration of the trends noted in the Short-Beam Strength data, it should be acknowledged that, due to the inelastic failure mode observed, the reported values of Short-Beam Strength cannot be taken as physical representations of the interlaminar shear strength in

the printed composite samples. For reference, a comprehensive numerical analysis of the Short-Beam Strength method was conducted in [43] and offered as supplemental content to those making experimental measurements of the interlaminar shear strength of unidirectional continuous fiber reinforced composites by means of the Short-Beam Strength method. The work performed in [43] emphasizes the commonality of failure modes in short-beam bending that do not entail shear fracture or splitting at the sample mid-plane, and as such, recommends using short-beam bending only as a screening test for interlaminar shear strength. Additionally, [43] indicates that classical estimates of maximum shear stress by means of ASTM D2344 can underestimate the maximum shear stress experienced by the sample by as much as 100 percent. This underestimation is attributed, in part, to the complex stress state the sample experiences directly under the loading nose where fracture is intended to occur [43]. In agreement with [43], other works have utilized Short-Beam Strength experimentation in accordance with the relevant ASTM, specifically with regard to thermoplastic matrix composite materials, and have also noted similar inelastic failure modes [21,44,45]. Acknowledging the prevalence of the inelastic failure mode in the literature, as well as the numerical analysis of the Short-Beam Strength method in [43], it is clear that the Short-Beam Strength method can only function as a means to compare processed composite material quality relative to manufacturing parameters, and not as a means to generate material properties.

In order to complete a discussion of the inelastic failure modes observed in this work, a brief discussion of the glass transition temperature of polypropylene is relevant. Although the glass transition temperature for the polypropylene thermoplastic in the commingled precursor was not empirically determined by means of DSC or DMA, it is generally accepted that the glass transition temperature of polypropylene can be located near 0 °C [46]. A variety of works have

investigated the effect of temperature, specifically temperature below and above the glass transition temperature, on the mechanical performance of polypropylene and polypropylene matrix composite materials and found a strong dependence therein [46,47]. More specifically, the work reported in [47] found that the yield stress of pure polypropylene as well as a polypropylene blend, as determined by uniaxial compression measurements, decreases by a factor of 2 and 3, respectively, when temperature is increased from 110 K to 230 K. Further, the yield stress for pure polypropylene was found to drop well below 100 MPa at temperatures around 300 K [47], a temperature similar to the environmental temperature experienced by the samples during the Short-Beam Strength testing in the current work.

Some relevant results from the work in [47] are displayed in Figure 24. It is intuitive that the sharp drop in the measured yield stress of polypropylene, with temperature, can be attributed in part to the increased mobility of polymer chains in amorphous regions of the semi-crystalline material. Due to the fact that the Short-Beam Strength testing performed for this work was performed in excess of the accepted glass transition range of polypropylene, it is reasonable to assume viscous flow contributed to the observed inelastic failure modes, as well as the Short-Beam Strength values, reported herein.
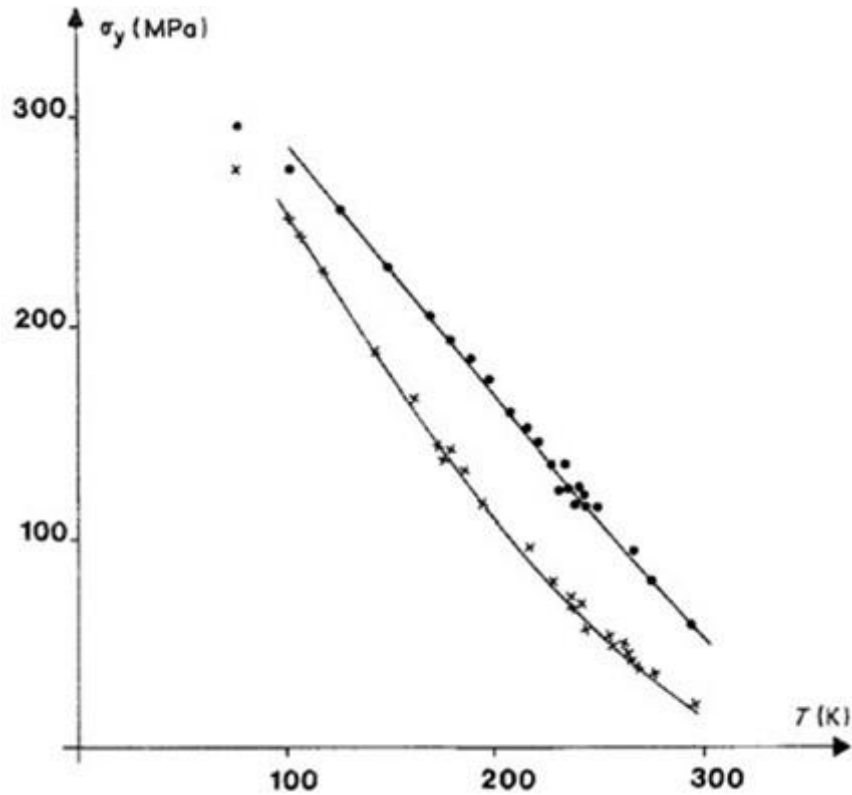
Figure 24: Yield stress versus temperature for pure polypropylene (.) and a polypropylene –
polyethylene blend (x) [47]

Moving forward, in terms of the metallographic results displayed earlier in Figure 23,

areas of poor wet-out are clearly visible in all three samples; however, areas of poor wet-out are

less prominent with increasing process temperature. Areas of poor wet-out (manufacturing

defects) are consistent with poor interlaminar properties, therefore the results presented suggest

that more optimal interlaminar properties can be realized through increasing processing

temperature, a means of increasing consolidation quality as well as subsequent composite

material quality. Similarly, matrix rich areas and localized reinforcement agglomerates are

apparent all representative samples, suggesting that the current method employed for applying

force to generate in-situ material compaction, or consolidation pressure, during processing is

inconsistent or inadequate. This inadequacy is addressed through hardware development in the

next section of this chapter.

2.1.12 Experiment Summary

The current effort successfully demonstrates a composite processing system capable of enabling a better understanding of the potential for innovative reinforcement placement, free of net-shape tooling, through the integration of common FDM hardware and the process of automated continuous fiber placement. Based on this preliminary study, investigating the processability of continuous commingled precursor material using the developed composite processing system, it is evident that interlaminar properties in the processed composites can be improved through increasing process temperature, ultimately a means of lowering the thermoplastic viscosity, improving reinforcement wetting, improving constituent consolidation and reducing manufacturing defects. Despite the increasing trend in measured Short-Beam Strength with increasing process temperature, the observed failure modes, in conjunction with the fact that the thermoplastic matrix was being loaded well above its glass transition temperature, indicate that the recorded Short-Beam Strength values cannot be portrayed as actual representations of the interlaminar shear strength of the processed composite, but rather qualitative evidence that consolidation in the composite material was marginally improved at higher process temperatures. While further processing details must be assessed, and in consideration of requisite hardware development moving forward, the results of this work demonstrate the potential for the realization of additively manufactured continuous fiber reinforced thermoplastic matrix composites with relatively high fiber volume fractions.

2.2 Development of a Consolidation Mechanism: Implementation & Experimentation

Additional purpose-built hardware was developed to modify the existing additive manufacturing system to allow for the application of controlled mechanical pressure during the processing of continuous fiber reinforced thermoplastic matrix composites from a continuous

commingled precursor. Experimental content includes information regarding the form and function of the new hardware, the materials in use, generation of process parameters, specimen preparation and test procedures. This is directly followed by results of the work. Results are reported in terms of a visual evaluation, mechanical evaluation and a metallographic evaluation.

2.2.1 Spring-Loaded End Effector

The purpose-built hardware relevant to this work is a spring-loaded end effector designed to integrate with the 3-axis (X, Y, Z) additive manufacturing system. The end effector utilizes a steel compression spring, of known stiffness (~ 7.5 N/ mm), to allow for the application of a known spring force at the point of material deposition during the printing process, seen in Figure 25 (a) and (b). Once relevant layer geometry (width and thickness) is developed empirically, in a method consistent with the earlier work, displacement control in the build direction (Z) allows for, in theory, the application of a near constant consolidation pressure during processing. Near constant consolidation pressure during processing is possible by means of programmed spring displacements that far exceed any small variations in the displacement of the spring as the print head moves across the sample. Using programmed spring displacements in the range of 1 – 2 mm, and assuming small variations in displacement of the spring during printing, in the range of 0.1 mm, total force variation is assumed to stay within the realm of ~ 1 N. In early proof-of-concept testing of the spring-loaded end effector, no spring movement during printing was visible by eye, therefore the assumption of only very small variations in displacement of the spring during printing is deemed tenable. This method is an improvement over the method used in the earlier work, where displacement control was used to apply consolidation pressure by means of a much stiffer spring and print bed combination, where similar variations in printing intuitively result in much larger variations in applied force and consolidation pressure.

Consistent consolidation pressure during a multilayer build is achieved through a net-zero change in spring travel each time a new layer is printed. Separately note that Figure 25 also shows two adjustable cooling ducts oriented at the tip of the nozzle. Cooling ducts were included in the design of the spring-loaded end effector as a means of quickly solidifying the commingled material after deposition on the print bed.

In addition to the spring-loaded end effector, the FDM style print bed used on the machine for past work was exchanged for a purpose-built, fully rigid substitute. Past work employed a glass plate mounted to a typical maker-style heated aluminum print bed. The print bed was affixed to another aluminum plate via a cornerwise, four point-of-contact system, utilizing M5 hardware to create a standoff between the print bed and the lower aluminum base plate. Due to the cornerwise, four point-of-contact mounting system, used for bed leveling purposes, the print bed was subject to significant and varying compliance across both the length and width of the printable area. As a result of this design, efforts at using the stiffness of the Z-axis of the machine, coupled with displacement control, for the purpose of applying in-situ consolidation pressure during processing were both unpredictable and uncontrollable. With the addition of a rigid print bed, affixed to the machine frame and vertically supported by the workbench the machine rests on, the overall compliance of the print bed was reduced to a point where it was deemed negligible. The rigid print bed, FDM style print bed and spring-loaded end effector are all pictured in Figure 26.
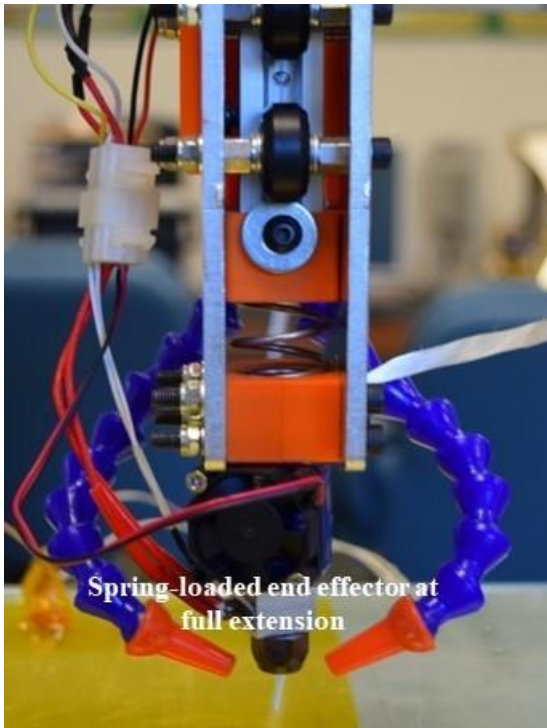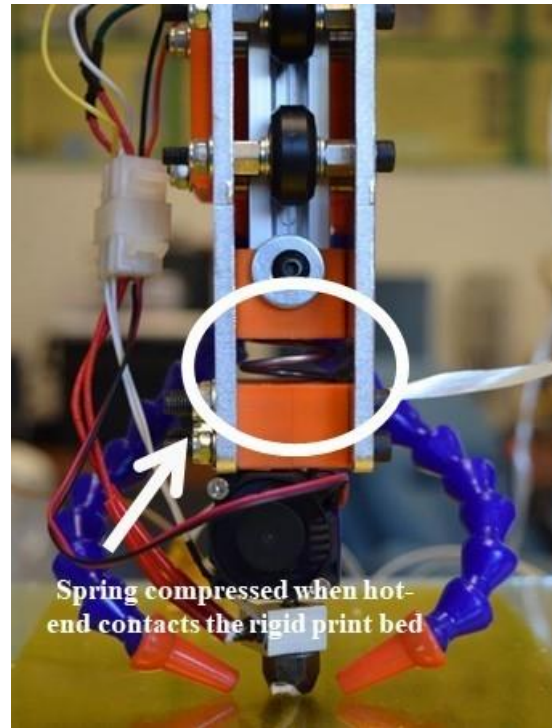
| (a) | (b) |

Figure 25: Spring-loaded end effector (a) at full extension or free hang (b) under compression, in contact with the rigid print bed
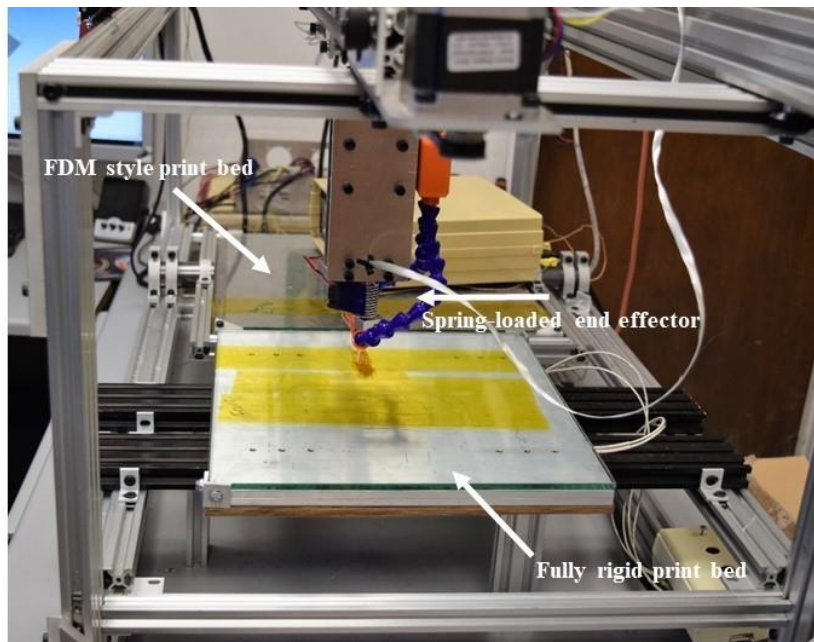
Figure 26: View of the FDM style print bed, the fully rigid print bed relevant to this work and the spring-loaded end effector

2.2.2 Materials

Consistent with earlier experimentation, the material employed in this work is a continuous commingled precursor, supplied as a single roving wound around a bobbin. In a departure from the earlier experimentation, a different commingled material combination was utilized, both to mitigate earlier issues with the printed commingled material warping on the print bed after deposition and to allow for mechanical evaluation of the composite material below the glass transition temperature of the included thermoplastic. The continuous commingled roving employed was composed, by weight, of 70 % E-Glass fiber and 30 % transparent PET thermoplastic strands, nominally equating to an unprocessed fiber volume fraction of 55 %.

Differential scanning calorimetry (DSC) was used to determine the glass transition region of the PET thermoplastic in the commingled product. Multiple temperature sweeps from 40 °C to 280 °C, using a heating rate of 10 °C per minute and a nitrogen purge gas, were conducted on what started as unprocessed commingled material. The range of mid glass transition temperatures, recorded from a total of 5 DSC sweeps, was identified as 70 – 72 °C, with a mean of 71.5 °C. From here forward, and unless specified otherwise, all references to the glass transition temperature of any relevant polymer will be specifically to the mid glass transition temperature. A representative DSC chart, cropped to show the glass transition region effectively, is displayed in Figure 27. For reference, it should be noted that no melt transformation was observed in the relevant temperature range observed in the DSC scans, implying the PET thermoplastic exhibits an amorphous microstructure. The range of the relevant temperature sweep was chosen such that any melt transformation would have been observed.
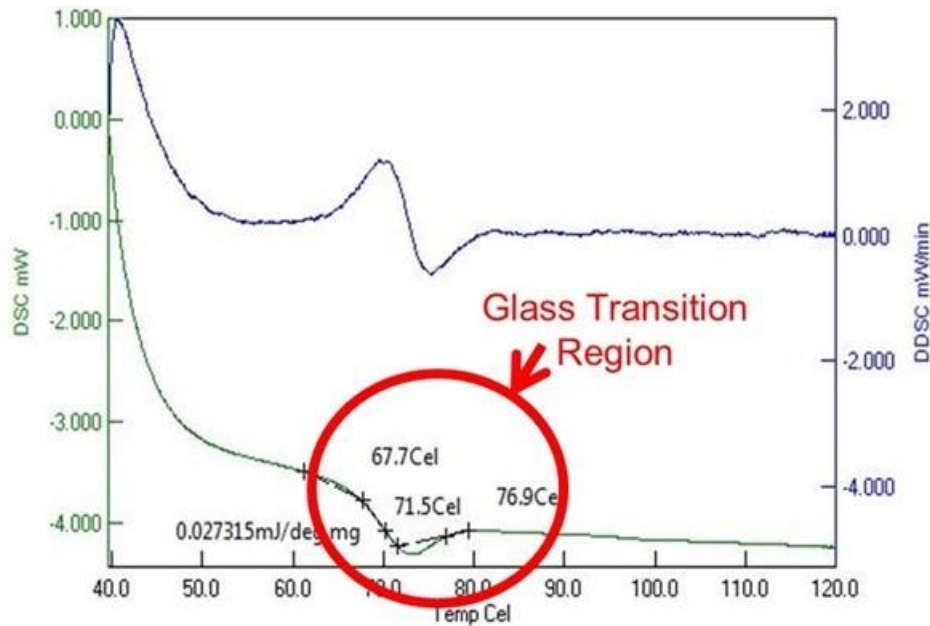
Figure 27: Representative DSC chart cropped to show the glass transition region for the E-Glass/ PET commingled material

Adhesive-back polyimide film, 0.002" thickness, is used as the deposition surface on the flat-plate substrate to facilitate enough tack to secure the deposited material, as well as ensure part removal, sans bonding to the substrate to avoid damaging the part. Polyimide film (amber in color) is visible on both the FDM and rigid print beds shown in Figure 26.

2.2.3 Process Parameters

Process parameters were determined based on a series of preliminary characterization experiments concerning the effects of variations of process/ print temperature, substrate temperature, print speed and applied spring force through displacement control on the consolidation quality of the printed commingled material. Consolidation was evaluated qualitatively from a visual standpoint, where "good" or "bad" consolidation was determined from the apparent transparency of single layer printed beam samples. Transparency was chosen as the metric for relative "goodness" based on the assumption that the coupling of a transparent polymer and transparent glass reinforcement could be combined into a relatively transparent

composite material, under the condition of no included void content. Therefore, the implication here is that any visual variation from transparency is correlated to void content.

For the purpose of investigating the effects of a controllable, applied spring force in the printing process, spring force was varied during sample preparation while all other process parameters were held constant. Print temperature, measured at the outlet of the nozzle with cooling enabled, remained constant at 220 °C. Substrate temperature was set at 72 °C, slightly above the glass transition temperature determined for the PET in the commingled precursor material. Print speed was set to 100 mm/ minute. It should be noted that a much slower print speed was chosen for this work, as compared to 600 mm/ minute, in an attempt to allow more time for the thermoplastic polymer to wet the glass reinforcement, and subsequently improve printed material consolidation (i.e. reduce void content).

Two different discrete spring forces were chosen to investigate the influence of controlled, constant applied force as a tune-able parameter in the printing process of continuous fiber reinforced thermoplastic matrix composite materials. A "low" magnitude applied force, 4.5 N, and a "high" magnitude applied force, 9 N, were implemented. A control sample was also printed using a rigid (i.e. rigid cylinder in place of the compression spring) end effector and the FDM style flat-plate substrate used in previous studies for the purpose of comparing the new method of displacement control to the methods employed in the first preliminary work. The rigid end effector is shown in Figure 28.
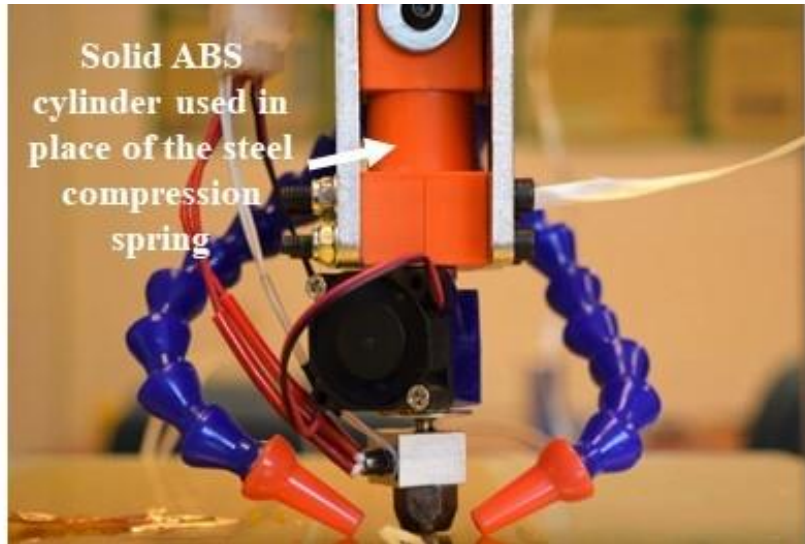
Figure 28: Image of the end effector using a rigid component in place of a compression sprint for printing of the control sample

Layer height for both applied force conditions was 0.4 mm; however, it should be acknowledged that the actual resulting layer heights determined for each spring force condition fell in the range of 0.40 – 0.45 mm, different by no more than five hundredths of a millimeter. This small discrepancy in layer height was not accounted for in the control code as it is beyond the resolution of the relevant 3-axis additive manufacturing system. Overall layer width for both cases was determined to be, nominally, 3.67 mm. Knowing the radius of the surface of the nozzle to be 5 mm, the cross-sectional area of the commingled material at the point of placement, and compaction or consolidation, is nominally 18.3 mm^2. Cross-sectional area of the commingled material at the point of placement is only relevant for determining the in-situ consolidation pressure, if and when desired.

2.2.4 Specimen Preparation

A series of specimens intended for mechanical and metallographic evaluation were prepared. Continuous fiber reinforced thermoplastic matrix beams, of rectangular cross-section, were processed from the supplied commingled feedstock under two distinct applied spring forces, as well as one control case using hardware and methods from the prior work. Print

61

temperature was held at 220 °C, substrate temperature was held at 72 °C, print speed was held at 100 mm/ minute and the applied force condition/ hardware was varied from 4.5 N, to 9 N to the control case. Without extensive experimentation, reaching beyond the scope of this work, the spring constant of the rigid end effector and 3-axis machine could not have been obtained, and is not considered. This hardware-centric value is assumed to change drastically across the length and width of the FDM style print bed used in the prior work. A composite beam during the printing process is shown in Figure 29.
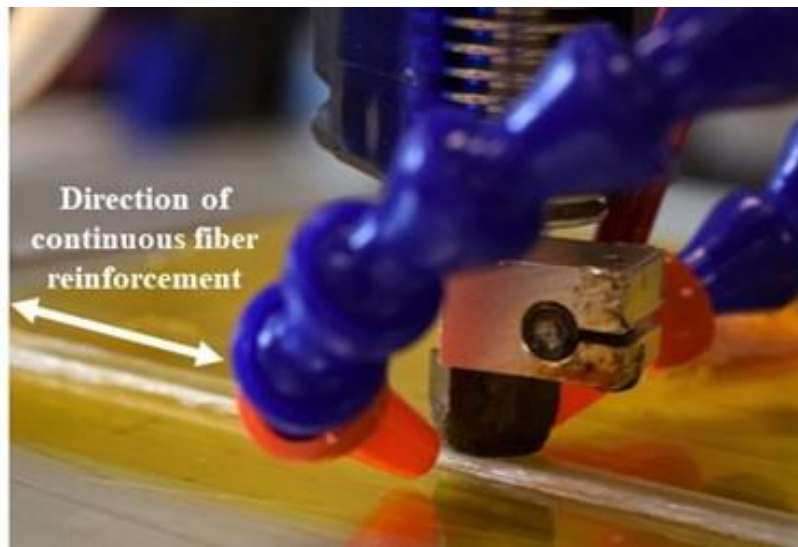
Figure 29: Continuous fiber reinforced thermoplastic beam during printing

2.2.5 Test Procedures

Short-Beam Strength (SBS) specimens were cut from the printed beams such that the continuous fiber reinforcement spanned the length of the specimen. The unidirectional glass fiber reinforced SBS samples were tested in accordance with ASTM D2344 in order to investigate quality variation with changing process condition of the 3D printed thermoplastic matrix composite specimen. Short-Beam Strength testing was chosen for this work, despite the nature of the results from the prior work, as a means to compare sample cross-sections, Short-Beam Strengths and failure modes in this study to those observed in the prior work.

Conventional loading pins, nominally 3.18 mm in diameter, and loading nose, nominally 6.35 mm in diameter, were employed using a loaded span of 12 mm. Sample dimensions were, nominally, 18 mm long by 3 mm tall by 6 mm wide. An illustration of a printed sample cross-section is shown schematically in Figure 30, clearly depicting the layer-wise build that makes up the sample. The loading rate used was 0.05 inches per minute as specified by the relevant ASTM [7]. Five specimens from each process condition were tested.

Quantitative volume fraction evaluation was performed using a procedure in accordance with ASTM D3171 [48]. A single representative E-Glass/ PET specimen from each of the three test groups was dried in a desiccator and weighed prior to determining the composite density via the Archimedes method. Each sample was then dried in a convection oven at 50 °C for four hours to remove gross amounts of moisture resulting from composite density determination. The PET matrix from each sample was then burned off in a muffle furnace at high temperature in air (5 hours at 550 °C), leaving the continuous glass reinforcement, which was then weighed. Known constituent densities were used to determine the fiber volume fraction and void volume fraction.
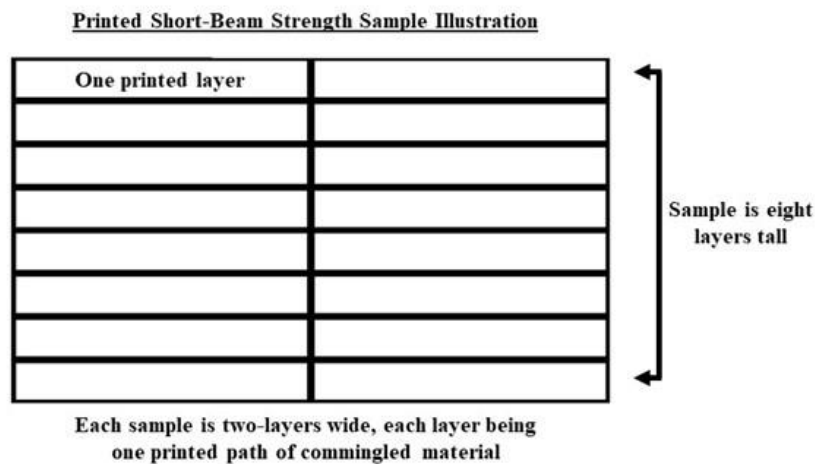
Figure 30: Illustration of a printed Short-Beam Strength sample cross-section processed using the current hardware (not to scale)

2.2.6 Results

Specimens were produced by melt processing a commingled continuous E-Glass/ PET

precursor using the 3-axis additive manufacturing system. Printed beams were visually

examined after being cut and sanded for geometric fidelity with respect to the ASTM standard

for Short-Beam Strength determination [7]. Metallographic evaluation was performed in order

to supplement the information acquired via Short-Beam Strength testing. Quantitative volume

fraction evaluation was performed on remaining samples to provide both a representative fiber

volume fraction and void volume fraction for the additively manufactured composites.

2.2.7 Visual Evaluation

Representative Short-Beam Strength specimen from each of the three cases, control,

4.5 N and 9 N are shown, left to right, in Figure 31 (a) for visual comparison of the beam

surfaces as well as the length-wise edges. It is noted that the surface of each sample is

comparable, showing little to no signs of any dry, and or, broken reinforcement. In contrast, the

length-wise edges of each sample all exhibit a nearly opaque appearance, with the opaque region

seeming to become more prominent in the control and 4.5 N cases. This opacity is considered to

be analogous to poor constituent consolidation and included void content.

The same opaque edge region is apparent, to a lesser degree, on single layers of the

processed commingled material as well, shown in Figure 31 (b). Figure 31 (b) serves as a visual

comparison of the transparency of the 9 N sample next to a comparable commercial continuous

glass reinforced PET prepreg. Transparency can be qualitatively compared via the black line,

black permanent marker on an aluminum caul plate, which runs normal to the two continuous

fiber reinforced thermoplastics. The two material samples show comparable transparency across

their widths.

It is noted that the transparency demonstrated by the single layer of commingled material in Figure 31 (b) is not directly transferred into the multi-layer 9 N Short-Beam Strength specimen at the far left of Figure 31 (a), despite being processed under the same process conditions. This can be attributed to a higher probability of included voids and matrix rich regions in between printed layers in the multi-layer beam.

| (a) | (b) |
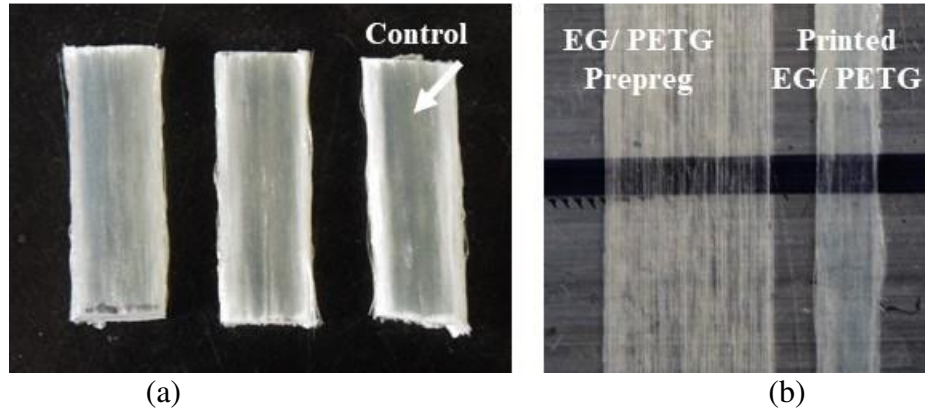
Figure 31: Visual evaluation (a) comparisons of un-tested SBS specimens; 9 N, 4.5 N and Control from left to right (b) comparison of one layer of printed commingled material at 9 N next to a comparable commercial EG/ PET prepreg

2.2.8 Mechanical Evaluation

Short-Beam Strength (SBS) testing was used as a quantitative analysis tool to investigate composite quality variation with changing process condition. SBS testing, following the relevant ASTM, was chosen as the sole mechanical analysis tool for this study as it provides insight into the interlaminar performance of a continuous fiber reinforced unidirectional composite as it relates to manufacturing defects [21]. Interlaminar performance investigation is useful to this study as it provides insight into the extent of the intimate contact, generated during processing, between the continuous reinforcing phase and the thermoplastic matrix phase. Information regarding interlaminar performance can also be correlated to any information obtained regarding the volume percentage, and location, of any included voids.

All SBS failures observed are classified as "inelastic", as depicted in the relevant ASTM document. Characteristics of this failure mode include, but are not limited to, significant permanent deformation without fracture and no definitive or visible cracking or shear failure at the mid-plane of the test specimen [7]. Tested specimens showed elastic behavior during loading up to a peak value, upon which the load plateaued and then decreased steadily at a pseudo-constant rate. Peak load values from the SBS tests were utilized to determine the nominal Short-Beam Strength (Equation 2.1) for each of the three sample groups as described in the ASTM standard for this form of failure. Table 2 compares the nominal Short-Beam Strength for each sample group with an associated sample standard deviation. Relevant representative fiber volume fraction and void volume fraction are compared as well.

Table 2: Properties comparison for commingled test samples

Specimen	Void Volume (%)	Fiber Volume (%)	SBS (Mpa)
Commingled EG/PETG – Control	5.7	50.3	25.6 ± 1.3
Commingled EG/ PETG – 4.5 N	2.4	52.5	26.2 ± 2.2
Commingled EG/ PETG – 9 N	5.6	49.8	27.6 ± 1.7

The resulting Short-Beam Strengths show an increasing trend, from a minimum for the control sample, to a maximum at the highest applied spring force, with the smaller applied spring force value falling in between the maximum and minimum. It should be noted that the magnitude of the standard deviation within the sample groups does not follow the same trend. Standard deviation within the sample groups, expressed as a percentage of the mean, are 5.0 %, 8.4 % and 6.1 % respectively.

Counterintuitively, there is not an immediate correlation between the representative void volume fractions and the mean Short-Beam Strengths. This trend follows for the representative fiber volume fractions as well. Separately, it is noted that the sum of the magnitudes of the void volume fractions and fiber volume fractions, for each representative sample, are nearly identical

to the specified 55 % fiber volume fraction of the dry, unprocessed commingled feedstock, with any discrepancies obviously attributed to changes in the volume fraction of thermoplastic matrix (not presented).

2.2.9 Metallographic Evaluation

Specimens were mounted and ground for the purpose of metallography. Representative micrographs of each process specific specimen are shown in Figure 32. Figure 32 is used as a qualitative tool to quickly verify representative fiber volume fractions determined through the relevant ASTM for polymer burn-off. In all samples, fiber distribution is reasonably consistent and a visual matrix-rich boundary exists at all points where one printed layer comes in contact with a new or adjacent layer. Figure 32 (c) shows that, for the 9 N sample case, matrix-rich seams between placed layers are reduced in terms of the apparent thickness. The placed layers are relatively consistent from sample to sample, indicating that the developed compaction hardware is performing as intended. The presence of included voids, indicated with white perimeters in Figure 32, is generally limited to the periphery of the beam cross sections, in predominately intralaminar (i.e. within layers of reinforcement) regions. Figure 32 (d) shows the 9 N sample at higher magnification for the purpose of verifying the apparent composite quality in terms of reinforcement wetting and fiber volume fraction. Black spots present at the edges of the reinforcement are artifacts, assumed to be fiber chipping, associated with the inherent difficulty of grinding continuous fiber reinforced thermoplastics for microscopy. Note that the grinding artifacts are distinguished from voids in Figure 32 (d).

(a)

(b)

68
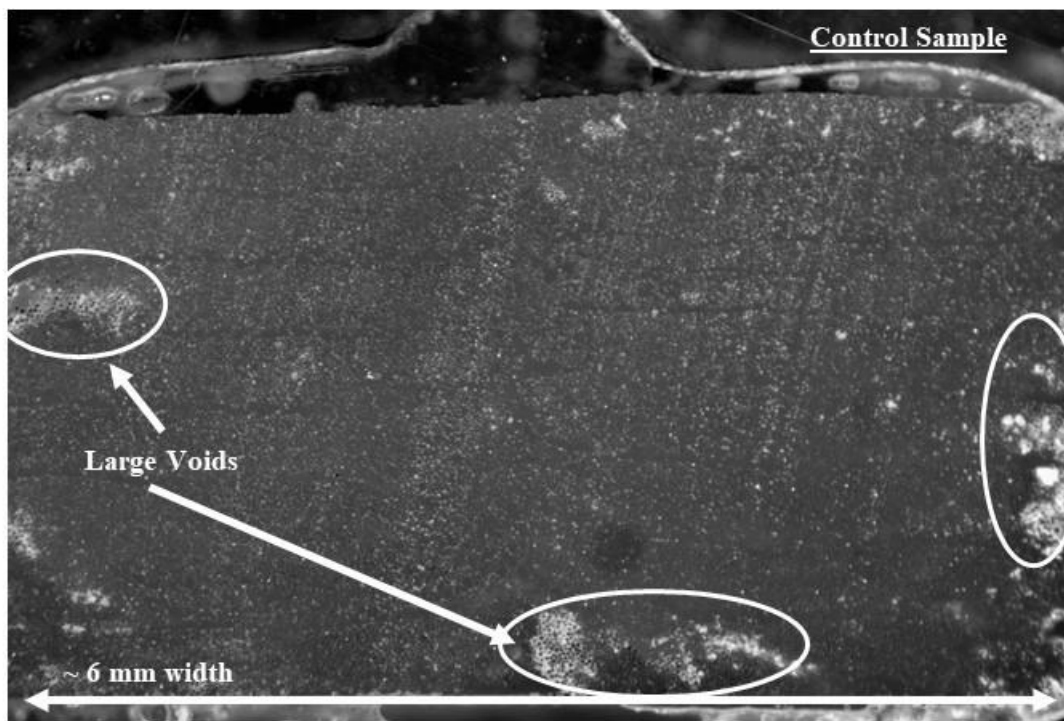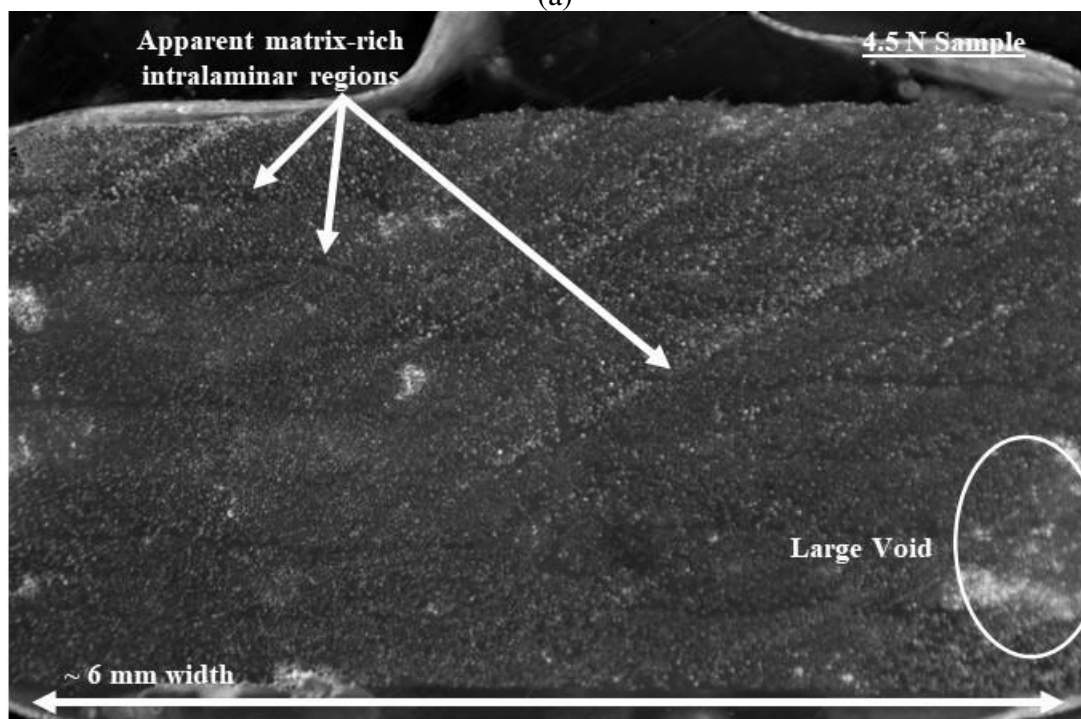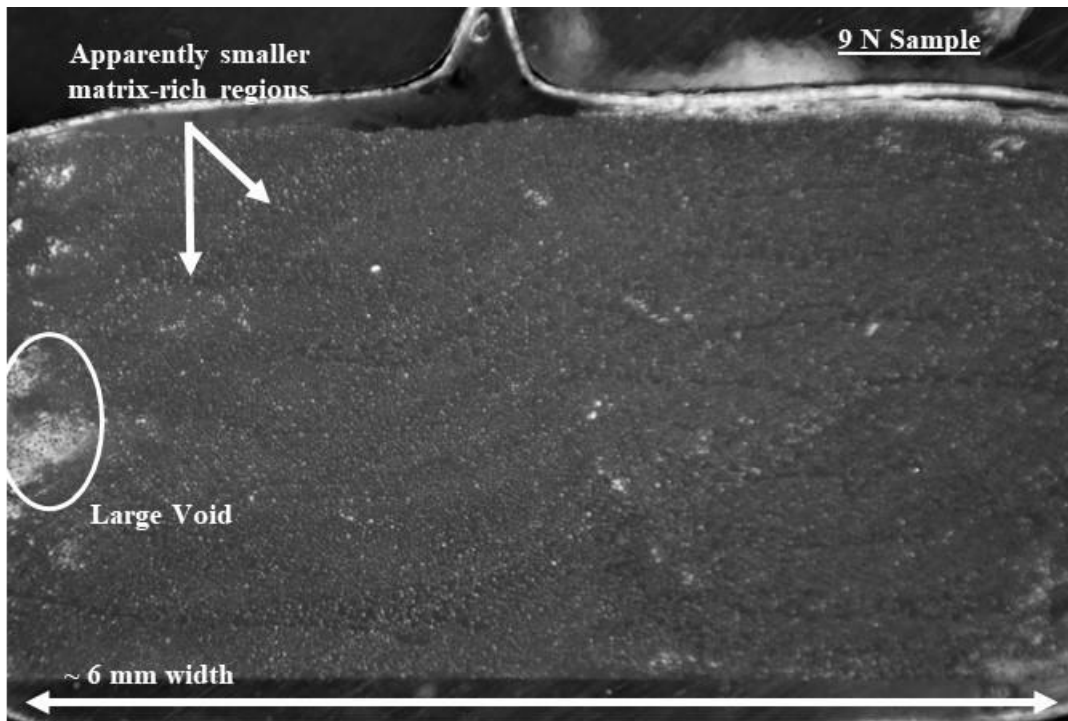
(c)
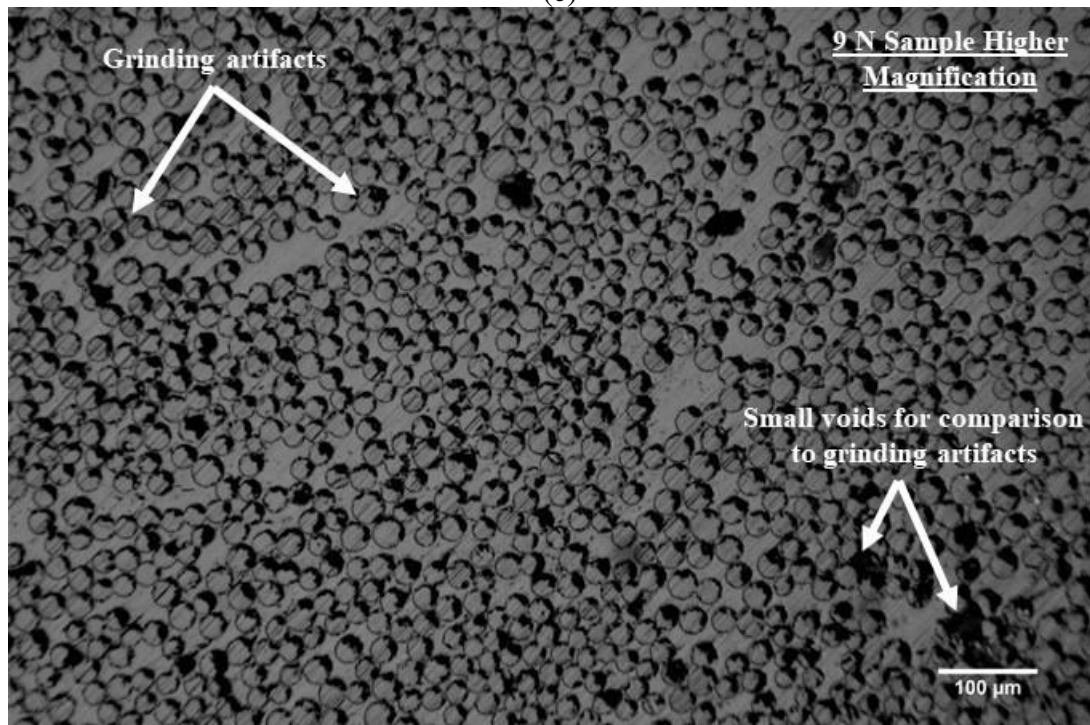
(d)

Figure 32: Metallographic evaluation (a) control sample (b) 4.5 N sample (c) 9 N sample (d) 9 N sample at higher magnification

2.2.10 Discussion

The goal of this preliminary study was to assess the effects of adding controllable applied pressure as a tune-able parameter in the additive manufacture of continuous fiber reinforced thermoplastic matrix composite materials. The effects of adding controllable applied pressure as a tune-able parameter were evaluated in terms of data obtained through Short-Beam Strength analysis as well as metallographic analysis. Data from the Short-Beam Strength analysis indicates an increasing trend in Short-Beam Strength with increasing applied consolidation pressure, with the worst performing sample being the control, made without the use of controlled, tune-able consolidation pressure. Images obtained for metallographic analysis of the processed samples supplement and expand upon the information obtained from mechanical testing. Included voids are clearly visible in all samples, with void content primarily confined to intralaminar areas at the periphery of the representative samples. Matrix-rich areas, specifically interlaminar areas between the printed layers, are also visible in all samples; however, they are less apparent in the 9 N sample. Consistently high fiber volume fractions are visually demonstrated in all processed samples.

As was the case in the first preliminary experiment, all observed Short-Beam Strength failures were classified as inelastic in accordance with the relevant ASTM. In contrast to the previous work, the thermoplastic matrix implemented in this work was tested at temperatures (20 – 25 °C) well below its empirically determined glass transition range, eliminating that factor from the discussion of the failure mode. For reference, other works relevant to both preliminary experiments performed for this work have recorded inelastic failures in Short-Beam Strength testing of thermoplastic matrix composites where testing was conducted well below the glass transition range of the relevant polymer [21,44,45]. With regard to the magnitude of the

recorded Short-Beam Strengths in this work, other works have reported Short-Beam Strengths for glass fiber reinforced PET/ PETG in the range of 20-35 MPa; however, without regard to fiber volume fraction or failure mode [49,50].

The increasing trend that is apparent in the Short-Beam Strengths in this work does not correlate well with the recorded representative void volume and fiber volume percentages. This is attributed to the fact that only a single representative sample for each sample group was subject to composite density measurement and polymer burnout. Short-Beam Strength samples for this work were cut from printed beams much longer than the requisite length for the Short-Beam Strength sample. As such, left-over sections from the as-printed sample beams were used for the void volume/ fiber volume measurements. In reference to the first preliminary experiment where the as-printed beam ends are pictured in the visual evaluation, see Figure 21, the as-printed beam ends in this work were also subject to varied consolidation quality as a result of the pick-up and put-down of the spring-loaded end effector, as compared to the fiber overlap seen in Figure 21. Note that the 180-degree turns were replaced by a pick-up and put-down protocol, with a requisite pause after end effector pick-up, to allow for manual cutting of the line of commingled material bridging from the print bed to the end effector. It is assumed that the sample used for determination of constituent content for the 9 N sample group in this experiment was likely taken from the end of an as-printed sample beam, and as such, was likely inclusive of more void content by volume than the samples taken from the middle of the as-printed beam that were used for Short-Beam Strength determination. This assumption is supported by the metallographic analysis as well, Figure 32, where from a visual standpoint, void content in the representative 9 N sample (taken from the middle of the as-printed beam) is less pronounced than the void content in both the control sample and the 4.5 N sample, albeit not significantly.

Further, with regard to the magnitude of the recorded Short-Beam Strengths relative to the recorded void content for each sample group, it is important to acknowledge the apparent lack of sensitivity in Short-Beam Strength to void content. From the control sample to the 4.5 N sample, a near 50 % decrease in included void content results in, approximately, a 2 % increase in Short-Beam Strength. This observed trend is consistent in direction, but not in magnitude, to other works which show more substantial, positive trends in Short-Beam Strength with decreasing void content, albeit in carbon/ epoxy laminates [33,51]. For reference, a 25 % decrease in SBS was recorded as a function of an approximate 6 % increase in void content (~ 4.2 % decrease in SBS per 1 % increase in void content by volume) [33]. In consideration of the SBS results from [33], coupled with the inelastic failure modes seen in both preliminary experiments, it is apparent that a more sensitive performance evaluation technique is necessary to assess the relative quality of the processed thermoplastic matrix composite materials in a meaningful way.

In closing, as was previously mentioned, it should be acknowledged that large visual discrepancies in terms of included void content are not apparent between the three sample groups. This serves as an indication that the force used for application of in-situ consolidation pressure was relatively similar, in effect, in the control, 4.5 N and 9 N sample groups. Despite this apparent similarity, minor visual and mechanical performance improvement across the range of samples serves as an indication that the spring-loaded end effector is functioning as intended, and has significantly improved upon the consistency of the printed continuous fiber reinforced thermoplastics as compared to the first preliminary experiment. Cross-sections from printed beams from both works, albeit shown with different magnification and color scheme, are shown in Figure 33 in defense of this claim. Notable differences between the two cross-sections in

Figure 33 include an obvious reduction in included void content in the current work compared to the previous work, a notable absence of large matrix-rich regions in the current work and more readily distinguishable layers with apparently consistent layer thicknesses in the current work.
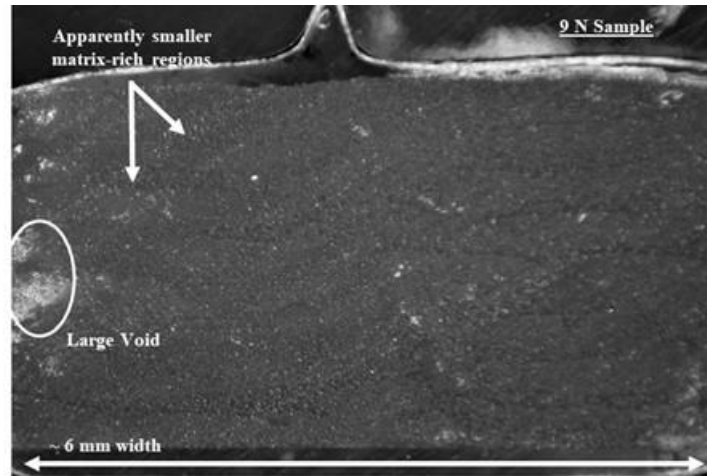
(a)
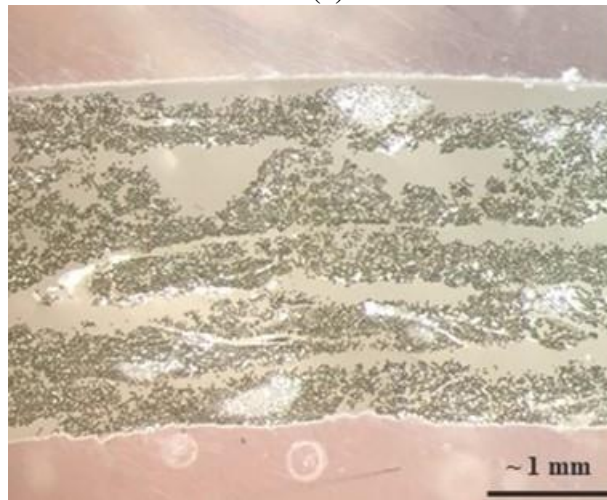
(b)

Figure 33: Comparison of cross-sections (a) the current preliminary experiment (b) the first preliminary experiment, note the reduced void content and matrix-rich regions in (a)

2.2.11 Experiment Summary

The current effort successfully demonstrates the addition of controllable, applied consolidation pressure as a tune-able parameter in the additive manufacturing of continuous fiber reinforced thermoplastic matrix composites from a commingled precursor. Based on this preliminary study, investigating the effect of applied consolidation pressure as a tune-able

parameter, it has been shown that interlaminar properties of the processed composites can be improved through increasing the applied consolidation pressure, a means of bettering constituent material consolidation and reducing manufacturing defects. Processed samples exposed to tune-able, controlled consolidation pressure during additive manufacture exhibited Short-Beam Strength values in excess of 27 MPa; however, processed samples exposed to uncontrolled consolidation pressure during additive manufacture exhibited Short-Beam Strength values in the range of 25 MPa. Similarly, although data regarding included void content was ultimately inconclusive, it is notable that a near 50 % decrease in included void content was associated with an approximate 2 % increase in Short-Beam Strength in the printed thermoplastic matrix composites. Ultimately, this serves as an indication that performance evaluation techniques that are more sensitive (in terms of property change per void content) to the presence of manufacturing defects are required to evaluate the quality of these additively manufactured thermoplastic matrix composite materials. While future work will address more sensitive approaches to evaluating processed additively manufactured continuous fiber reinforced thermoplastics, the results of this work demonstrate the capability of the current additive manufacturing system to process continuous fiber reinforced thermoplastics with consistently high fiber volume fractions and relatively controllable consolidation as compared to the first preliminary work.

3 Major Experimental Effort

The following chapter presents experimental efforts directed at evaluating processed composite material quality, as a function of included void content, by means of Dynamic Mechanical Analysis. The relevant additive manufacturing hardware, coupled with the continuous commingled feedstock, remain unchanged from the latter preliminary experiment regarding the spring-loaded consolidation mechanism coupled with the continuous commingled E-Glass and PET thermoplastic (EG/ PET). Motivation for this work is presented in terms of DMA-relevant examples from the additive manufacture of CFRTP composites literature as well as other notable uses of DMA for quality evaluation and manufacturing defect characterization within the continuous fiber reinforced polymer matrix composite arena. Following a statement of the motivation for this work, an overview of the working principles of DMA is presented such that it precedes sub-sections concerned with the relevant hardware, feedstock material, process parameters, specimen preparation and test procedures. Results of the work will succeed the experimental overview, which will be presented specifically in terms of DMA measurements and metallography. Results of the work are supplemented by brief discussion, preceding an expanded discussion that is presented in Chapter 4.

3.1 Motivation

In consideration of the results of the preliminary experimentation, more specifically the latter preliminary experiment, it was concluded that conventional means of correlating processed composite material quality with manufacturing parameters by means of Short-Beam Strength were not ideal for the material system relevant to this work. The preliminary experimentation demonstrated that the fiber placement/ additive manufacturing system, coupled with the use of a

continuous commingled precursor, was sufficiently capable of processing continuous fiber reinforced thermoplastic matrix composites with fiber volume fractions in the structurally-relevant range of 50 %, but not without included void content. Printed samples with representative void content in the range of ~ 6 % exhibited a 2 % decrease in Short-Beam Strength as compared to printed samples with representative void content in the range of ~ 2.5 %. This trend, although intuitive in terms of direction, is not consistent in magnitude with other works that have explored the relationship between interlaminar properties and included void content [33,51]. In coupling of the observed lack of sensitivity in measured Short-Beam Strength to void content in the printed CFRTP with the observed inelastic failure modes in Short-Beam Strength testing, it is clear that a more sensitive approach to processed composite material quality evaluation is requisite to adequately characterize the effects of manufacturing defects in the relevant material system.

As mentioned in Chapter 1, the use of Dynamic Mechanical Analysis (DMA) has been employed sparingly in the relevant literature regarding the additive manufacture of continuous fiber reinforced thermoplastics [19,20]. To reiterate the brief description of Dynamic Mechanical Analysis provided in Chapter 1, DMA can be most readily described as a thermomechanical analysis technique, most common to polymers and polymer matrix composites, where a material specimen is cyclically loaded while the viscoelastic deformation response of the specimen is tracked with regard to time, temperature or some combination of both. The viscoelastic deformation response is commonly separated into three components or properties, the storage modulus, loss modulus and the loss tangent or damping factor. The storage modulus represents a viscoelastic material's ability to elastically store energy, the loss modulus represents a viscoelastic material's ability to dissipate energy through viscous internal

motions, and the loss tangent or damping factor is mathematically equal to the ratio of the loss modulus to the storage modulus and qualitatively represents a material's ability to damp or dissipate energy.

As a result of the thermomechanical utility provided by the use of DMA, thermal transitions in a viscoelastic polymer/ polymer matrix composite are readily observed as a function of notable changes in one or more of the three viscoelastic properties described above. As such, the use of DMA in the literature regarding additive manufacture of continuous fiber reinforced thermoplastics has been primarily focused on quantifying the glass transition temperature, a readily observed thermal transition, of processed composite material systems [19,20]. In this context, DMA is ideal for identifying/ quantifying the glass transition temperature due to the sample size constraints imposed by other thermal analysis methods, such as DSC. A notable, and relevant, exception in [20] should however be acknowledged. The investigation in [20] was purposed with assessing the effects of pre-process fiber surface modification, specifically to facilitate the development of intimate fiber/ matrix contact and interface generation, on the tensile, flexural, thermal and fracture morphology of additively manufactured continuous carbon fiber reinforced polylactic acid (PLA) composites. Pre-process fiber surface modification resulted in marked improvements in tensile modulus as well as flexural modulus, an intuitive conclusion analogous to the effects of applying a sizing to fiber reinforcement used in a thermoset matrix composite; however, the effects of pre-process surface modification on the relevant thermal properties were more notable to this work. For reference, representative tensile and flexural properties from [20] are shown in Figure 34.
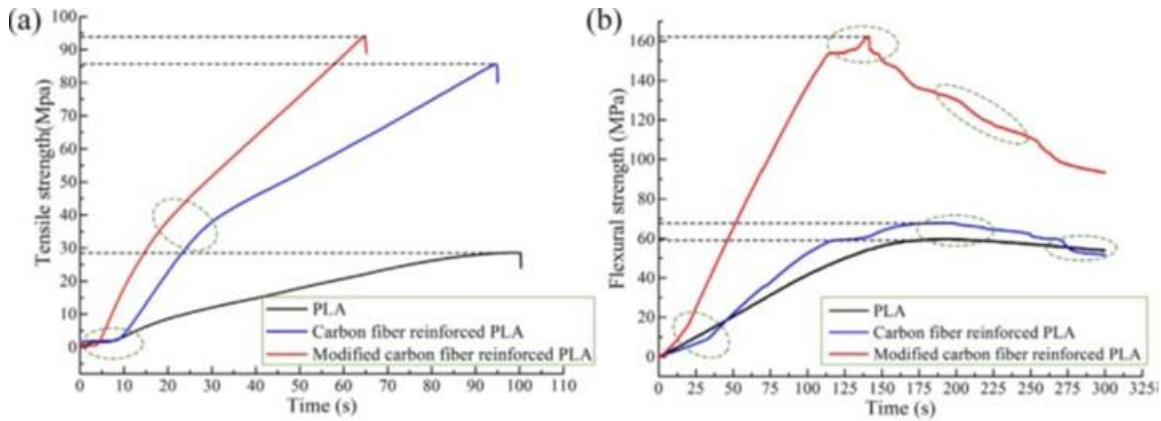
Figure 34: Tensile and flexural properties of 3D printed composites as a function of pre-process fiber surface modification [20]

In [20], DMA scans were performed at 1 Hz using a 3-point bending fixture and a relevant temperature sweep (room temp to 250 °C at 5 °C per minute) on printed specimens with and without pre-process fiber surface modification as well as on neat PLA specimens. The effects of the pre-process fiber surface modification were reported in terms of storage modulus, loss tangent and glass transition temperature. In terms of the DMA results, it is most notable that the specimen group subjected to pre-process fiber surface modification exhibited both the highest recorded storage modulus and glass transition temperature, while also exhibiting the lowest recorded loss tangent [20]. Adding to the impact of the pre-process fiber surface modifications, the reported storage modulus for the additively manufactured composite specimens without fiber surface modification, exhibited a value (typically reported in GPa) well below that of the neat PLA specimen, indicating a loss in the materials ability to elastically store energy. The authors of [20] attributed these results to the enhanced interfacial bond, and subsequent load transfer from matrix to fibers, in the printed composites utilizing the modified reinforcement, coupled with the lack of interfacial bonding and the presence of manufacturing defects, namely voids along the interface, in the untreated composite specimens. Relevant DMA results from [20] are shown in Figure 35.
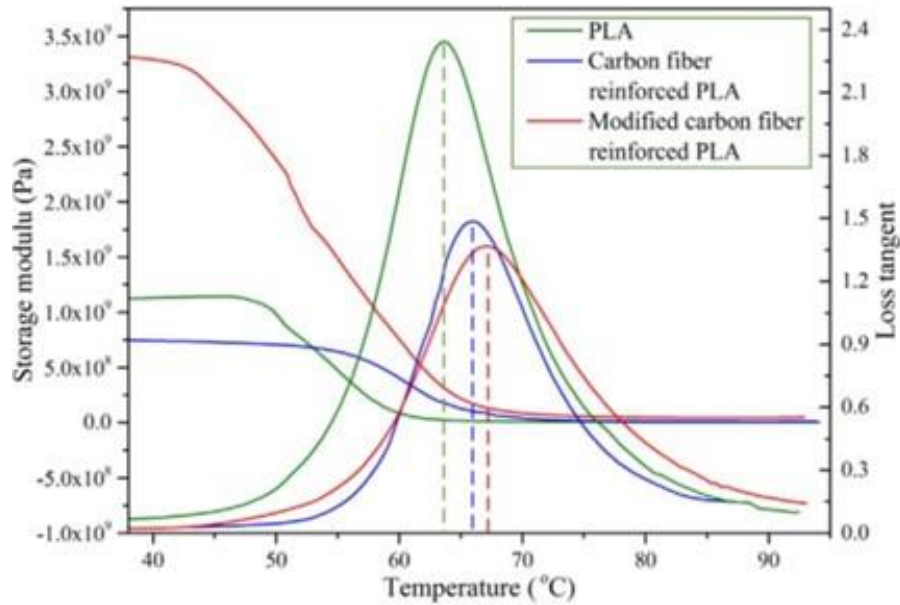
Figure 35: Storage modulus and loss tangent for three kinds of printed materials [20]

Figure 35 shows a total of six curves, three of which describe measured storage moduli (curves which appear to be bound by two horizontal asymptotes) while the remaining three curves describe measured loss tangents (those curves resembling a downward-opening parabola). Note the legend in Figure 35 which correlates curve color to the relevant material specimen being evaluated. Although it is not explicitly stated in [20], the DMA experiments that were performed clearly indicate that Dynamic Mechanical Analysis is potentially an appropriate method for evaluating the defect-based quality, both mechanically and thermally, of additively manufactured continuous fiber reinforced thermoplastics. DMA as a defect-based quality evaluation tool is novel in this literature, but has been utilized in a similar manner in other arenas. Outside of the realm of additive manufacturing and continuous fiber reinforced thermoplastics, DMA has been successfully utilized to track the effects of manufacturing defects, namely void content and fiber waviness, on the mechanical and thermal properties of woven, cross-ply carbon fiber/ epoxy laminates [37]. In agreement with the aforementioned results from [20], the work performed in [37] demonstrated that the measured stiffness (reported in N/ m) of

carbon fiber/ epoxy laminates is negatively impacted by the presence of manufacturing defects, as is the peak value of the loss tangent. Similarly, the results from [37] also demonstrate a notable decrease in the measured glass transition temperature (taken as the temperature at which the peak value of tan δ is measured) as defect (void content) concentration increases.

Using the work in both [20] and [37] as experimental evidence of both the utility and sensitivity of DMA with regard to material and processing related defects, it should be clear that DMA exhibits the potential to be a powerful defect-based quality evaluation tool in the additive manufacture of continuous fiber reinforced thermoplastics. The additive manufacturing hardware relevant to this work has demonstrated the capabilities required to process continuous fiber reinforced thermoplastics with high volume fractions on a flat print substrate, albeit inclusive of manufacturing defects, namely void content. Preliminary experiments presented in Chapter 2 have shown that conventional comparative evaluation techniques for continuous fiber reinforced polymers, specifically Short-Beam Strength analysis, fall short of adequately characterizing the effects of included void content on the processed continuous fiber reinforced thermoplastic matrix composites. This inadequacy could be addressed with a thorough investigation of the effects of included void content on the thermomechanical performance of additively manufactured continuous fiber reinforced thermoplastics by means of DMA, and as such, an investigation of this nature is the subject of this chapter. Prior to the presentation of the experimental hardware, materials, preparation and procedure, a background of DMA as a thermomechanical measurement technique is presented.

3.2 Dynamic Mechanical Analysis – Function & Theory

Dynamic Mechanical Analysis (DMA) is a thermomechanical analysis technique, founded in rheological principles, that is most typically reserved for the analysis and evaluation

of neat polymers and polymer matrix composite materials. Modern DMA equipment can take on a variety of functional forms, most commonly utilizing either rotational or linear schemes to excite the relevant material specimen, as well as perform a variety of experiments purposed with characterizing the viscoelasticity of polymeric material systems. Some of these experiments include, but are not limited to, creep-recovery, stress relaxation, quasi-static stress/ strain measurement and dynamic stress/ strain measurement. For the purpose of this work, only dynamic stress/ strain experiments using a linear sample excitation scheme will be relevant. A representative schematic of a typical DMA with a linear sample excitation scheme is shown in Figure 36.
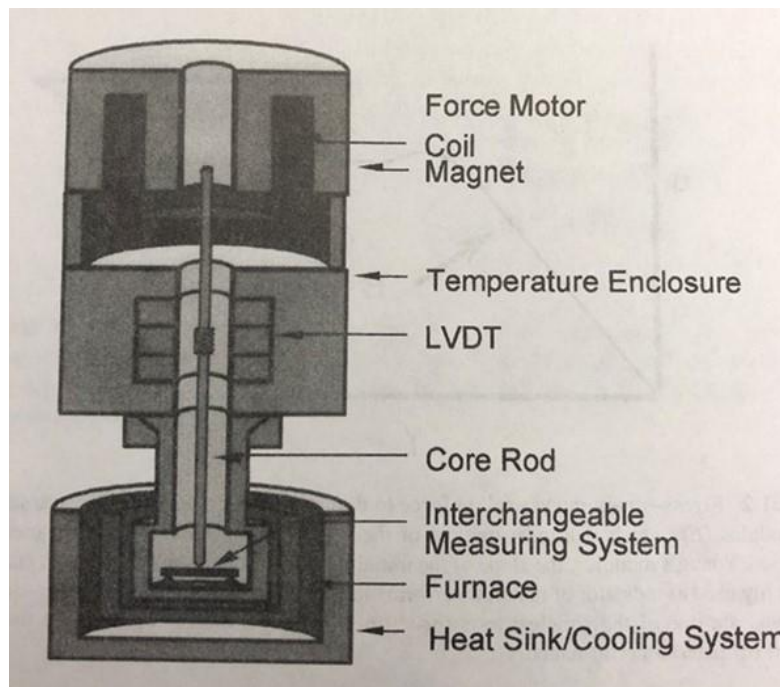
Figure 36: Representative schematic of the basic components within a typical DMA utilizing a linear sample excitation scheme [52]

Dynamic stress/ strain experiments in a DMA can be most readily described as the action of applying an oscillating, sinusoidal in this case, force to a material specimen while measuring the specimens deformation response to the applied force as a function of either time, temperature, or some combination of both [53]. The sinusoidal stress (arising from the excitation

force) gives rise to a sinusoidal strain which lags behind the stress by a phase angle, between 0 and 90 degrees, typically denoted as δ, Figure 37. Note that this phase angle lag is analogous to the definition of a viscoelastic material in that a perfectly elastic material response will have a 0-degree phase lag between stress and strain while a perfectly viscous material response will have a 90-degree phase lag. As long as the recorded phase lag exhibits a magnitude between 0 and 90 degrees, the relevant material specimen is viscoelastic, and the phase lag can be correlated to the materials ability to dissipate energy through internal molecular motions, commonly referred to as damping. Using recorded measurements of the specimen deformation response to the sinusoidally applied force, or stress, viscoelastic material properties can be calculated in the form of the specimen resistance to deformation, or storage modulus (E'), the samples tendency to flow, or loss modulus (E"), and the mathematical ratio of E" to E' known as the damping or loss factor (tan δ).
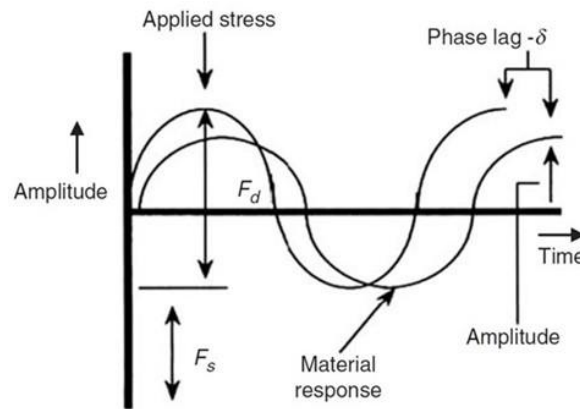
Figure 37: Viscoelastic deformation response to a sinusoidally applied excitation force [53]

As mentioned in the last paragraph, a viscoelastic material specimen exposed to a sinusoidal excitation force (stress) has some amount of deformation (strain) at the peak of the sine wave coupled with an angle defining the lag between the stress sine wave and the strain sine wave [52]. By measuring the stress sine wave relative to the strain sine wave, the storage

modulus (E'), loss modulus (E") and damping or loss factor (tan δ) can all be calculated. The equations used to determine E', E" and tan δ are given by 3.1-3.3 [52].

$$E' = (\sigma_0/\epsilon_0) \cos \delta = (f_0/bk) \cos \delta \tag{3.1}$$

$$E'' = (\sigma_0/\epsilon_0) \sin \delta = (f_0/bk) \sin \delta \tag{3.2}$$

$$\tan \delta = E''/E' \tag{3.3}$$

In equations 3.1 – 3.3, the subscript zero (e.g. σ_0) typically refers to the associated value at the peak of the relevant sine wave. To define the variables used to form equations 3.1 – 3.3, stress is represented by σ, strain is represented by ϵ, the mechanical excitation force is represented by f, the agglomerated specimen geometry and fixture boundary conditions term is represented by b, the specimen displacement at peak is represented by k and finally the phase angle is represented by δ. As shown, the measured storage modulus and loss modulus, E' and E" respectively, are both defined as functions of the applied excitation force, the specimen shape and fixture boundary conditions and the specimen displacement at the peak of the strain sine wave. As such, it should be intuitive that the specimen size, as well as the mechanical test fixture in use, are critical to the appropriate use of DMA.

A variety of fixtures are common to commercial DMA technology, including, but not limited to, tensile, double cantilever (DCB or clamped-clamped bending), single-cantilever, shear, compression and 3-point bending. Similar to quasi-static mechanical testing in a conventional load frame, the choice of the test fixture places global limits on specimen geometry. In DMA, limits on specimen geometry are further convoluted by the size of the test chamber (the interior geometry of the insulated furnace, see Figure 36) as well as the measurement range (range of applicable load) of the DMA in use. All commercial DMA equipment are subject to limits, both minimum and maximum, on the applicable force available for specimen excitation.

As such, specimen geometry is affected by a third variable, (the first two being fixture type and test chamber size) which is the expected elastic modulus, or elastic stiffness, of the relevant material. For example, the deformation response of a rectangular beam specimen in a bending fixture will be a function of the flexural stiffness of the beam (assuming no viscous contribution), commonly simplified as EI, where E represents the elastic modulus of the specimen material and I represents the moment of inertia of the beam cross-section. To stay within the measurable limits of the DMA hardware, it is common practice to decrease the moment of inertia of the specimen, by decreasing the specimen thickness, as the elastic modulus of the specimen material increases. Practically this implies that, again for the sake of example, a neat epoxy specimen will likely have a maximum allowable thickness in excess of that available for a carbon fiber reinforced epoxy specimen for a given fixture. For reference, and in consideration of common DMA equipment, a sample size in the range of 50 mm by 5 – 10 mm by 1 – 2 mm (length by width by thickness) is generally acceptable. These statements are supported by ASTM D4065-12 which gives recommendations for determination and report of procedures for DMA [54].

As previously mentioned, dynamic stress/ strain measurements in a DMA are typically performed as a function of time, temperature or some combination of both of these parameters. It is typical for most commercial DMA systems to be able to achieve controlled heating/ cooling rates ranging from less than 1 °C per minute up to as much as 20 °C per minute. Additionally, it is typical for most commercial DMA systems to be able to excite a specimen at a variety of individual frequencies, or superimposed frequencies, ranging from less than 1 Hz up to as much as 200 Hz. By coupling heating and cooling programs with mechanical specimen excitation at either discrete or superimposed frequencies, commonly referred to as synthetic waveforms, mechanical and thermal material phenomena can be observed in the same experiment. This

unique ability afforded by DMA allows for enhanced sensitivity, as compared to Differential

Scanning Calorimetry (DSC) and Differential Thermal Analysis (DTA), when it comes to

observing thermal transitions in polymers and polymer matrix composite materials [52].

Ultimately, with an appropriate experimental procedure, DMA can not only be used to quantify

the mechanical performance of a polymer or polymer matrix composite in terms of storage

modulus and damping factor, but also to identify both gross, and subtle, thermal transitions in the

material. Pertaining to DMA, identifiable thermal transitions range all the way from gross melt

transitions/ transformations, to the glass transition region, to coordinated movements in

microstructurally amorphous regions, to side chain movements and even bond bending and

stretching [52].

These aforementioned thermomechanical sensitivities afforded by DMA clearly posture

DMA as the most applicable and informative analysis tool available, specifically with regard to

evaluating polymers and polymer matrix composite materials. It is for this reason that DMA is

the sole analysis tool utilized in the experimental efforts outlined in this chapter.

3.3 Experimental Hardware

The hardware required by this portion of the experimental work remains unchanged from

the latter section of the preliminary experimentation that is outlined in Chapter 2. A 3-axis

additive manufacturing system, retrofitted with a custom spring-loaded end effector for

continuous commingled precursor payout, is utilized to process continuous fiber reinforced

thermoplastic matrix composite samples. The spring-loaded end effector is pictured in Figure

38, the entire additive manufacturing system is pictured in Figure 39.
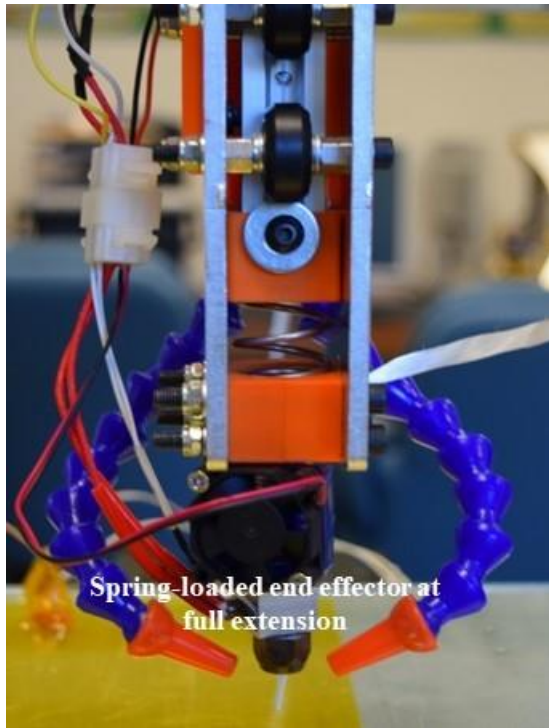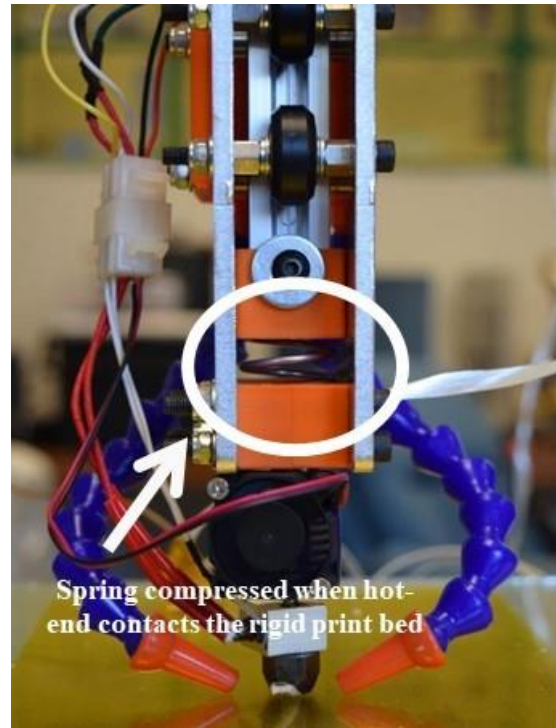
| (a) | (b) |

Figure 38: Spring-loaded end effector (a) at full extension (b) under compression in contact with the rigid print bed
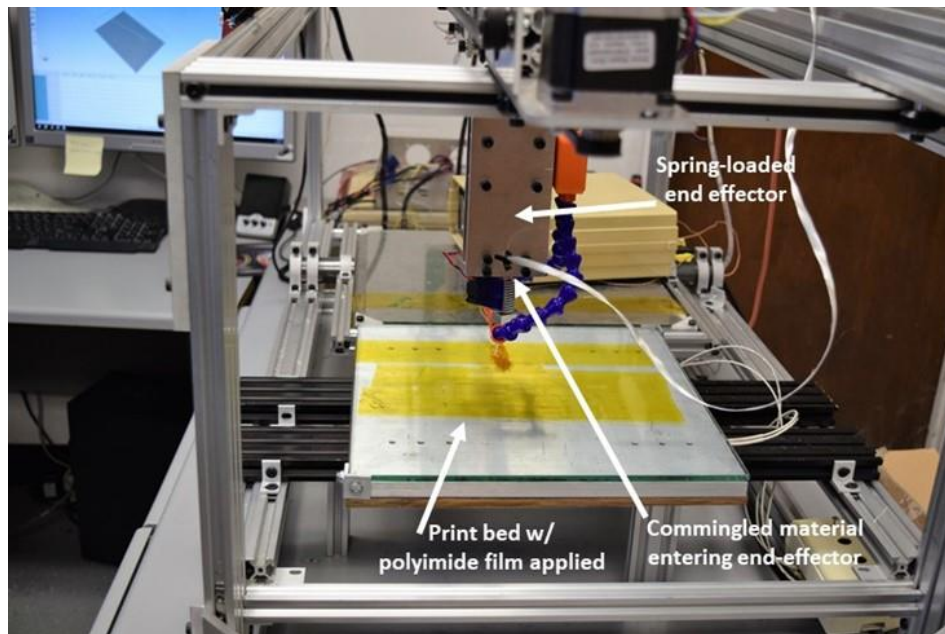
Figure 39: 3-axis composite processing system with relevant components highlighted

3.4 Materials

Consistent with earlier experimentation, the material employed in this work is a continuous commingled precursor, supplied as a single roving wound around a bobbin. The continuous commingled roving employed was composed, by weight, of 70 % E-Glass fiber (2.62 g/ cm^3) and 30 % transparent PET thermoplastic strands (1.27 g/ cm^3), nominally equating to an unprocessed fiber volume fraction of approximately 55 %. Note that the constituent densities were provided by the manufacturer of the continuous commingled manufacture, these were not explicitly measured.

Earlier work, outlined in Chapter 2, utilized DSC to determine the glass transition region of the amorphous PET thermoplastic in the commingled product. Multiple temperature sweeps from 40 °C to 280 °C, using a heating rate of 10 °C per minute and a nitrogen purge gas, were conducted on what started as unprocessed commingled material. The range of mid glass transition temperatures, recorded from a total of 5 DSC sweeps, was identified as 70 – 72 °C, with a mean of 71.5 °C. Additionally, and unchanged from the latter preliminary experimentation in Chapter 2, adhesive-back polyimide film is used as the deposition surface on the print bed to facilitate enough tack to secure the deposited material while also allowing for easy part removal upon print completion. The polyimide film, for visual reference, is shown in Figure 39.

3.5 Process Parameters

Process parameters for this experiment are based on the process parameters used in the latter preliminary experiment presented in Chapter 2. Despite the fact that the void content measurement associated with the 9 N sample case, see Chapter 2, did not coincide well with the observed trend in Short-Beam Strength, or the relevant micrographs, the 9 N process parameters

were chosen as the baseline parameters for this work. For reference, the 9 N process parameters provided the most optically transparent printed composite samples, where relatively low void content was verified through microscopy. As the purpose of this study is, in essence, to examine any apparent thermomechanical trends in additively manufactured composite material performance as a function of void content, by means of DMA, apparent void content in samples made using the baseline process parameters is non-critical as long as void content can be functionally modified in a known direction through small, controlled changes in those baseline process parameters. This is the governing assumption used to justify use of the 9 N sample case process parameters as a baseline. This assumption is verified later in the work.

The baseline parameters, derived from the 9 N sample case in Chapter 2, are defined again here for reference. Print temperature, measured at the outlet of the nozzle with cooling enabled (the ducting apparent in Figure 38) is held constant at 220 °C. Print bed temperature is held constant at 72 °C, slightly above the glass transition temperature determined for the PET thermoplastic in the commingled precursor material. Applied spring force, by means of the spring-loaded end effector, is 9 N, resulting in a programmed printed layer height of 0.4 mm. Print speed relevant to the baseline parameters is held at 100 mm/ minute; however, as will be discussed, print speed is the process variable used to functionally modify the included void content in the printed specimens required for this work.

Intuitively, in a thermoplastic matrix composite melt processing approach, there are three primary process variables that can be altered to functionally change the quality (i.e. void content in this context) of the processed composite material. The three process variables being referenced are, in the relevant vernacular, print temperature, applied compaction force (pressure) for constituent consolidation, and print speed (effectively the time the material is under

consolidation pressure). A relevant study concerned with the effects of void content on the structural, flexural performance of unidirectional glass fiber reinforced polypropylene utilized the method of varying time under molding pressure, albeit in a compression molding type process, to produce thermoplastic matrix composites with void content ranging from 1 – 14 %, and as such this same approach was employed for this work [55].

From the baseline print speed of 100 mm per minute, print speed was increased in increments of 50 mm per minute up to 400 mm per minute, providing a total of seven print speeds (100, 150, 200, 250, 300, 350, 400) that are used to print specimens with varying void content for this work. All other process parameters are held constant.

3.6 Specimen Preparation

A series of specimens intended for Dynamic Mechanical Analysis were prepared according to geometric constraints placed on specimen geometry by both the DMA test chamber and the relevant test fixture. The DMA used for this work is a Seiko DMS6100, with a cylindrical test chamber geometry defined by a 78 mm height and a 64 mm diameter, Figure 40. The fixture relevant to this work is a double cantilever beam bending device (DCB or clamped-clamped bending) with an outboard clamp to outboard clamp span of 50 mm, maximum clampable width of 15 mm and maximum clampable thickness of 5 mm. Note that these dimensions represent absolute maximums put on clampable specimen geometry, not implied suggestions on specimen geometry. In this fixture, the relevant specimen is rigidly clamped at its length-wise extremities as well as at its mid-span, where the mid-span (inboard) clamp is rigidly connected to the loading shaft of the DMA. The DCB fixture is shown in Figure 41.
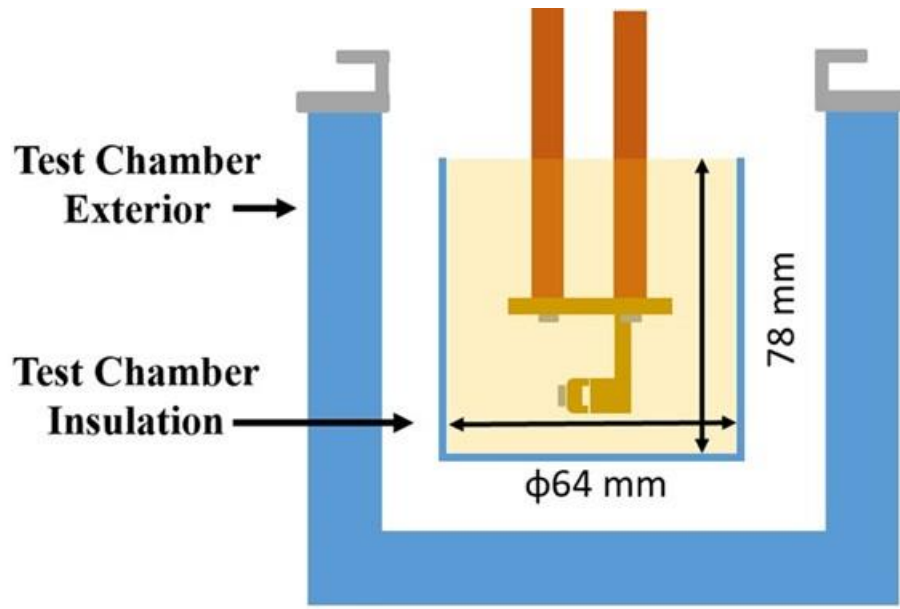
Figure 40: Graphical cross-section of the Seiko DMS6100 test chamber, loading shaft not shown, tensile fixture shown in yellow (provided by Hitachi)
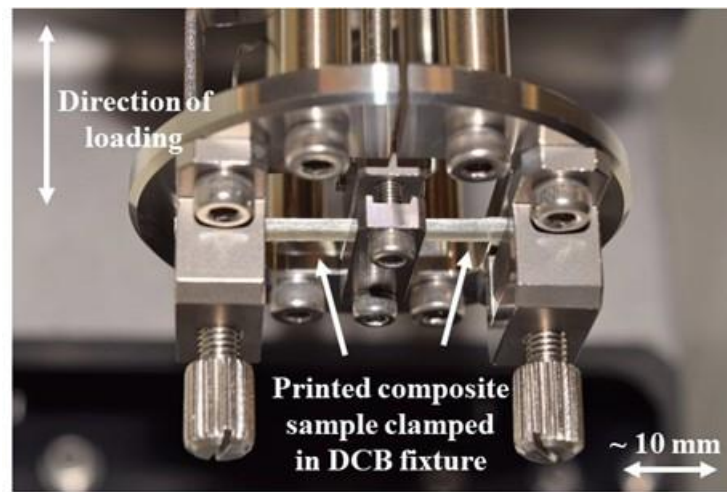
Figure 41: Printed composite sample in the double cantilever beam fixture relevant to this work

Continuous E-Glass/ PET beams, of rectangular cross-section, were processed from the supplied commingled feedstock using seven distinct print speeds, 100 – 400 mm per minute in increments of 50 mm per minute, while all other process parameters were held constant. Print temperature was held constant at 220 °C with the cooling ducts enabled, print bed temperature was held constant at 72 °C and applied spring force for consolidation pressure was held constant

90

at 9 N via the use of control code-based displacement control of the end effector. Specimens were printed such that the specimen cross-section was comprised of four unidirectional (UD) printed plies of the continuous commingled precursor, commonly referred to in laminated composites vernacular as a $[0°_2]_s$ laminate, or simply as a four ply UD laminate.

As a result of printing the samples at varying print speeds, analogous to varying the time under consolidation pressure, the nominal sample thickness for each print speed group increased as a function of increasing print speed. This is a trend consistent with other works discussed earlier in this chapter [37,55]. This trend is intuitive under the assumption that viscous flow of the thermoplastic polymer in the commingled material, in the low viscosity state experienced during processing, occurs almost entirely due to mechanical pressure applied by the spring-loaded end effector via the hot-end nozzle (gravity is acknowledged but neglected). This implies that the slower print speeds, with all other parameters held constant, will generally correspond to thinner samples, as a slow print speed provides a longer period of time for the low viscosity polymer to flow in the un-impeded direction (the direction of printed layer width) away from the hot-end nozzle. Consequently, the changes in sample thickness with print speed were accompanied by changes in the sample width with print speed (i.e. cross-section variation). As the thickness of each ply increased with increasing print speed, the width of the ply decreased accordingly. This concept is illustrated graphically in Figure 42.
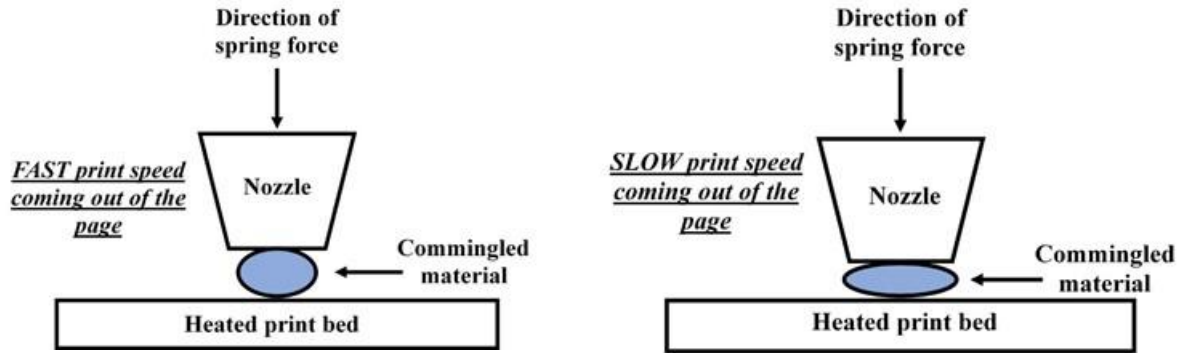
Figure 42: Graphical representation of correlation between print speed and layer cross-section according to viscous flow of the thermoplastic

All beam specimens were printed to have a nominal, as printed, length of 120 mm. This was intended to give more than enough room to remove the length-wise extremities of the as-printed specimens, by means of a rotary diamond blade, which are subject to varying levels of consolidation quality as a result of the pick up and put down action of the spring-loaded end effector. Removing the ends of the as-printed specimen is desirable as it allows for a cut-to length DMA specimen with pseudo uniform consolidation quality across the specimen length. This method provides for a means of testing the effects of manufacturing defects which occur in steady-state manufacture, as opposed to defects which occur in the transient pick-up and put-down action of the spring-loaded end effector. Effects on printed material consolidation due to the transient pick-up and put-down action of the spring-loaded end effector can be mitigated through the integration of a cut and re-feed mechanism for the spring-loaded end effector, (i.e. additionally hardware development) and as such, is not of interest to this study. Note that further hardware development to this end is not the subject of this work.

A total of six continuous E-Glass/ PET specimens were printed at each print speed. The length-wise extremities of the as-printed specimens were removed such that the remaining specimen length was nominally 60 mm, roughly corresponding to the maximum length allowed by the test chamber of the DMS6100. Following length-wise extremity removal, all specimens

were finely sanded, using 400 grit SiC sand paper, along their length to provide a pseudo-planar surface for subsequent specimen width measurements. Sanding along the top and bottom of the specimens was not required as the surface finish of both the top and bottom of the specimens is effectively tooled, during printing, by the print bed and the hot-end nozzle.

All specimen lengths were measured using a digital Vernier caliper, whereas all specimen widths and thicknesses were measured with a digital micrometer. One length measurement was taken for each post-processed beam specimen, whereas four measurements of specimen width and thickness were taken and averaged for each DMA specimen. One length measurement for each specimen was acceptable in consideration that the total specimen length has no influence on the DMA results (beam span is defined by the fixture). An example of an as-printed beam specimen compared to a post-processed DMA specimen is shown in Figure 43. The respective nominal dimensions of each group of DMA specimens (seven total groups, each composed of six specimens), separated by print speed, are reported in Table 3.
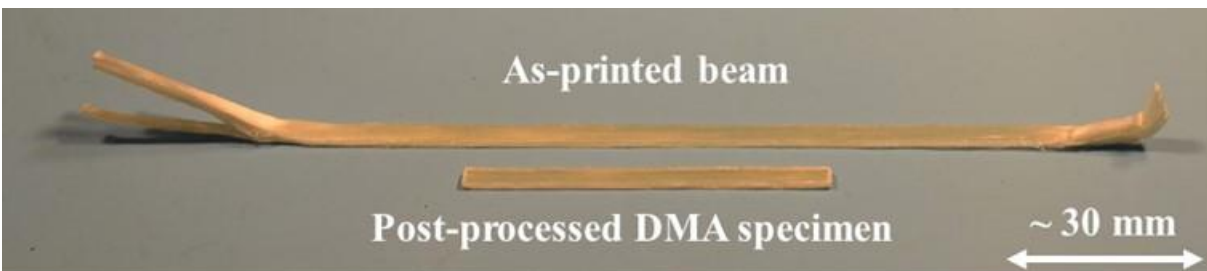
Figure 43: As-printed EG/ PET beam as compared to a post-processed DMA specimen, note the extremeties of the as-printed beam

Table 3: Nominal dimensions of each group of DMA specimens, separated by print speed, with associated sample standard deviations, expressed as a percent of the mean

Print Speed (mm/min)	Length (mm)	Length St.Dev (%)	Width (mm)	Width St.Dev (%)	Height (mm)	Height St.Dev (%)
100	58.65	0.50	4.302	1.55	1.335	1.08
150	58.29	0.48	3.959	1.25	1.458	1.77
200	58.30	0.77	3.810	1.99	1.542	1.53
250	58.72	0.78	3.708	2.09	1.579	2.14
300	58.65	0.49	3.632	1.66	1.658	1.96
350	58.57	0.73	3.590	2.10	1.717	2.06
400	58.57	1.07	3.599	1.62	1.740	2.78

3.7 Test Procedures

Specimens for Dynamic Mechanical Analysis were cut from the as-printed beams such that the continuous E-Glass fiber reinforcement spanned the length of the specimen. The printed, unidirectional specimens were tested with methods in accordance with ASTM D4065-12 where applicable. The same DMA scan was performed on every printed composite specimen from every print speed group. The relevant DMA scan is defined as follows: a temperature program ranging from 30 °C to 90 °C at a heating rate of 5 °C per minute, a five-frequency synthetic oscillation mode (0.5 Hz, 1 Hz, 2 Hz, 5 Hz and 10 Hz), and a 5 μm mid-span specimen displacement (by means of the loading shaft or probe as it commonly referred to). Use of a 5 μm mid-span specimen displacement translates to a maximum oscillatory strain in the range of 0.40 – 0.52 %, depending on nominal sample thickness, as determined by Equation 3.4. Note that ε represents oscillatory strain, a represents maximum beam displacement, t represents nominal DMA specimen thickness and l represents the unclamped, or free length of one half of the double cantilever beam.

$$\varepsilon = 12\left(\frac{at}{l^2}\right) \tag{3.4}$$

It should be acknowledged here that a 5 μm mid-span specimen displacement is a recommended starting point for measurements using the synthetic oscillation mode made available by the DMS6100. This recommendation is intended to keep the maximum possible beam displacement, analogous to the maximum possible oscillatory strain, low enough to stay within the linear viscoelastic region of the relevant polymer. The technical manual for the DMS6100 specifically states that, as a result of the synthetic oscillation mode, the relevant specimen may experience peak oscillatory displacements five times that of the programmed displacement. The maximum oscillatory strain range, 0.40 – 0.52 %, reported above was calculated accordingly, where 25 μm was used instead of 5 μm as the term a in Equation 3.4. It is generally accepted that maximum oscillatory strains less than 1 % are sufficient to stay within the linear viscoelastic range, as specified by ASTM D4065-12 [54].

As no external cooling was available at the time of experimentation, the starting temperature for the DMA scan was required to be in excess of room temperature to ensure control over the starting conditions of the experiment. As such, 30 °C was deemed to be a suitable starting temperature. The finishing temperature for the DMA scan, that being 90 °C, was chosen to ensure that measurements were taken throughout the glass transition of the thermoplastic matrix in printed composite specimen, ~ 72 °C. As the PET thermoplastic matrix is known to have an amorphous microstructure, determined via DSC, scanning temperature well past the glass transition in the interest of observing any other thermal transitions in the material was deemed unnecessary and non-critical to this work. The heating rate of 5 °C per minute was chosen as it provides for relatively short scan times, in the range of 12 minutes per scan, while also showing sensitivity to the glass transition of the thermoplastic polymer.

Although it is common for DMA scans to be run at a single, constant frequency, 1 Hz for example, a synthetic oscillation mode was chosen for this work as it allows for 5 frequencies of sample excitation concurrently. The use of a synthetic oscillation mode allows for a DMA scan to measure both temperature and frequency dependent phenomena in the same scan, while also generating more (as in excess) useful data in a single scan for a single specimen. The synthetic oscillation mode schematically resembles five superimposed sine waves, representing the five varied excitation frequencies, as opposed to a five discrete sine waves. This concept is graphically displayed in Figure 44. In addition to acquiring information about temperature and frequency dependency in a single scan, the use of a synthetic oscillation allows for potential construction of viscoelastic master curves, through the principles of time/ temperature superposition, using a single experiment. This topic is addressed in commentary on future work.
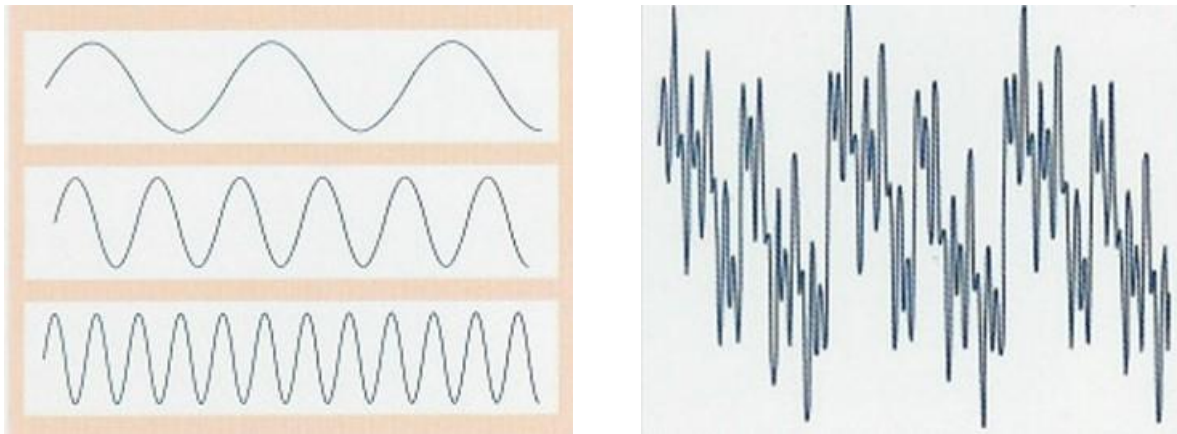
Figure 44: Three single, discrete frequencies (left) as compared to a synthetic superposition of five frequencies (right). Image adapted from Seiko EXSTAR DMS6100 brochure

Following evaluation of the various specimen by Dynamic Mechanical Analysis, quantitative constituent volume fraction evaluation was performed using a procedure in accordance with ASTM D3171 [48]. In an effort to mitigate the chances of constituent volume fraction being biased by an outlier, all six DMA specimen from each of the seven total print speeds were subjected to the methods suggested by the relevant ASTM. Each specimen was

dried in a desiccator and weighed prior to determining the composite density via the Archimedes method. In this experiment, all specimens were painted on all sides with a thin acrylic coating, of known density, prior to density determination. This was done with the intent of mitigating water uptake in the specimens. Specimens were weighed following the application of the acrylic coating and as such the volume of the acrylic coating was accounted for in the relevant calculations. Following composite density determination, the PET matrix from each sample was then burned off in a muffle furnace at high temperature in air (5 hours at 550 °C), leaving the continuous glass reinforcement. The leftover continuous glass reinforcement was then weighed, and constituent volume fractions (fiber, matrix and void) were determined via the use of known constituent densities.

3.8 Results

Specimens were produced by melt processing, and placing, a commingled continuous E-Glass/ PET precursor using the 3-axis additive manufacturing system. Printed specimens were visually examined before and after analysis by DMA. Printed specimens were thermomechanically evaluated in the DMS6100, using a double cantilever beam bending fixture, a five-frequency synthetic oscillation mode and a temperature scan from 30 °C to 90 °C at a 5 °C per minute heating rate. Following thermomechanical evaluation, specimens were subjected to composite density determination and subsequent constituent volume fraction determination for the purpose of correlating any observed trends in thermomechanical material performance to the presence of void content. Metallographic evaluation of representative specimens was performed in order to supplement the information garnered from thermomechanical evaluation by means of Dynamic Mechanical Analysis (DMA).

3.9 Print Speed & Void Content

The fundamental assumption made in the design of this experiment is that void content in the printed composites can be functionally modified through changes in the print speed process parameter. As such, this assumption must be verified before the thermomechanical results of the DMA scans can be presented. As was mentioned earlier in the work, while all other process parameters were held constant, specimens purposed for DMA were printed at seven print speeds, ranging from 100 mm per minute to 400 mm per minute in increments of 50 mm per minute. A total of six DMA specimens were printed at each of the seven print speeds. Nominal void content measurements from the printed continuous fiber reinforced thermoplastics, with associated standard deviations, are presented as a function of print speed in Figure 45. The same data is tabulated and presented in Table 4.
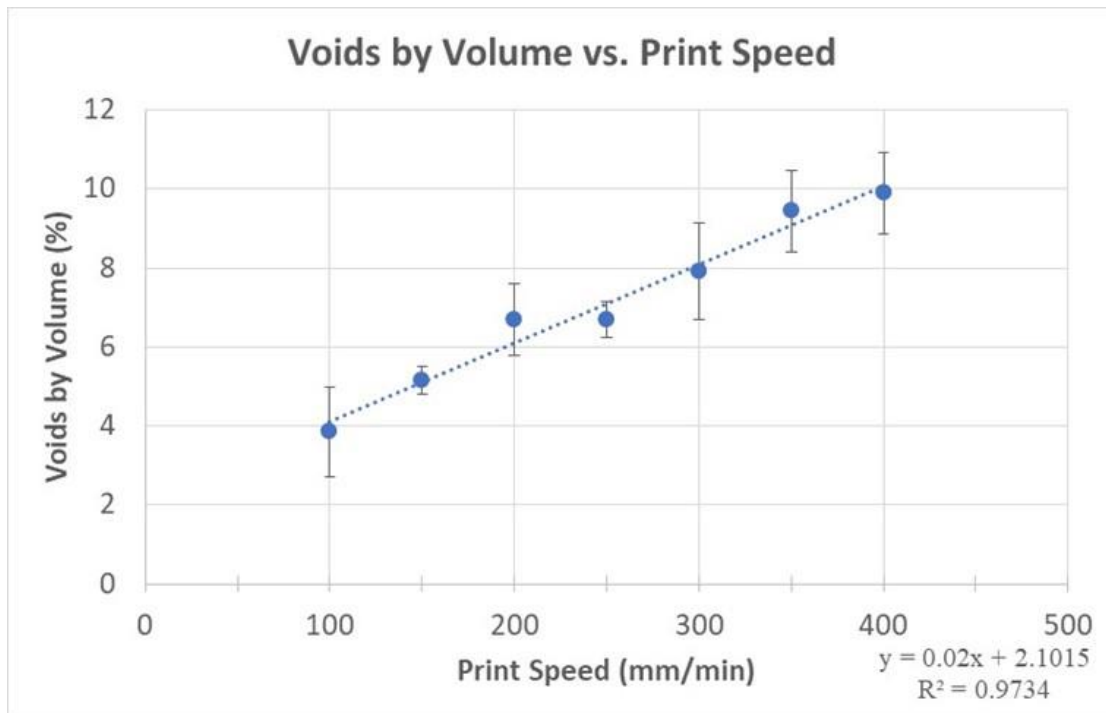
Figure 45: Nominal void content, with sample standard deviations, for each of the seven print speeds

Table 4: Nominal void content, with sample standard deviations, for each of the seven print speeds

Print Speed	Nominal Void Content (%)	Sample St.Dev (%)
100	3.85	1.14
150	5.15	0.34
200	6.69	0.92
250	6.69	0.47
300	7.93	1.23
350	9.44	1.02
400	9.90	1.03

As shown in Figure 45, nominal void content in the printed composites tends to increase as print speed is increased, verifying the assumption made earlier in this work. A trendline was added to Figure 45 for the purpose of showing the general linearity of the observed relationship between void content and print speed. The nominal value of void content increases with increasing print speed at all print speeds, with the exception of the 200 mm per minute and 250 mm per minute print speeds. This phenomenon is difficult to resolve as the average and sample standard deviation for the 250 mm per minute group falls within the sample standard deviation for the 200 mm per minute group. Similarly, there is no reason to believe that the magnitude of the sample standard deviation for any of the nominal void content measurements reported follows any trend in direction or magnitude. In consideration of the global trend in the data, the localized phenomenon in the 200 – 250 mm per minute range is not considered to be significant in the preliminary presentation of the results of the experiment.

Separately, for the point of clarifying the data presented in both Figure 45 and Table 4, it must be acknowledged that the sample standard deviations are not being presented as percent values of the mean (i.e. plus or minus 10%) but rather in the same dimension as the nominal void content measurements, which happen to be expressed as a percent by volume.

3.10 Visual Evaluation

Representative DMA specimens from the 100, 250 and 400 mm per minute groups are shown, top to bottom, in Figure 46. Note that Figure 46 shows specimens prior to thermomechanical evaluation in the DMS6100.
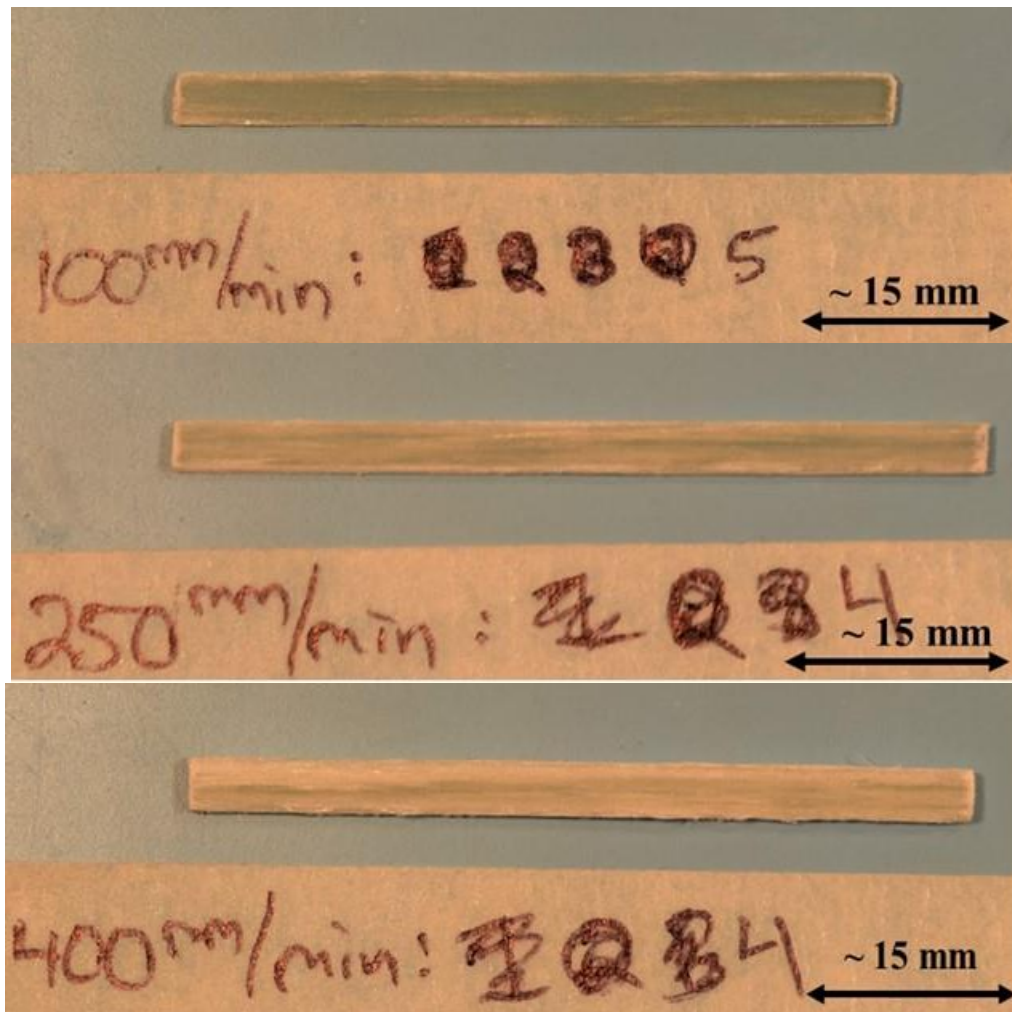
Figure 46: Visual comparison of some representative DMA specimens before evaluation in the DMS6100

The three specimens shown in Figure 46 were chosen specifically to illustrate the differences in processed composite material transparency, or lack thereof, as the apparent opacity relates to included void content. In examining Figure 46, it should be clear that the top image, the 100 mm per minute specimen, is the most transparent while the bottom image, 400 mm per

minute, is the most opaque, while the middle image, 250 mm per minute, falls somewhere in between the two other specimens. Similar to visible differences in the three specimens shown, it should be noted that the three specimens also exhibit varying cross-sectional geometry which is not readily apparent in the images. The differences in cross-sectional geometry are analogous to the differences in nominal specimen geometry that were presented in Table 3 in the Specimen Preparation section of this chapter.

Seeing as Figure 46 illustrates the appearance of representative DMA specimens prior to evaluation in the DMS6100, it is appropriate to show the same representative DMA specimen following the thermomechanical evaluation. In Figure 47, the same three DMA specimens are shown for the purpose of highlighting the visible clamping artifacts left on the specimen surfaces from the double-cantilever beam fixture. In consideration of the clamping artifacts, it should be acknowledged that all of the DMA specimens were clamped in the DCB fixture with nominally the same clamping pressure. This was achieved by scaling the tightening torque applied to the bolts (where torque is applied with a torque wrench) on the inboard and outboard clamps of the fixture to account for changes in the sample width.
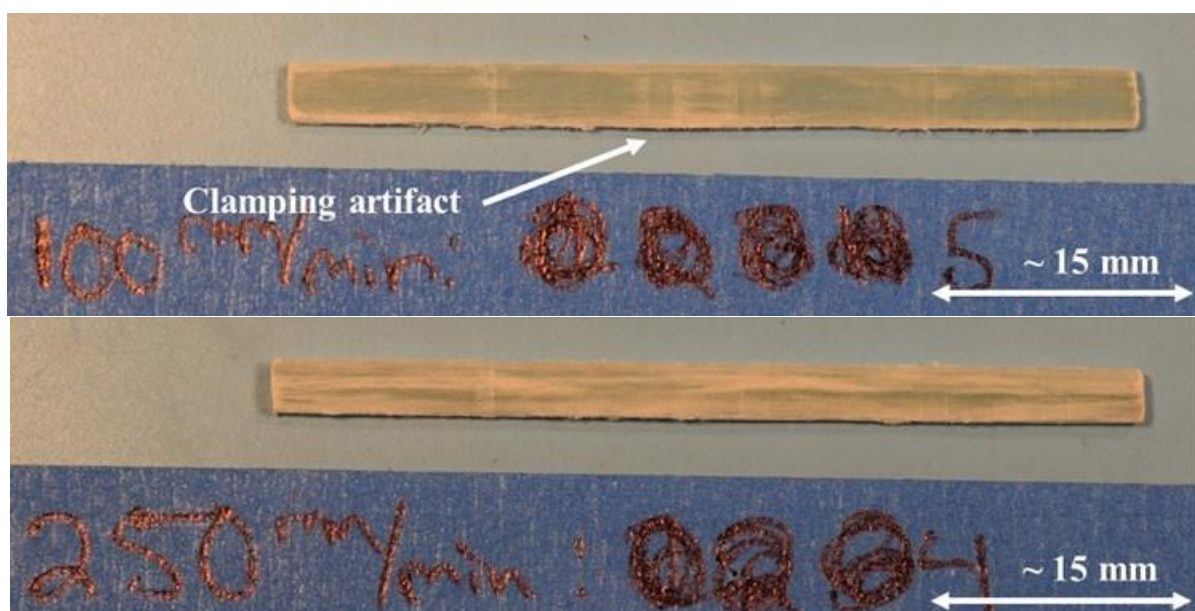
Figure 47: Visual comparison of some representative DMA specimens following evaluation in the DMS6100

3.11 Thermomechanical Evaluation – Dynamic Mechanical Analysis

Dynamic Mechanical Analysis was used as a thermomechanical material evaluation method to investigate the effects of included void content on the additively manufactured continuous fiber reinforced thermoplastic matrix composite specimen. All specimens were cyclically loaded using a five-frequency synthetic oscillation mode (0.5, 1, 2, 5 and 10 Hz) throughout a temperature sweep, controlled at 5 °C per minute, from 30 °C to 90 °C in order to observe both pseudo room temperature behavior as well as behavior throughout the glass transition region for the thermoplastic polymer matrix. The software package associated with the DMS6100 provides a spectrum of output data, both in tabular and graphical format, including E', E" and tan δ as a function of temperature. A typical graphical output provided by the DMS6100 software package is shown in Figure 48. In examining Figure 48, note that there is a total of 15 curves, sub-divided into three color coordinated subsets of five curves each. Each color coordinated subset of curves, green, red and blue, corresponds to one of the three measured material properties, E', E" and tan δ (tanD on the relevant axis) respectively. Similarly, each color coordinated group is made up of five curves, which correspond to the five frequencies imposed by the synthetic oscillation mode, 0.5, 1, 2, 5 and 10 Hz.
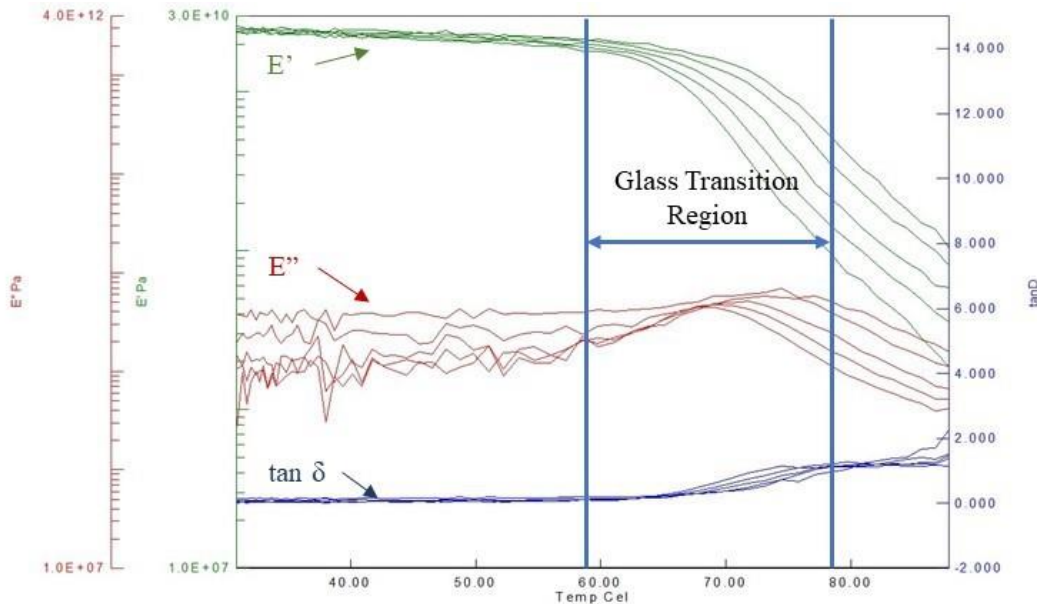
Figure 48: Typical graphical output provided by the DMS6100 software package showing the three measured properties as a function of temperature (E', E" and tanD or tan δ)

In addition to showing the various frequencies, as well as the relevant measured material properties, Figure 48 also shows some trends in those measured material properties that are typical in DMA outputs for both polymers and polymer matrix composites. Intuitively, the properties in an amorphous thermoplastic polymer, like PET, go through their most drastic changes in and around the glass transition region of the polymer. These drastic changes are attributed to the transition from the hard, glassy state associated with relatively low temperatures to the soft, rubbery state associated with relatively high temperatures. The transition from the hard, glassy state to the soft, rubbery state is most readily attributed to a localized increase in free volume, which in turn allows for large segments of the polymer chains to coordinate movement in response to both current and residual mechanical stimuli [52]. The existence of this coordinated movement is a functional analog to a decrease in the viscosity of the amorphous polymer, implying less resistance to flow and, similarly, less elastic load bearing capability.

During the glass transition, the storage modulus (E') and the loss modulus (E") go through opposing changes, where the elastic storage modulus undergoes a marked decrease in

magnitude, to some pseudo steady-state, while the viscous loss modulus concurrently undergoes an increase in magnitude, albeit up until a point of apogee, where the loss modulus then tapers off to a pseudo steady-state as well, Figure 48. This pseudo steady-state is visually analogous to the rubbery plateau that is observable in semi-crystalline polymers up until the melting temperature. Similar to the phenomenon experienced by E" around the glass transition, tan δ also undergoes a similar increase in magnitude up to a point of local apogee and then a subsequent decrease in magnitude according to the ratio of E" to E' through the temperature program. The phenomenon described, with regard to tan δ, is not particularly apparent in Figure 48, but is much more apparent in Figure 35. This topic will be discussed later in this chapter.

Typically, results from a Dynamic Mechanical Analysis study are reported in terms of frequency specific plots of the storage modulus (E'), loss modulus (E") and damping factor (tan δ) as a function of temperature, as well as single values of one or more of these parameters at a given temperature of interest to highlight mechanical performance or the glass transition temperature [20,34–38]. As such, the results of this work will be reported in consideration of these trends, but also in consideration of this work's specific goal of evaluating the measured material properties in terms of included, gross void content. Results of this work are herein presented in terms of the maximum measured storage modulus (E'), the maximum measured loss modulus (E"), the glass transition temperature as measured according to the peak measured value of E", and the maximum measured value of damping factor (tan δ). Commentary regarding the justification for this presentation scheme will be provided as it becomes relevant and necessary.

3.11.1 Maximum Measured Storage Modulus as a Function of Void Content

The maximum measured storage modulus (E') was determined for all six specimens belonging to each of the seven print speed-based specimen groups. In this case, the maximum

measured storage modulus, which typically occurs in the range of 30-50 °C, as shown in Figure 48, serves as an analog to the flexural elastic stiffness of the printed composite material at or around room temperature. It has been assumed that the flexural storage modulus of a composite material at a given temperature, say room temperature or even 30 °C, is conceptually similar to the flexural modulus as determined by a quasi-static mechanical test in accordance with the relevant ASTM [53]. In consideration of this assumption, results summarized in [53] from other works in the arena, as well as empirical evidence generated by the authors of [53], specifically with regard to a three-point bending scheme and carbon/ epoxy laminates, have shown that although the flexural storage modulus and the quasi-static flexural modulus are conceptually similar, their magnitudes can vary by as much as 50% depending on specimen preparation and the idiosyncrasies of the measurement technique applied (i.e. specimen prep, fixture type etc.).

In consideration of the chance of discrepancy between the measured flexural storage modulus and the quasi-static flexural modulus, as well as the fact that quasi-static mechanical testing in accordance with the relevant ASTM (ASTM D790) was not performed for this work, the magnitude of the data to be presented is of less interest than any trends therein. As such, the average of the maximum measured storage modulus for each print speed specimen group was calculated and subsequently plotted as a function of void content. Note here that nominal void content will be used interchangeably with print speed going forward as the empirical relationship between the process parameter, print speed, and the resulting void content in the printed composite material has already been established. For the nominal values of void content that represent each print speed group of DMA specimens, see Table 4. The average of the maximum measured storage modulus, as a function of void content, is shown in Figure 49 for all five tested frequencies (0.5, 1, 2, 5 and 10 Hz). Note that color coordinated lines are used to join the

nominal values of maximum measured storage modulus for each specimen group for the purpose of more readily distinguishing the five data sets from one another.

In examining Figure 49, it is clear that there is a notable negative trend, at all measured frequencies, in the maximum measured storage modulus with increasing void content in the printed composite specimens. Based on the nominal data presented, with small discrepancies in accordance with the relevant frequency, the maximum measured storage modulus decreases by approximately 33-35% with an approximate 6% increase in void content. This gross decrease in the maximum measured storage modulus translates to, approximately, a 5% decrease per 1% added void content. This data is presented in Table 5. Separately, the data presented in Figure 49 clearly shows that although the magnitude of the maximum measured storage modulus at a given void content is frequency dependent, the observed negative trend seen in the relevant measurement is, based on these empirical results, frequency independent. Finally, for the sake of due diligence, the maximum measured storage modulus data from the 1 Hz data set, as a function of void content, is presented with associated error bars indicating the sample standard deviation in Figure 50. Note that a linear trendline was added to Figure 50 to show a basic linear relationship in the empirical data. In acknowledgement of the linear trendline in Figure 50, as well as other occurrences of the linear fit in this chapter, note that this work is only demonstrating a generalized linear trend within the relevant experimental window.
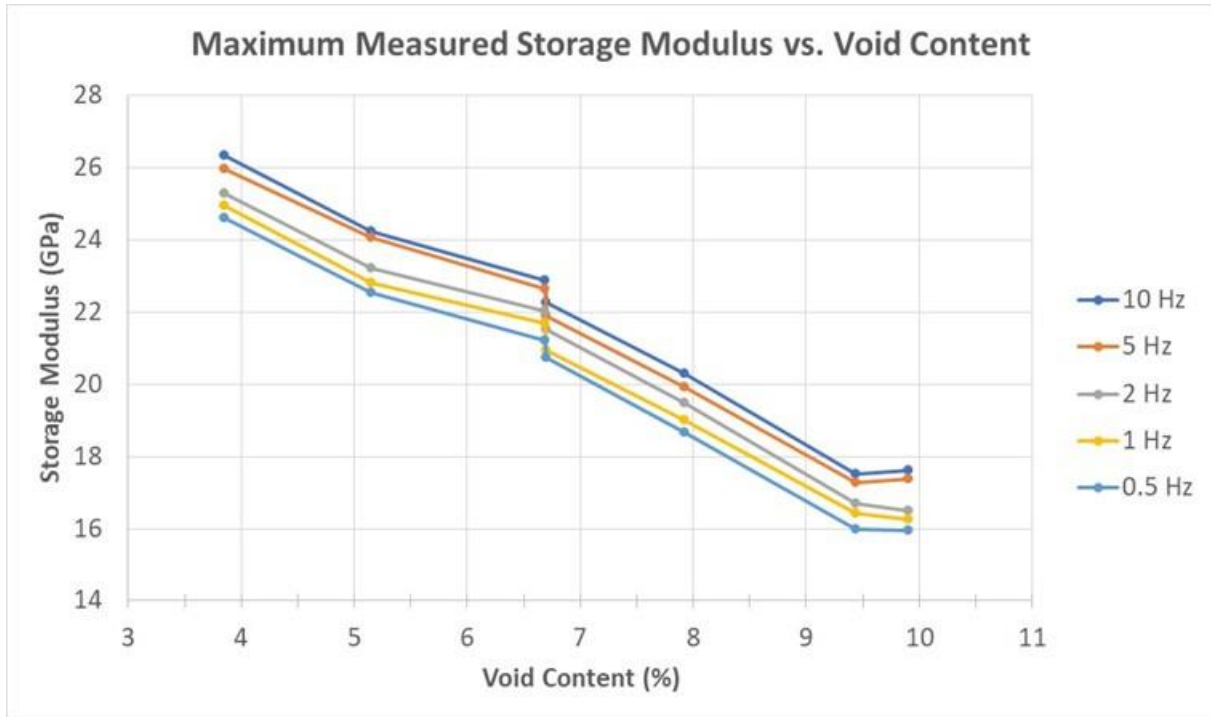
Figure 49: Maximum measured storage modulus (E'), at five frequencies, as a function of void content

Table 5: Frequency-based percent decrease in the maximum measured storage modulus (E') over the entire empirical range and per 1% added void content

Test Frequency (Hz)	Total Decrease in E' (%)	Decrease in E' per % void (%)
0.5	35.09	5.80
1	34.80	5.75
2	34.71	5.74
5	33.09	5.47
10	33.10	5.47
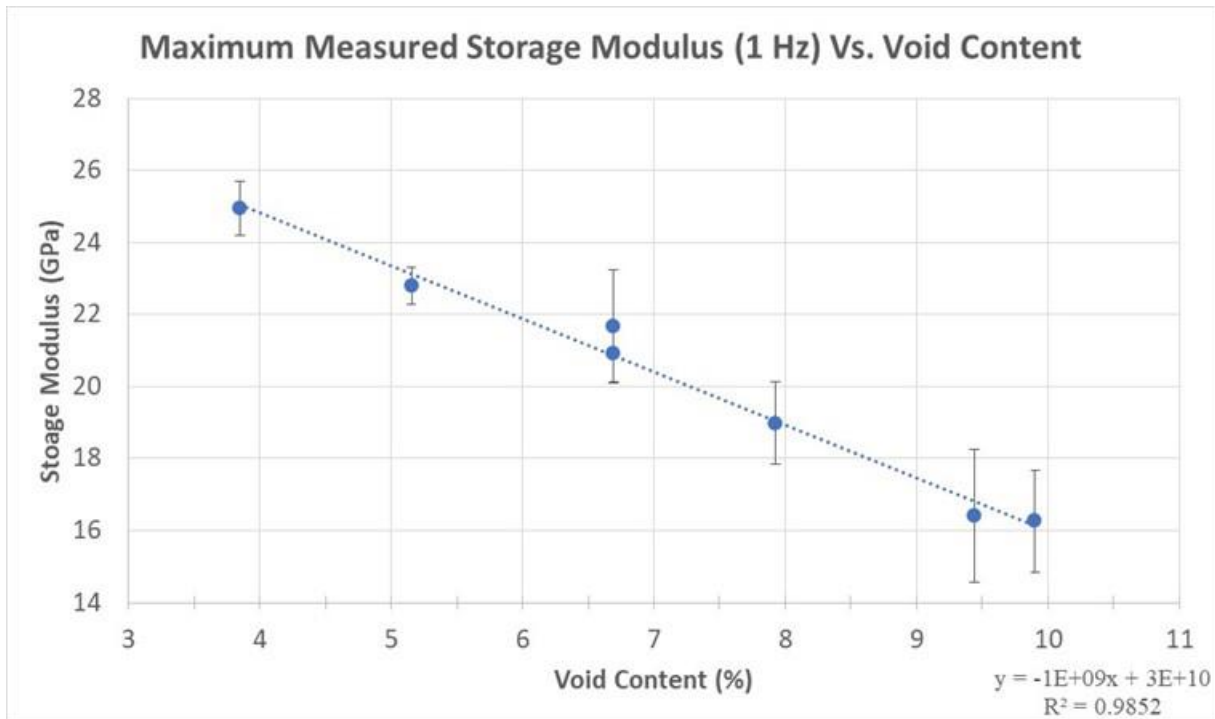
Figure 50: Maximum measured storage modulus, at 1 Hz, with associated standard deviations

An important phenomenon to acknowledge in this section, with regard to both Figure 49 and Figure 50, is the appearance of vertically coincident data points in the void content range of approximately 6.7 % voids by volume. These vertically coincident data points correlate directly to the same two overlaid points in Figure 45 (nominal void content vs. print speed) which correspond to the 200 and 250 mm per minute print speed specimen groups. In recollection of the contents of Table 4, note that these two print speed groups exhibited nearly identical nominal void contents by volume. Figure 50 clearly shows that the magnitude of the maximum measured storage modulus (a nominal value in this case) of the two nearly coincident data points is very similar; however, the included standard deviations, shown as error bars, make it impossible to contend that the separate nominal values are statistically different. The nominal values of maximum measured storage modulus, at 1 Hz, that are graphically displayed in Figure 50 are tabulated with their associated standard deviations for reference in Table 6. The two vertically coincident data points are highlighted in Table 6.

Table 6: Maximum measured storage modulus with associated standard deviations, at 1 Hz, for the different specimen groups

Print Speed (mm/min)	Void Content (%)	E' at 1 Hz (GPa)	St.Dev (GPa)
100	3.85	24.9	0.75
150	5.15	22.8	0.51
200	6.69	21.7	1.58
250	6.69	20.9	0.79
300	7.93	19.0	1.15
350	9.44	16.4	1.85
400	9.90	16.3	1.41

3.11.2 Maximum Measured Loss Modulus as a Function of Void Content

The maximum measured loss modulus (E") was determined for all six specimens belonging to each of the seven print speed-based specimen groups. In this case, the maximum measured loss modulus is typically observed during the glass transition region, and can be used as an indicator of the glass transition temperature [38,52]. A single, nominal value of the maximum measured loss modulus was calculated for each of the seven print speed-based specimen groups according to each of the five tested frequencies. These nominal values, for all five frequencies, are plotted as a function of void content in Figure 51. Note that color coordinated lines are used to join the nominal values of maximum measured loss modulus for each specimen group for the purpose of more readily distinguishing the five data sets from one another.
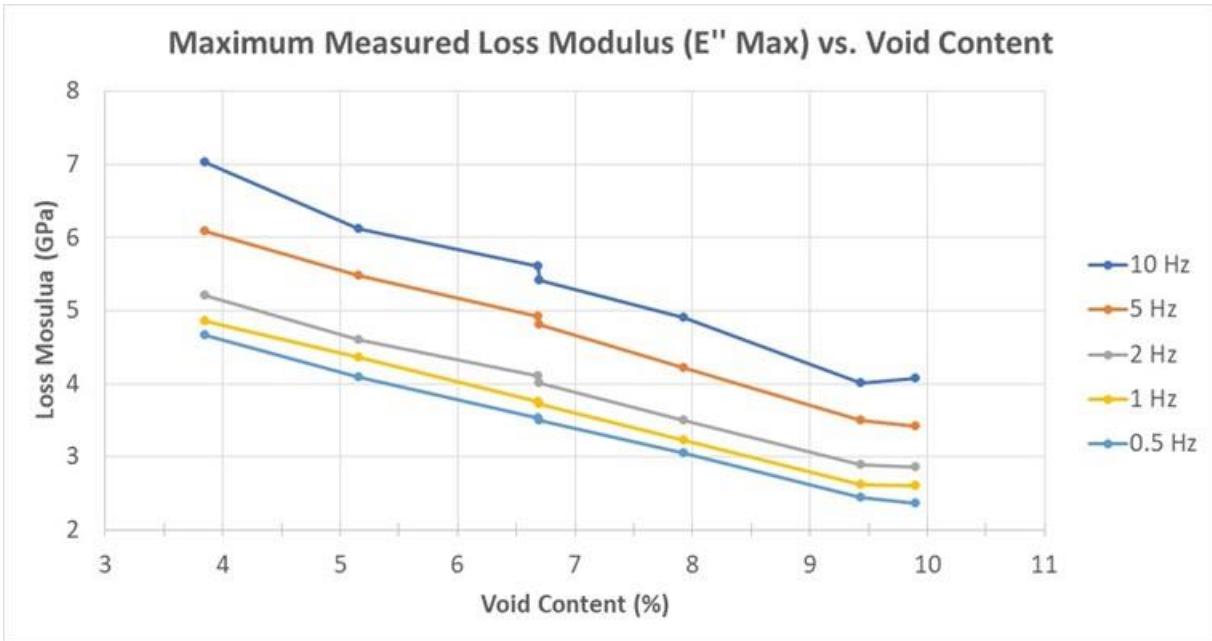
Figure 51: Maximum measured loss modulus (E"), at all five frequencies, as a function of void content

In examining Figure 51, it is clear that there is a notable negative trend, at all measured frequencies, in the maximum measured loss modulus, with increasing void content in the printed composite specimens. Based on the nominal data presented, with small discrepancies in accordance with the relevant frequency, the maximum measured loss modulus decreases by approximately 42 – 49 % with an approximate 6 % increase in void content. This gross decrease in the maximum measured loss modulus translates to, approximately, a 7 – 8 % decrease per 1 % increase in void content. This data is presented in Table 7 for reference. Similar to the maximum measured storage modulus data presented in Figure 49, the data presented in Figure 51 clearly shows that, although the magnitude of the maximum measured loss modulus at a given void content is frequency dependent, the observed negative trend seen in the relevant measurement is, based on these empirical results, frequency independent.

Table 7: Frequency-based percent decrease in the maximum measured loss modulus (E") over the entire empirical range and per 1% added void content

Test Frequency (Hz)	Total Decrease in E" (%)	Decrease in E" per % void (%)
0.5	49.24	8.21
1	46.47	7.74
2	45.20	7.53
5	43.84	7.31
10	42.03	7.01

Similar to the format used to present the maximum measured storage modulus, at 1 Hz, as a function of void content, the maximum measured loss modulus, with associated sample standard deviations, is presented in Figure 52. As has been the standard up to this point, a linear trend line was added to Figure 52 for the purpose of showing a seemingly linear relationship in the empirical data, only within the experimental window. Similar to what was seen in the maximum measured storage modulus data, the maximum measured loss modulus data is also subject to two stacked, or vertically coincident, data points at 6.7 % void content on the x-axis. This is shown in both Figure 51 as well as Figure 52. As was the case prior, these stacked data points correspond directly to the nominal 200 mm per minute and 250 mm per minute specimen groups which exhibit nearly identical nominal void content. In keeping with the storage modulus trend, the nominal values for maximum measured loss modulus at these two points, at 1 Hz, lie within the sample standard deviations of each other, and as such, cannot be readily distinguished as being significantly different from one another. The data that is presented in Figure 52 is tabulated in Table 8 for reference. The two vertically coincident data points are highlighted in Table 8.
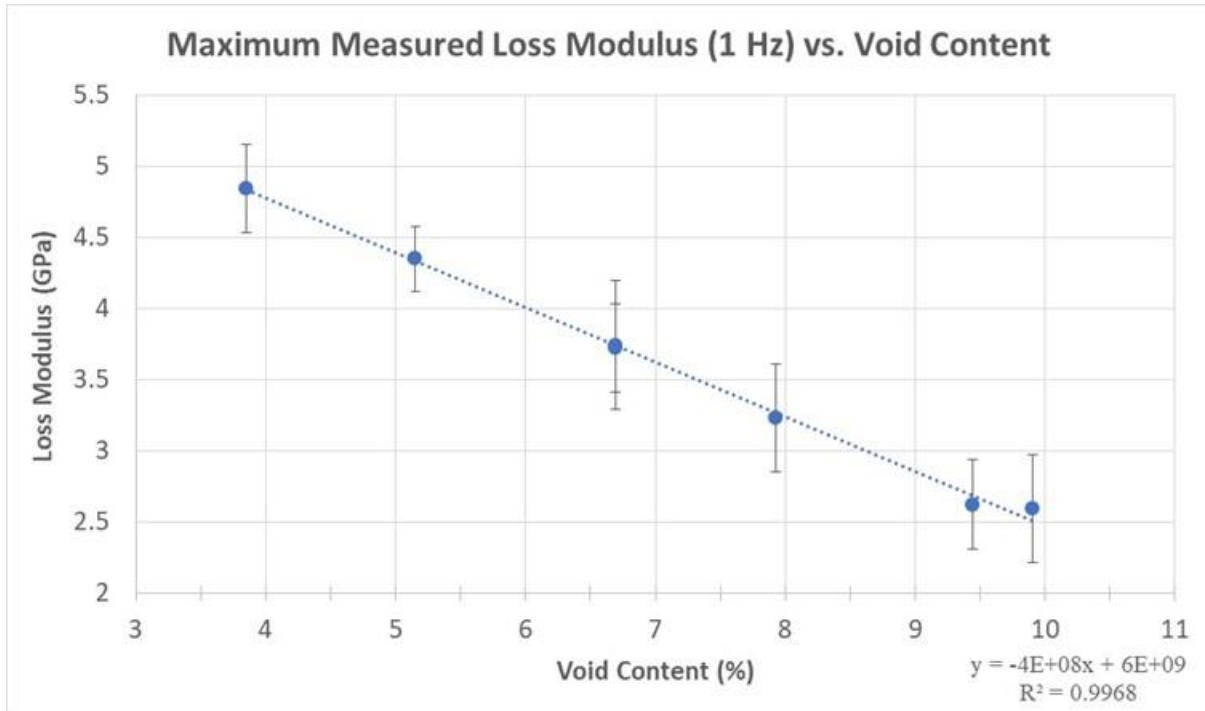
Figure 52: Maximum measured loss modulus, at 1 Hz, with associated sample standard deviations

Table 8: Maximum measured loss modulus, at 1 Hz, with associated sample standard deviations

Print Speed (mm/min)	Void Content (%)	E" at 1 Hz (GPa)	St.Dev (GPa)
100	3.85	4.85	0.31
150	5.15	4.35	0.23
200	6.69	3.75	0.45
250	6.69	3.73	0.31
300	7.93	3.23	0.38
350	9.44	2.63	0.32
400	9.90	2.60	0.38

3.11.3 Glass Transition Temperature (Tg) as a Function of Void Content

There are a variety of methods that can be used to determine the glass transition temperature for a neat polymeric, or polymer matrix composite, specimen using the results of a temperature scanning DMA experiment. In general, all methods utilize the appearance of specific phenomena in the data obtained for either the storage modulus (E'), loss modulus (E") and or the damping factor (tan δ) and then correlate that phenomena to the temperature at which it occurs. Typical methods to determine the glass transition temperature include using the onset

of the increase in the tan δ curve, the peak of the tan δ curve, the onset of the E' drop, the onset of the increase in the E" curve or the peak of the E" curve [52]. Choosing a method for the determination of Tg is largely dependent on idiosyncrasies that relate to the particular goals of the relevant study, coupled with the background of the experimentalist. The relevant ASTM for the determination and reporting of dynamic mechanical properties, ASTM D4065, recommends using the peak of the tan δ as general practice, while also acknowledging that the other phenomena previously described can also indicate the glass transition temperature [54].

For the purpose of this work, the glass transition temperature is determined based on the peak value of the E" curve at 1 Hz. Literature concerning the correlation between both DMA and DSC based methodology for determining the glass transition temperature of polymers indicates that choosing Tg based on the maximum value of the loss modulus (E"), explicitly at 1 Hz, corresponds to the mid Tg observed in DSC [56]. For reference, it has been reported that, in isolated cases, differences between Tg determined from the maximum E" and the mid Tg from DSC can be as much as $\pm$ 10 °C; however, it should be noted that there is much less correlation between the mid Tg from DSC and the Tg as determined by the peak of the tan δ curve [56].

The glass transition temperature was determined for all six DMA specimen within each of the seven print-speed based specimen groups. As mentioned previously, the glass transition temperature was taken as the temperature at which the measured loss modulus (E") of the relevant specimen reached a maximum, graphically this is expressed as the peak of the E" curve, during the 1 Hz scan. The seven sets of six glass transition temperatures were used to determine nominal values of the glass transition temperature for each print speed, or void content, based specimen group. These nominal values, with associated sample standard deviations, are

113

graphically displayed in Figure 53. Note that a linear trend line has been added for the purpose

of showing the general linearity, or lack thereof, in the window of empirical data.
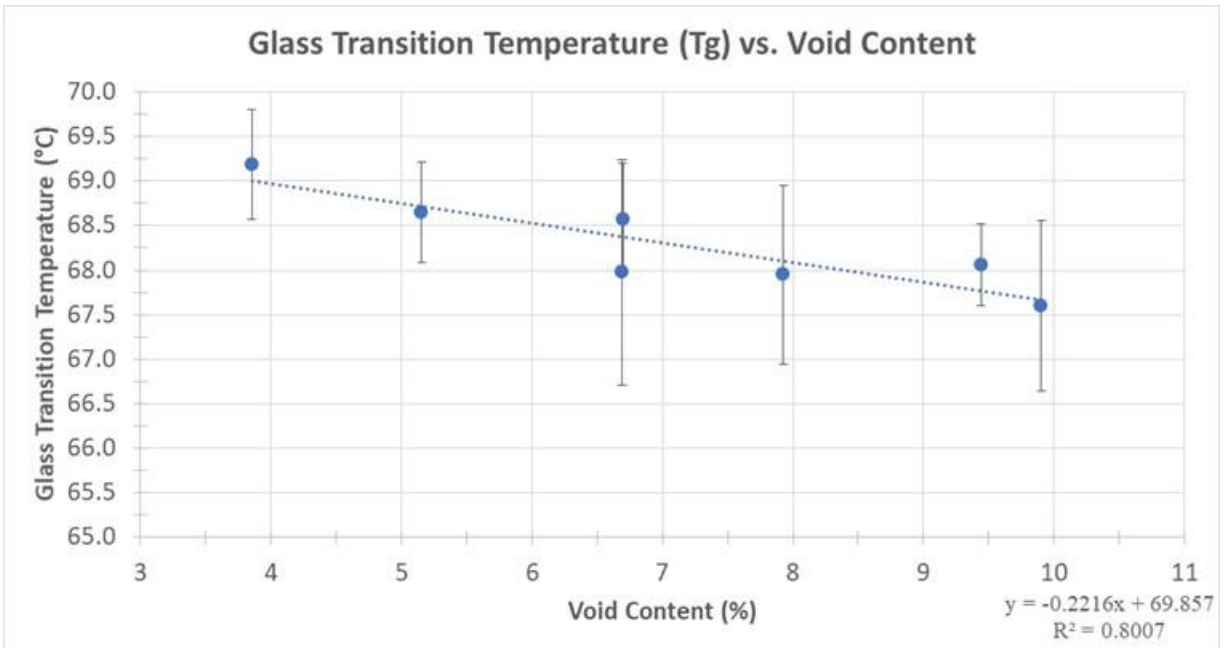
Figure 53: Glass transition temperature as a function of void content

In examining Figure 53, it is apparent that the two data points that share the same

nominal void content, those belonging to the 200 mm per minute and 250 mm per minute

specimen groups, are again stacked in such a way that the associated standard deviations make it

difficult to discern one nominal value as being statistically different from the other nominal

value. That being said, a general negative trend is seen in the glass transition temperature as

void content in the printed composites is increased. Despite the seemingly small range of

measured glass transition temperatures, as well as the relatively large sample standard deviations,

this apparent negative trend is tenable based on the first (graphically the left-most data point) and

last (graphically the right-most data point) data points coupled with their associated sample

standard deviations. Based on the nominal data presented in Figure 53, an approximate 6 %

increase in nominal void content correlates with a nominal 1.6 °C (2.3 % from the baseline) drop

in the measured glass transition temperature. The data that is graphically displayed in Figure 53 is tabulated for reference in Table 9 with the 200 and 250 mm per minute data points highlighted.

Table 9: Glass transition temperature from E" max at 1 Hz with associated sample standard deviations

Print Speed (mm/ min)	Void Content (%)	Tg from E" $_{max}$ (°C)	St.Dev (°C)
100	3.85	69.2	0.62
150	5.15	68.7	0.57
200	6.69	68.0	1.27
250	6.69	68.6	0.63
300	7.93	68.0	1.00
350	9.44	68.1	0.46
400	9.90	67.6	0.96

3.11.4 Maximum Measured Damping Factor (tan δ) as a Function of Void Content

The maximum measured damping factor (tan δ) is a commonly reported, and or discussed, value in the relevant literature regarding DMA temperature scans of polymers and polymer matrix composites [19,20,34–38]. The maximum measured damping factor, as previously mentioned, represents the mathematical ratio of E" to E' at any temperature within a given DMA temperature scan. As such, the maximum measured damping factor provides a quantitative, dimensionless representation of a given material's ability to dissipate mechanical strain energy as heat. Typically, the maximum measured damping factor occurs within the glass transition region of the relevant polymer or polymer matrix composite. This phenomenon is most readily attributed to the notable decrease (multiple orders of magnitude) in storage modulus (E'), coupled with the notable increase in loss modulus (E") that results as a function of the relatively drastic increase in polymer chain mobility that occurs during the glass transition. Typical graphical outputs of the damping factor, as measured over a given temperature range which is inclusive of a glass transition, tend to resemble something analogous in appearance to a bell curve, where the maximum (or peak) value is observed at the point of apogee. Typical graphical outputs of the damping factor for three different additively manufactured specimens

from the relevant literature, and not from this work, are shown for reference in Figure 54 [20].

Note that the point of apogee is distinguished for the three damping factor curves (loss tangent in

the cited work) in Figure 54.
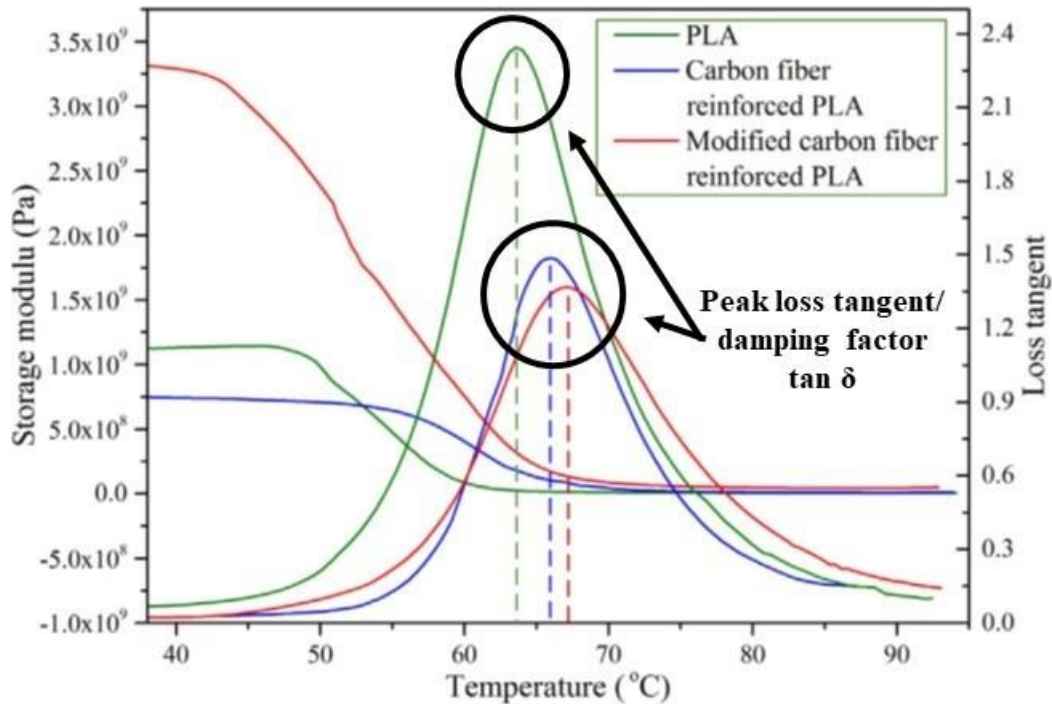
Figure 54: Example of the typical graphical appearance of the damping factor during a
temperature sweep through the glass transition region [20]

Seeing as Figure 54 shows what is common in the DMA literature for graphical outputs

of the damping factor tan δ, it is appropriate to show the graphical output of the damping factor

as measured in the current work. Figure 48 shows a representative graphical output from a DMA

scan relevant to this work; however, the relatively atypical appearance of the damping factor

curves was not addressed in the section containing Figure 48. As such, Figure 55 has been

included for the purpose of emphasizing the atypical nature of the graphical representation of the

damping factor over the temperature sweep used for the DMA scans relevant to this work.

Figure 55 illustrates this atypical behavior, for all five tested frequencies, for a DMA specimen

from the 100 mm per minute specimen group. Note that the damping factor in Figure 55 does

not resemble a bell curve with a discrete point of apogee, as shown in Figure 54, but rather

shows an expected increase in damping factor around the glass transition temperature of the PET

thermoplastic matrix (~ 71 °C), followed by a more gradual increase up until the final

temperature of the scan (~ 90 °C). Note that this atypical damping factor behavior is apparent at

all tested frequencies, for all tested specimens from all of the print speed based specimen groups.
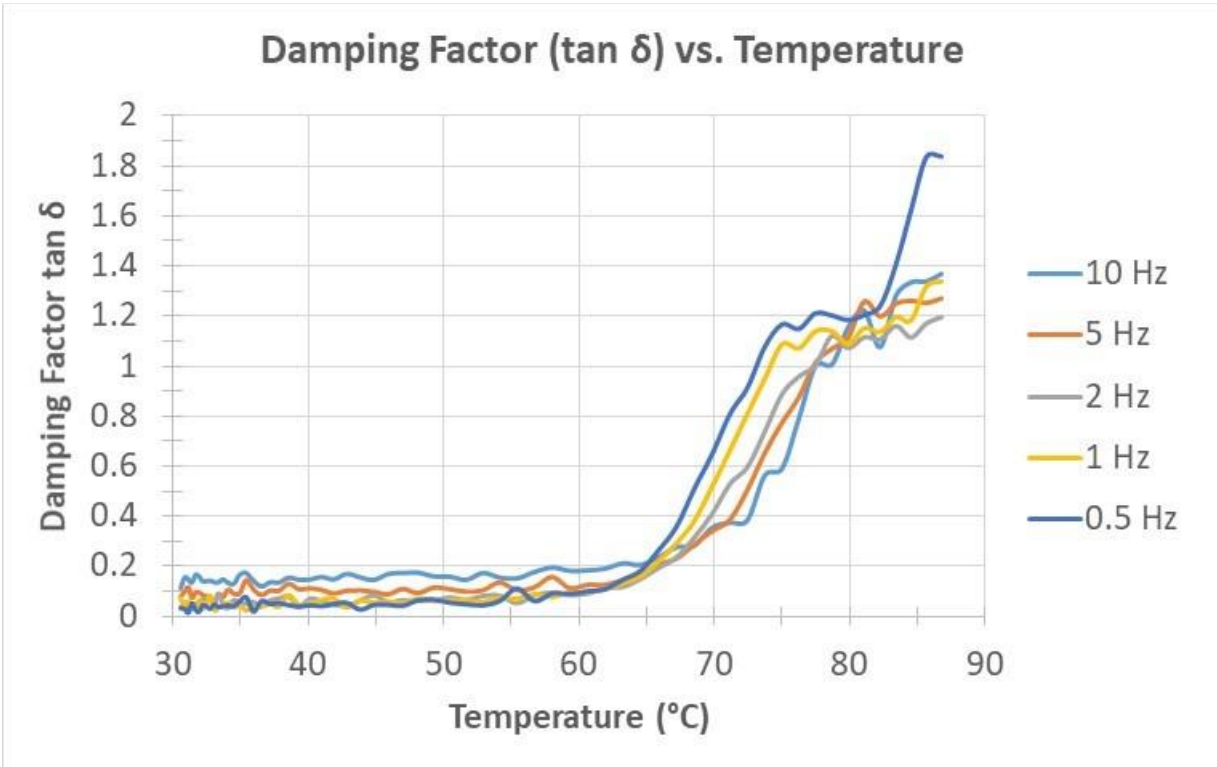
Figure 55: Damping factor, at all tested frequencies, as a function of temperature for a single
specimen from the 100 mm/ minute group

In consideration of the atypical damping factor behavior that was common to all tested

samples in this work, the maximum measured damping factor typically occurred well beyond the

glass transition region of the PET thermoplastic matrix, almost always at the final temperature in

the applied temperature scan. As such, the nominal value of maximum measured damping factor

for each specimen group, averaged over all six tested specimen per group, are coincidentally

atypical. Nominal values of the maximum measured damping factor for each of the seven print

speed based specimen groups are plotted as a function of the nominal void content associated

with the relevant specimen group, for all tested frequencies, in Figure 56. Note that color coordinated lines are used to join the nominal values of maximum measured damping factor for each specimen group for the purpose of more readily distinguishing the five data sets from one another.
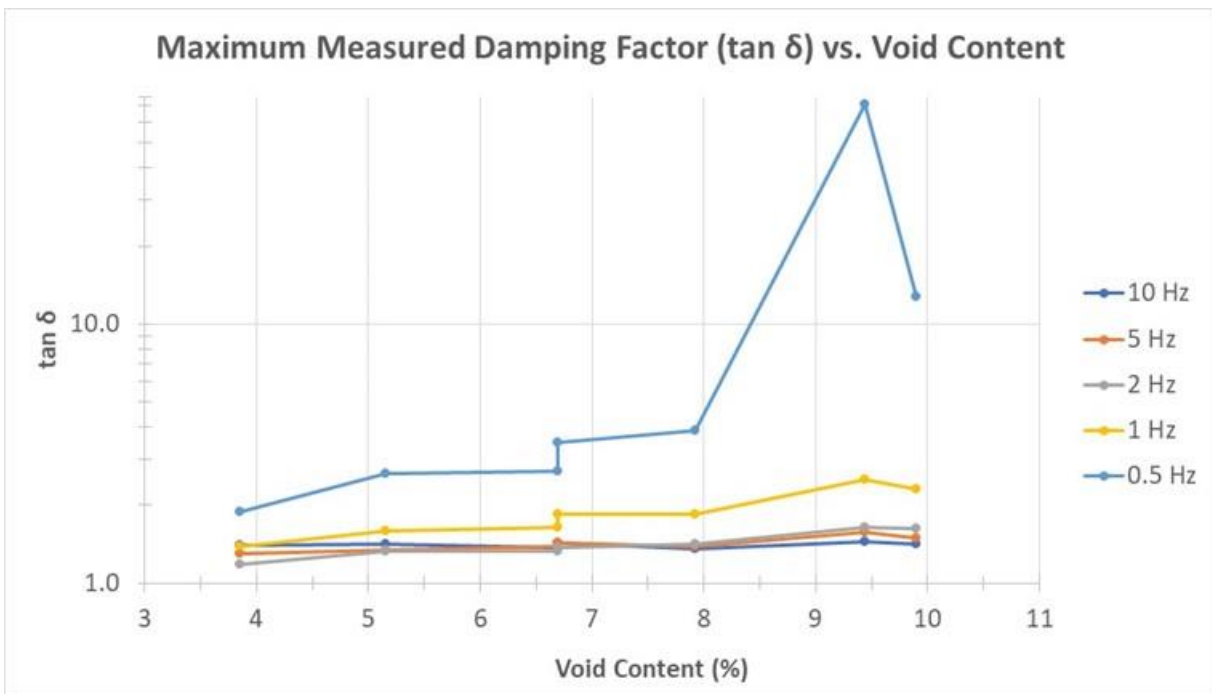
Figure 56: Maximum measured damping factor as a function of void content, note the log scale used for damping factor (y-axis)

In examining the data of Figure 56, a variety of phenomena must be acknowledged. Firstly, note that a log scale was required for the y-axis, in this case the magnitude of the damping factor, tan δ. A log scale was required to facilitate viewing of all of the relevant data points, as the nominal values of maximum damping factor for the 0.5 Hz frequency exhibited very large magnitudes relative to data points for the other four tested frequencies. Secondly, it should also be noted that Figure 56 also shows the same stacked, or vertically coincident data points at ∼ 6.7 % void content. This is consistent with the entirety of the data presented up to this point. In keeping with the standard of presentation of the results up to this point, percent changes in the maximum measured damping factor for all frequencies as a function of void

118

content are included in Table 10. Note that the percent increase in the maximum measured

damping factor decreases drastically from 0.5 Hz to 10 Hz. A similar decrease in the percent

damping factor increase per percent increase in void content is also apparent. Clearly these

results indicate some level of frequency dependence; however, it is unclear if the apparent

frequency dependency of the percent changes in the maximum measured damping factor is

significant as the maximum measured damping factor occurs outside of the typical, expected

range. Note that the expected range was established in Figure 27, which shows the entire glass

transition is complete by approximately 80 °C.

Table 10: Percent changes in the maximum measures damping factor over the empirical range

Test Frequency (Hz)	Total Increase in tan δ (%)	Increase in tan δ per % void (%)
0.5	85.21	14.20
1	39.73	6.62
2	27.03	4.51
5	12.24	2.04
10	1.60	0.27

Moving forward, and in keeping with the presentation of results up to this point, the

maximum measured damping factor for each print speed specimen group, at 1 Hz, is presented in

Figure 57 with associated sample standard deviations. Note that a linear trend line was added to

Figure 57 to show the general linearity of the empirical data within the relevant experimental

window. The data graphically presented in Figure 57 is tabulated in Table 11 for reference, with

the 200 and 250 mm per minute data points highlighted.
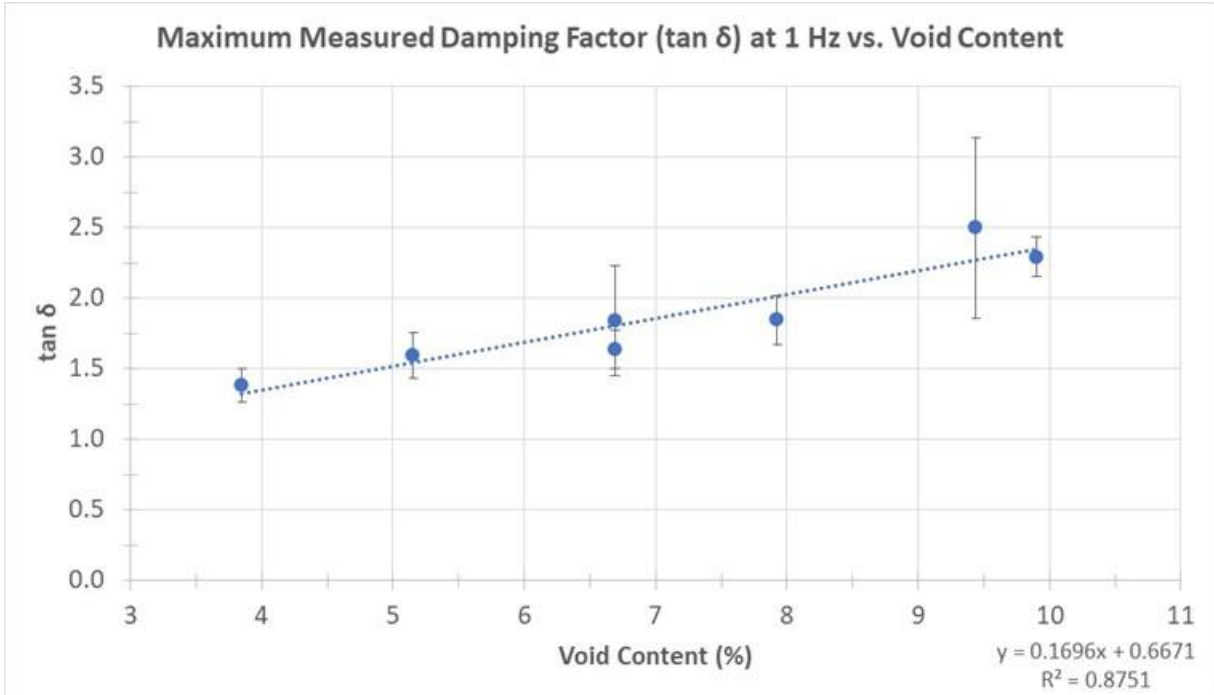
Figure 57: Maximum measured damping factor, at 1 Hz, with associated sample standard deviations

Table 11: Maximum measured damping factor, at 1 Hz, with associated sample standard deviations

Print Speed (mm/ min)	Void Content (%)	Max Measured tan δ	St.Dev (tan δ)
100	3.85	1.38	0.12
150	5.15	1.59	0.16
200	6.69	1.64	0.13
250	6.69	1.84	0.39
300	7.93	1.85	0.18
350	9.44	2.50	0.64
400	9.90	2.30	0.14

3.12 Metallographic Evaluation

Measurement of void content in the as-tested DMA specimens requires complete consumption of the specimens in a high temperature muffle furnace, leaving only the continuous reinforcement behind, and as such, metallography of the as-tested specimens is impossible. In consideration of the unavoidable destruction of the DMA specimens, additional specimens for each of the print speed groups were additively manufactured during the specimen preparation phase and allocated for use as representative metallographic samples. Following DMA analysis

and void content measurements, these pre-allocated specimens were mounted in acrylic resin and

ground for the purpose of comparing cross-sectional geometry, visual void content and void size

and location. Representative specimens from the 100 mm per minute, 250 mm per minute and

400 mm per minute print speed groups are shown in Figure 58. Figure 58 is used as a qualitative

tool to quickly verify the previously reported measurements of both specimen cross-section

variation and void content.
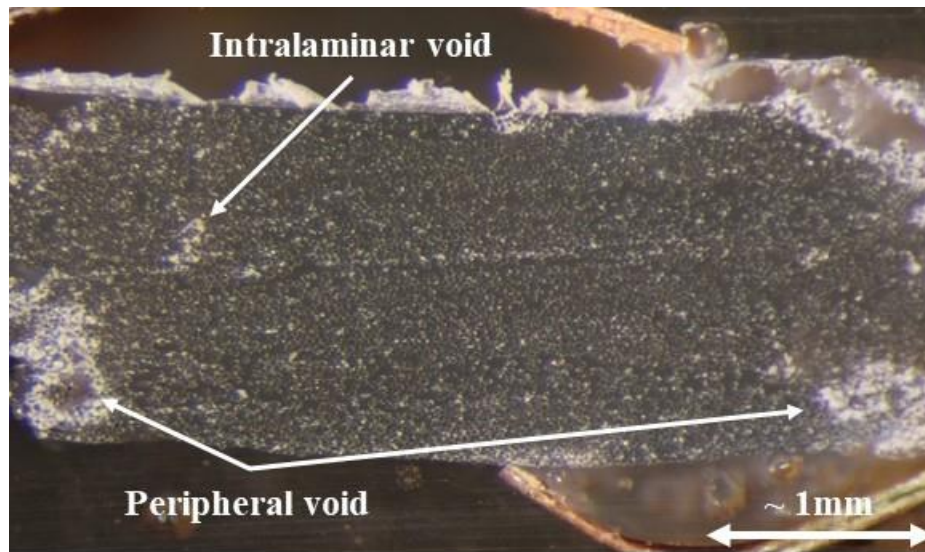
(a)
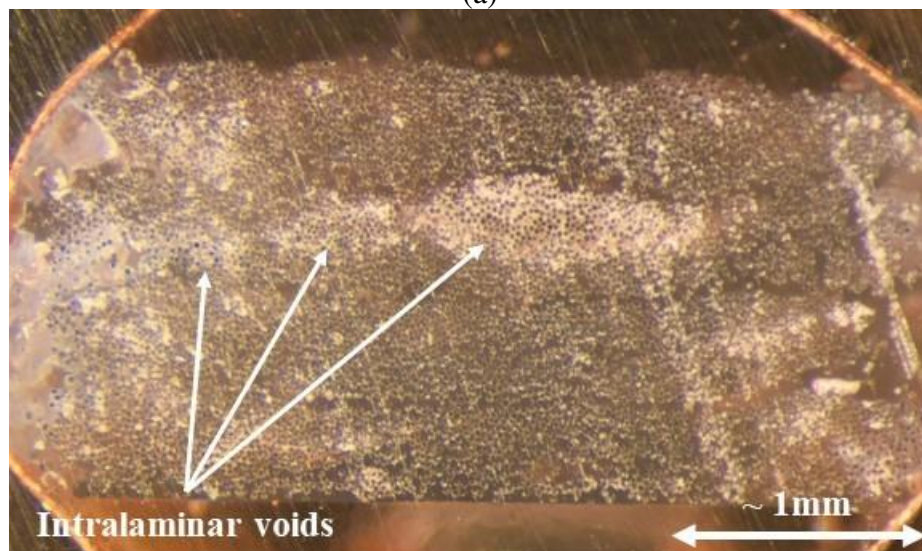
(b)
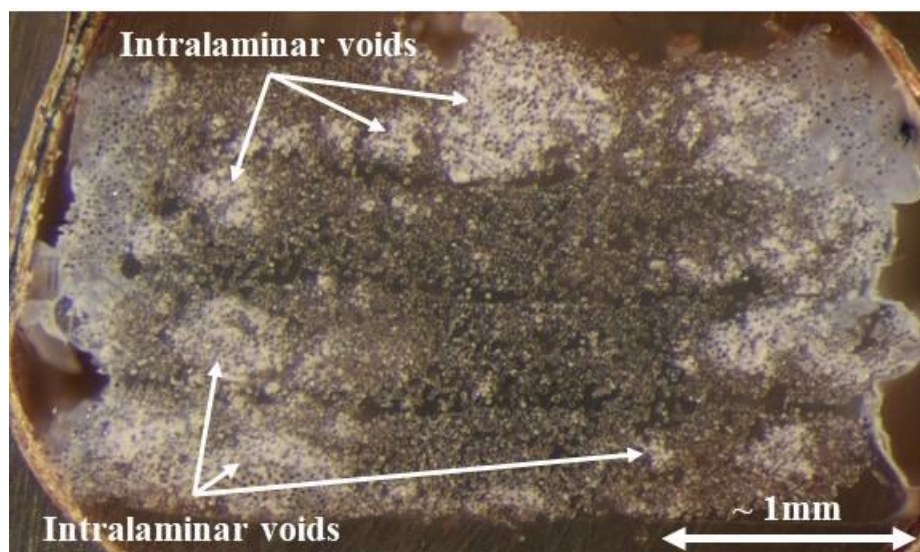
(c)

Figure 58: Representative DMA cross-sections for geometry and void content comparison (a) 100 mm/ minute (b) 250 mm/ minute (c) 400 mm/ minute

Examination of the three cross-sections shown in Figure 58 should yield an immediate visual correlation between the print speed used to additively manufacture the representative specimens and the void content therein. Void content clearly increases with increasing print speed, with the location of the void content almost exclusively in intralaminar regions or at the periphery of the representative specimens. Intralaminar void content is indicated, to differing extents, in all cross-sections shown in Figure 58. Note that void content at the periphery of the cross-sections is present in all cross-sections, but only explicitly indicated in cross-section (a). Separately, the variation in sample cross-section should be readily apparent, where variation is most pronounced in comparing cross-section (a) and cross-section (c). A final, notable visual takeaway from Figure 58 is the appearance of larger interlaminar regions between the printed layers of the representative DMA specimens as print speed is increased. These regions are not explicitly measured; however, as all of the images were taken under the same conditions, it is reasonable to assume that the visual discrepancy in interlaminar thickness, which is a matrix rich

region, is tenable. Cross-sections (a) and (c) are shown again in Figure 59 for comparison of the visual discrepancies in interlaminar thickness.
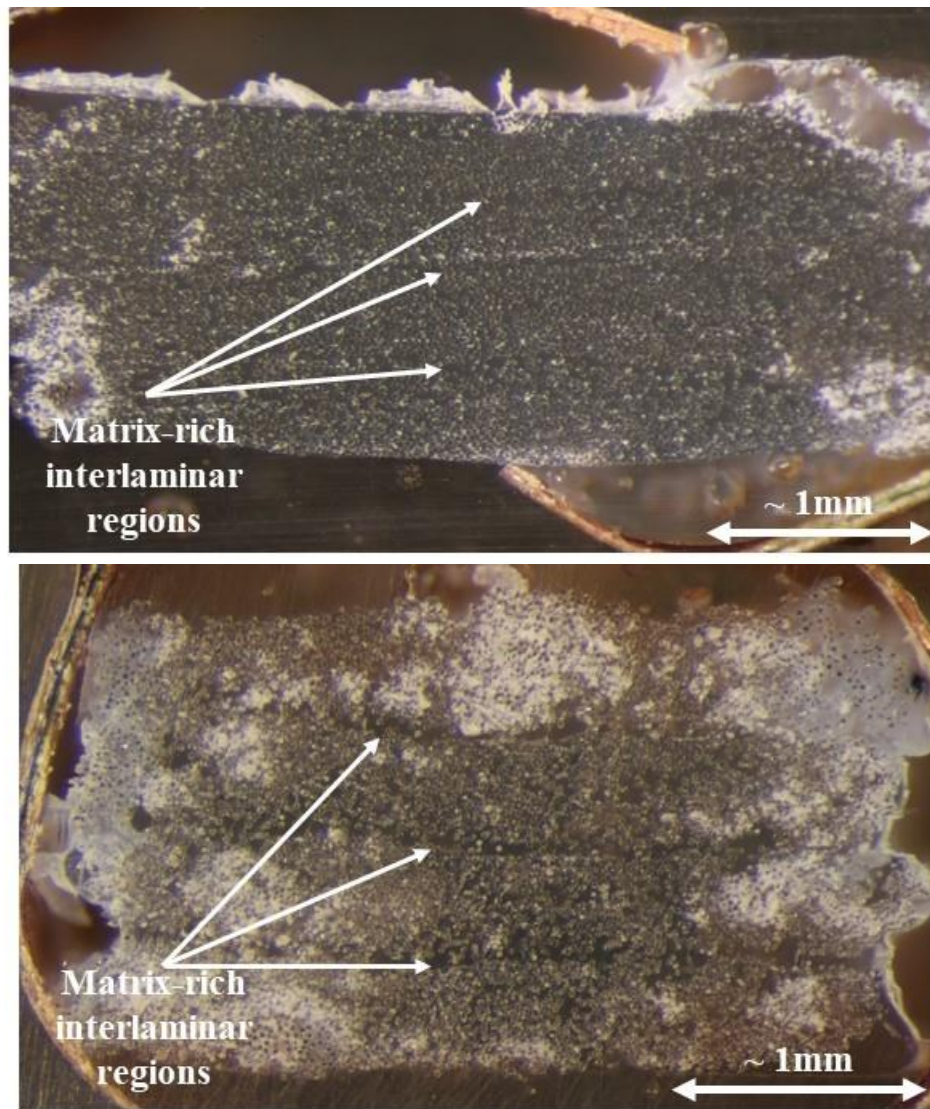
Figure 59: Visual comparison of the 100 mm/ minute and 400 mm/ minute cross-sections with matrix-rich interlaminar regions indicated

4 Expanded Discussion – Major Experimental Effort

The following chapter serves to more thoroughly interpret and discuss the results of the major experimental effort, specifically in terms of trends in the data and relevant analogues from literature. Notable results will be revisited in terms of specific follow-up experimentation, based on themes from the major experimental effort. Following discussion of the results of the major experimental effort, prospective future work is proposed to conclude the chapter.

4.1 Print Speed & Void Content

The fundamental assumption driving the major experimental effort was that void content in the printed composites could be functionally modified through changes in the print speed process parameter. This assumption was verified by the results of the void content measurements from the DMA specimens, where the nominal void content for each of the seven print speed based specimen groups increased with increasing print speed. The increasing trend in nominal void content was consistent at the majority of the data points, with a notable exception being a shared nominal void content between the 200 mm per minute and 250 mm per minute specimen groups. For reference, the data relevant to this conversation is presented again in Table 12, with the 200 mm per minute and 250 mm per minute data highlighted for quick reference.

Table 12: DMA specimen print speed relative to nominal void content and the associated sample standard deviation

Print Speed	Nominal Void Content (%)	Sample St.Dev (%)
100	3.85	1.14
150	5.15	0.34
200	6.69	0.92
250	6.69	0.47
300	7.93	1.23
350	9.44	1.02
400	9.90	1.03

The highlighted data in Table 12 shows that the 200 mm per minute and 250 mm per minute data points share a nominal void content of ~ 6.7 % by volume, with associated sample standard deviations that effectively overlap each other. As a result of this empirical phenomenon, it is difficult to resolve whether the two relevant data points are statistically different from one another. As previously mentioned, there is no reason to believe that the magnitude of the sample standard deviation for any of the nominal void content measurements reported follows any trend in direction or magnitude, and as such, a standard deviation-based explanation of the shared nominal void content between in the 200 mm per minute and 250 mm per minute specimen groups is not reasonable. In consideration of the data, the most readily available explanation of the shared nominal void content between the 200 mm per minute and 250 mm per minute specimen groups is likely founded in some chance interaction between the relevant process parameters. Note that the relevant process parameters are print speed, print temperature, print bed temperature and applied spring force.

Shown graphically in the last chapter, the empirical relationship between print speed and nominal void content is reasonably well fit with a linear regression, within the relevant experimental window. Relevant work exploring the effects of void content on continuous fiber reinforced thermoplastics from a commingled glass/ polypropylene precursor found a similar relationship in terms of void content as a function of time, at process temperature, under applied

consolidation pressure [55]. The empirical results from this work are graphically compared to

the empirical results from [55] in Figure 60. Note that the range of void content from [55] that is

relevant to this work is encircled for visualization.
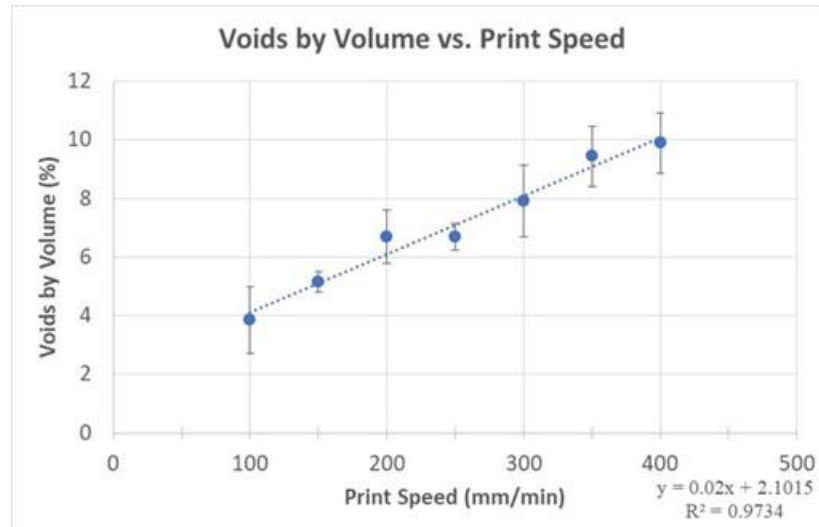
(a)
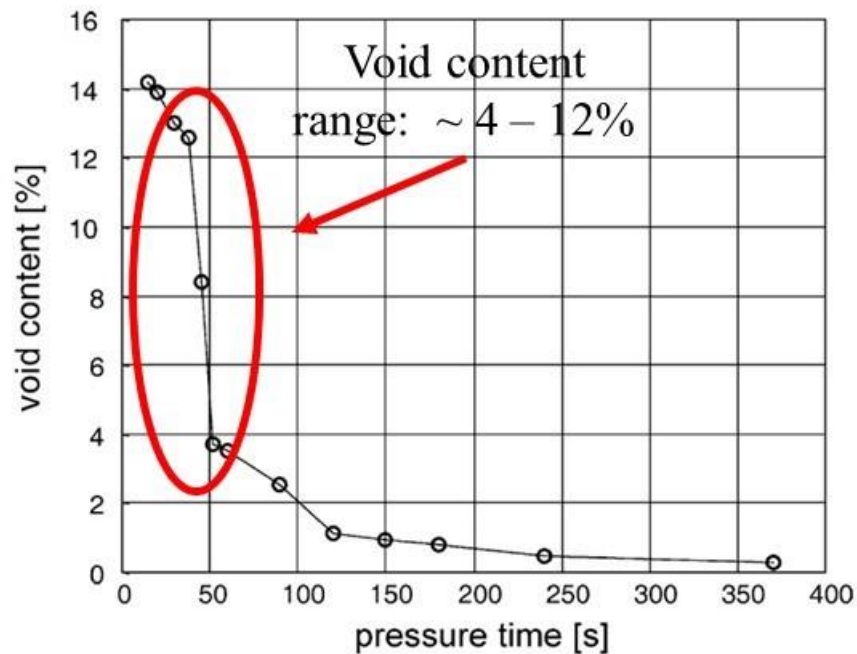
(b)

Figure 60: Comparison of (a) void content vs. print speed from this work and (b) void content versus pressure time from [55]

The comparison made in Figure 60 should serve only as a verification of the direction of

the void content vs. print speed relationship recorded in the current work. In the current work, as

print speed is increased, the available time for in-situ consolidation of the commingled precursor is decreased. This is a direct analogue to the scheme of the horizontal axis used in Figure 60 (b), where "pressure time" increases from zero seconds to 400 seconds. For clarification, the use of different schemes for the horizontal axes in Figure 60 (a) and (b) explains the difference in the sign of the slope that is notable when cross-examining the images. Similarly, note that Figure 60 (b) displays discrete data points joined by solid lines, likely for visualization, whereas Figure 60 (a) displays discrete data points with a linear regression fit to the data set.

4.2 Visual Evaluation

The images presented in Chapter 3 for visual evaluation of the printed continuous fiber reinforced DMA specimens are presented again in Figure 61. Note that the pre-DMA and post-DMA specimens are shown adjacent to each other to facilitate direct comparison of the specimen surfaces. As previously stated, it is clear that the relative opacity of the DMA specimens increases with increasing print speed. In consideration of the changing opacity, it is reasonable to assume that visible changes in the transparency of the DMA specimens can be related to the increasing void content that was recorded with increasing specimen print speed. This relation is further supported by the micrographs presented in the metallographic evaluation in Chapter 3, where the presence of intralaminar void content increases in the representative specimen, most notably from the 100 mm per minute specimen to the 400 mm per minute specimen. The relevant micrographs, specifically the 100 mm per minute (a) and the 400 mm per minute (b), are included again in Figure 62 for reference.
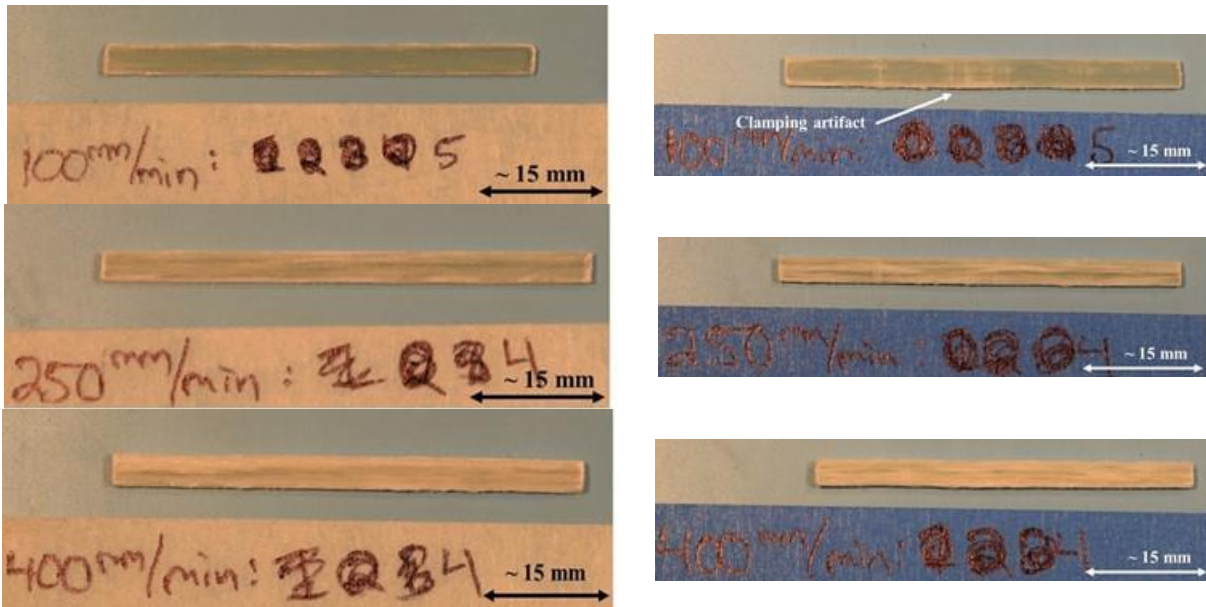
Figure 61: Visual comparison of DMA specimens before (left) and after (right) DMA evaluation

(a)   (b)
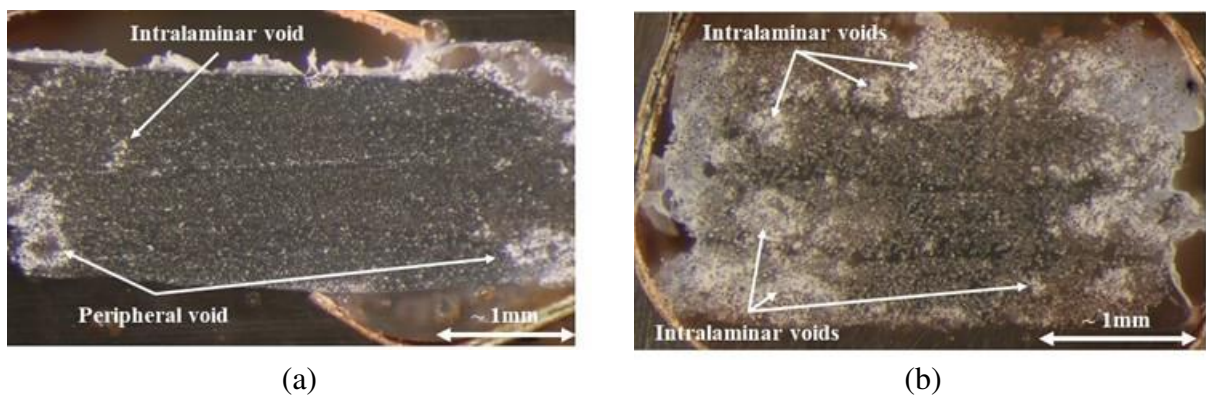
Figure 62: Representative DMA cross-sections showing notable, visible differences in intralaminar void content between the (a) 100 mm/ minute and (b) 400 mm/ minute conditions

As mentioned in Chapter 3, visible clamping artifacts imparted by the DCB fixture in use are apparent in the tested DMA specimen, with some exemplary specimens shown in Figure 61. It is notable that the clamping artifacts are most visible on the 100 mm per minute specimen and least visible on the 400 mm per minute specimen. This is intuitive in consideration of the increasing opacity, which correlates to void content, in the images shown in Figure 61 and Figure 62. Seeing as clamping artifacts were present in all tested DMA specimens, any potential effects of the artifacts in the context of damage to the specimen are not considered to vary in impact or significance with respect to the thermomechanical data. Fundamental literature

regarding Dynamic Mechanical Analysis suggests that a certain amount of shearing strain is imposed upon a relevant specimen when it is clamped in a single or double-cantilever fixture at both the mid-span and outboard clamps [52]. As such, it is likely that the visible artifacts on the DMA specimens after evaluation in the DMS6100 are related to this fixture-imparted shearing strain.

4.3 Maximum Measured Storage Modulus as a Function of Void Content

The notable outcome of examining maximum measured storage modulus (E') as a function of void content in the printed continuous fiber reinforced thermoplastic matrix composite DMA specimens is the presence of a clear negative trend in storage modulus with increasing void content. The observed trend is in direct agreement with two highly relevant studies that have already been cited in relation to the current work, one regarding the effects of pre-process fiber modification on the mechanical performance of additively manufactured continuous fiber reinforced PLA [20] and the other regarding the effects of void content on the thermomechanical performance of carbon/ epoxy laminates by DMA [37].

The work performed in [20] found that pre-process fiber surface modification resulted in a drastic increase in the maximum measured storage modulus of printed DMA specimens as compared to specimens printed with untreated reinforcement. The increase in maximum measured storage modulus was directly attributed to an enhanced interfacial bond in the printed specimens using the modified reinforcement, in conjunction with the presence of defects (voids) in the printed composite material using the untreated reinforcement. The work performed in [37] found that, by introducing various levels of void content in the processed carbon/ epoxy laminates, the measured elastic stiffness of the DMA specimen (similar to storage modulus) exhibited a negative trend with increasing void content. Graphical results from both [20] and

[37] are shown in Figure 63. In examining Figure 63, it should be clear that the results of the

current work, in terms of storage modulus as a function of void content, are consistent with what

has been observed in the relevant literature.

(a)

(b)
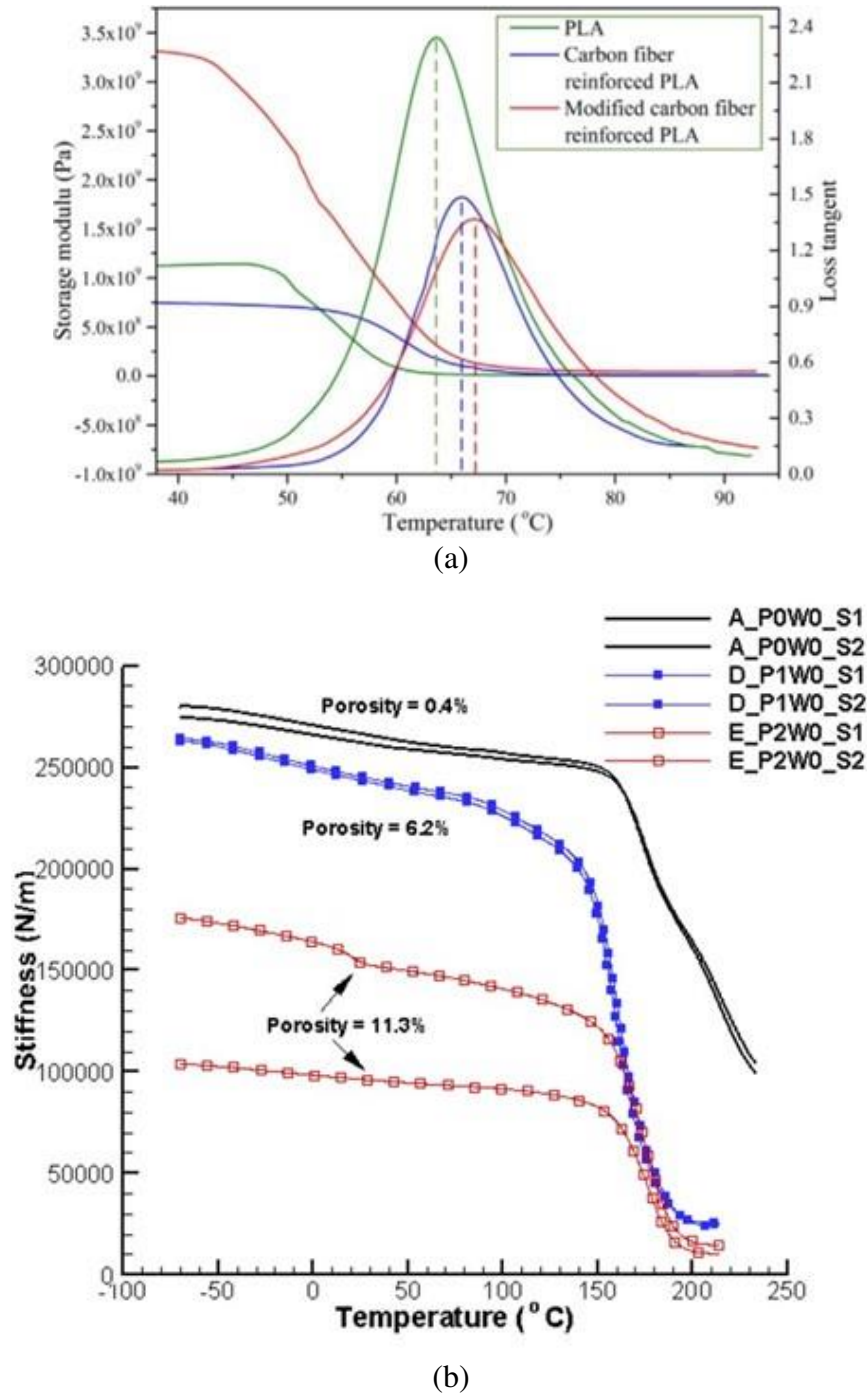
Figure 63: Results comparison from (a) [20] and (b) [37] showing a negative trend in E' with increasing defects

In determination of the constituent content, by means of the relevant ASTM standard [48], for the printed DMA specimens in this work, notable variation in fiber volume fraction was observed with increasing print speed. It should be intuitive that as void content increases, either matrix content, fiber content, or some combination of both phases, must decrease in order to accommodate any volume of void content in a given geometrically constrained specimen. Using a basic Rule of Mixtures (ROM) approach for prediction of the elastic modulus of a unidirectional continuous fiber reinforced composite material with relatively high fiber volume fraction (~ 50 %), it should be clear that the elastic modulus of the reinforcing fiber is the dominant material property in the calculation of the elastic modulus of the composite material. This is attributed to the relatively large elastic modulus inherent to the reinforcing fibers, as compared to the relatively small (typically one or two orders of magnitude smaller) elastic modulus inherent to the polymer matrix. In consideration of the dominance of the reinforcement properties, any comparative analysis of the mechanical performance of composite materials should take this fiber volume content variation into account. Variation in fiber volume content in the printed DMA specimens, as a function of print speed (analogous to void content) is shown in Figure 64. The data presented in Figure 64 is tabulated for reference in Table 13.
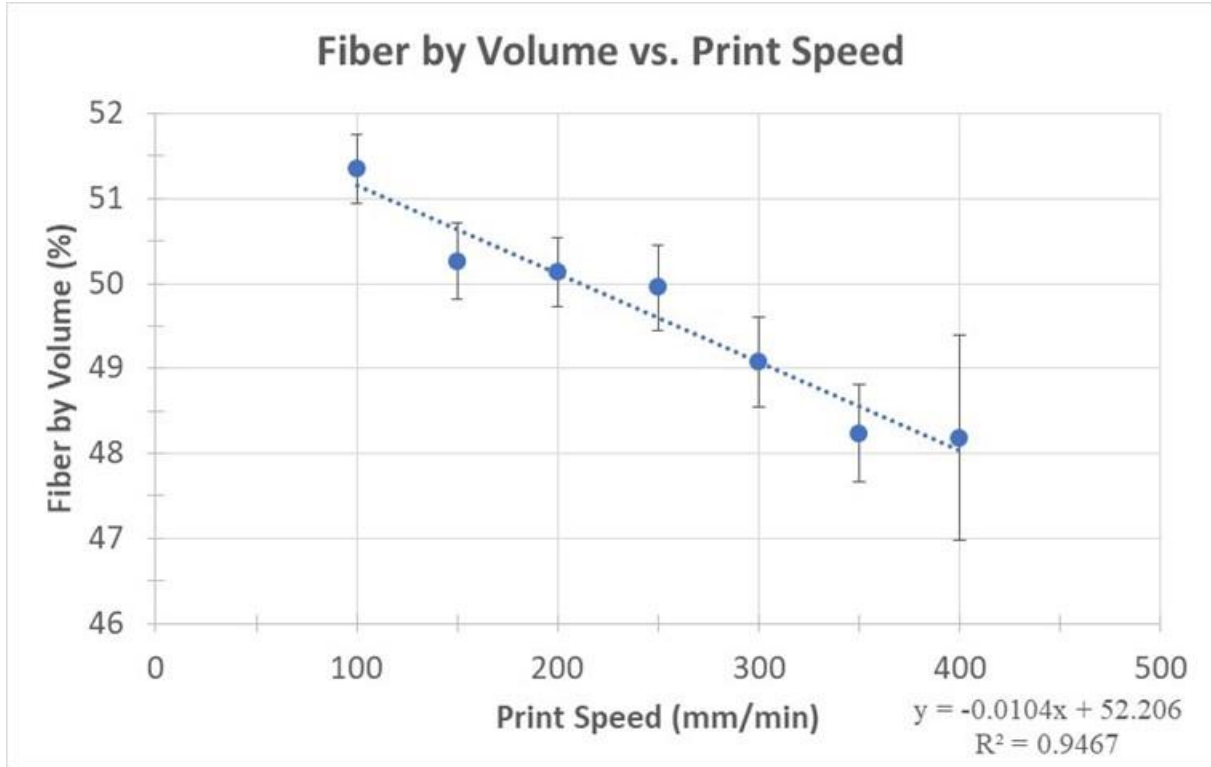
Figure 64: Nominal fiber volume content, with sample standard deviations, as a function of DMA specimen print speed

Table 13: Nominal fiber volume content, with sample standard deviations, as a function of DMA specimen print speed

Print Speed	Nominal Fiber Volume Content (%)	Sample St.Dev (%)
100	51.35	0.41
150	50.26	0.45
200	50.13	0.40
250	49.95	0.51
300	49.08	0.53
350	48.24	0.57
400	48.18	1.21

Using nominal values (MatWeb [57]) for the elastic moduli of E-Glass fiber (~ 72 GPa) and amorphous PET thermoplastic (~ 2.8 GPa) as well as the maximum and minimum nominal fiber volume contents from this work, Table 13, a simple Rule of Mixtures (ROM) prediction of the in-plane (fiber direction in this case) elastic modulus of a unidirectional E-Glass/ PET composite can be made (assuming no void content). Using both the maximum (51.35 %) and

132

minimum (48.18 %) fiber volume contents from the current work, ROM yields in-plane elastic

moduli for the composite material ranging from ~ 38 GPa to ~ 36 GPa respectively.

The in-plane elastic modulus is known to correlate with the flexural elastic modulus, and

as such, the flexural storage modulus by DMA. Under the assumption that the flexural storage

modulus is analogous, but not identical, to the flexural in-plane elastic modulus measured using a

quasi-static mechanical test, these simple ROM calculations imply that the effect of the measured

variation in nominal fiber volume content on the maximum measured storage modulus, across

the range of DMA specimens, is minimal in comparison to sum total effect of void content. In

consideration of the measured variation in the fiber content by volume, it is important to note

that there is similar variation in the matrix content by volume, ranging from ~ 44.8 % (100 mm

per minute) to ~ 41.9 % (400 mm per minute). Seeing as the contribution of the PET matrix to

the magnitude of the elastic modulus of the composite material is minimal compared to the

contribution of the reinforcement, the variation in matrix content by volume is deemed negligible

in this context. For reference, the variant of ROM used to determine the in-plane elastic modulus

for the void-less, unidirectional E-Glass fiber reinforced PET composite material used in the

example above is provided, Equation 4.1. Note that E_f is the fiber elastic modulus, E_m is the

matrix elastic modulus and V_f is the fiber volume content.

$$E_{Composite} = E_f V_f + E_m (1 - V_f) \qquad\qquad (4.1)$$

4.4 Maximum Measured Loss Modulus as a Function of Void Content

The results of this work indicate a negative trend in the maximum measured loss modulus

(E") with increasing void content. As mentioned earlier in the current work, the maximum

measured loss modulus is typically observed within the glass transition region and is often used

as an indicator of the glass transition temperature of the relevant polymer or polymer matrix

composite. More generally, the loss modulus serves as a representation of a polymers ability to dissipate strain energy, as heat, through internal motions. In consideration of the relevant DMA literature, it is not uncommon for studies to report differences in the maximum measured loss modulus relative to the temperature at which the maximum E" is measured; however, it is uncommon to see commentary on the significance of the magnitude of E" at this point in the DMA scan, despite the fact that it serves as a local maximum in the experiment [34,36,38].

With regard to this work, within the tested temperature range, it is assumed that the viscoelastic material response is heavily influenced by the amorphous PET thermoplastic matrix, as well as the interface between the PET matrix and the continuous E-Glass reinforcement. As such, it is likely that the negative trend in the maximum measured loss modulus, with increasing void content, can be generally related to the fiber volume content and the matrix volume content. Measured variation in fiber volume content with increasing specimen print speed was presented in the previous sub-section. Similar variation in the matrix volume content with increasing print speed was also observed. Figure 65 graphically displays the nominal measured matrix content by volume as a function of DMA specimen print speed. The data graphically presented in Figure 65 is tabulated in Table 14 for reference.
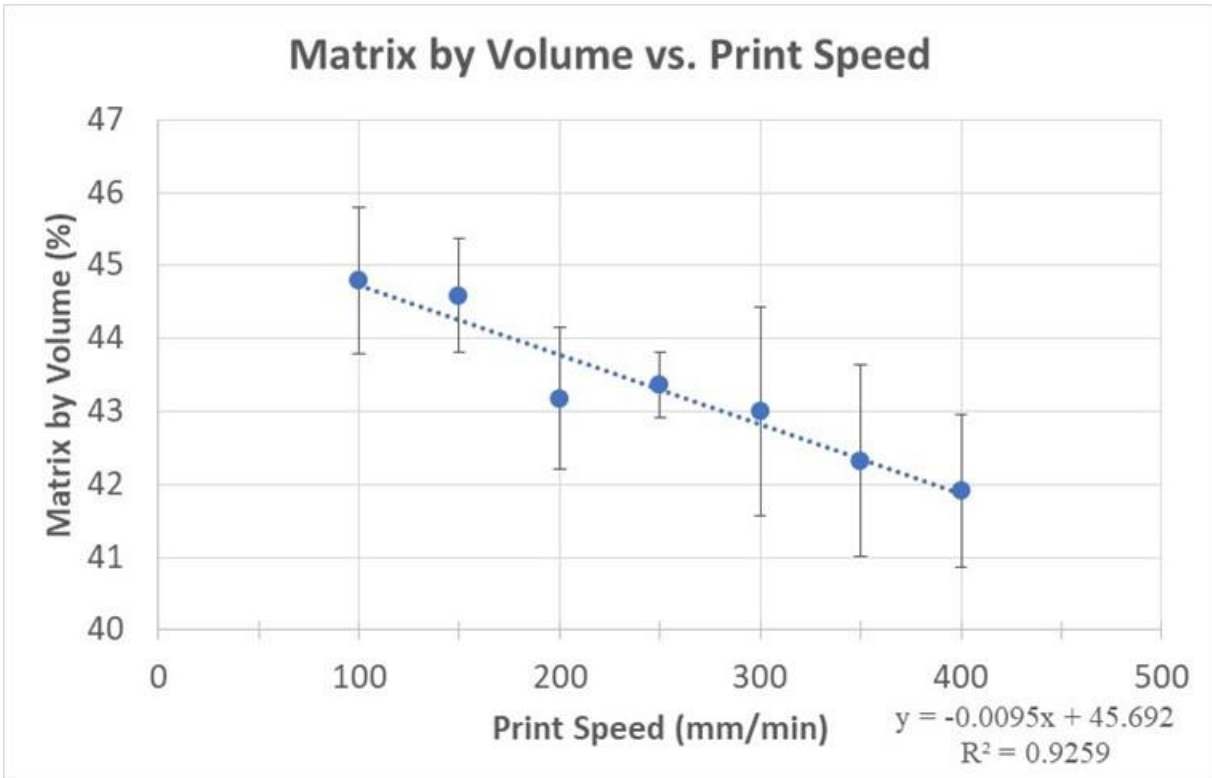
Figure 65: Nominal matrix volume content, with sample standard deviations, as a function of DMA specimen print speed

Table 14: Nominal matrix volume content, with sample standard deviations, as a function of DMA specimen print speed

Print Speed	Nominal Matrix Volume Content (%)	Sample St.Dev (%)
100	44.80	1.00
150	44.59	0.78
200	43.18	0.97
250	43.36	0.45
300	43.00	1.43
350	42.32	1.32
400	41.92	1.05

The constituent content data for the seven print speed based DMA specimen groups, presented in Figure 64, Figure 65, Table 13 and Table 14, clearly indicates that both the nominal fiber volume and matrix volume content decrease with increasing DMA specimen print speed, and as such, increasing void content as well. It is difficult to attribute the entirety of the negative trend in maximum measured loss modulus to the decrease in constituent content with increasing void content; however, it is also difficult to eliminate the possibility of the decrease in

135

constituent content contributing to the decrease in maximum measured loss modulus. Due to the

relative ambiguity of the significance of the magnitude of the maximum measured loss modulus

in this context, development of a better understanding of the magnitude of the loss modulus is

requisite to providing any further discussion of the empirical trends reported in this work. As

such, development of said understanding of the magnitude of the loss modulus, specifically with

regard to the effects of void content, is logical to propose as a topic for future work.

4.5 Glass Transition Temperature (Tg) as a Function of Void Content

The maximum measured loss modulus (E") at the 1 Hz test frequency was used as an

indicator of the glass transition temperature of the printed DMA specimens. Using the peak E"

as the indicator for Tg, the results of this work indicate a negative trend in Tg with increasing

void content. This data is graphically revisited in Figure 66, and tabulated for reference in Table

15.
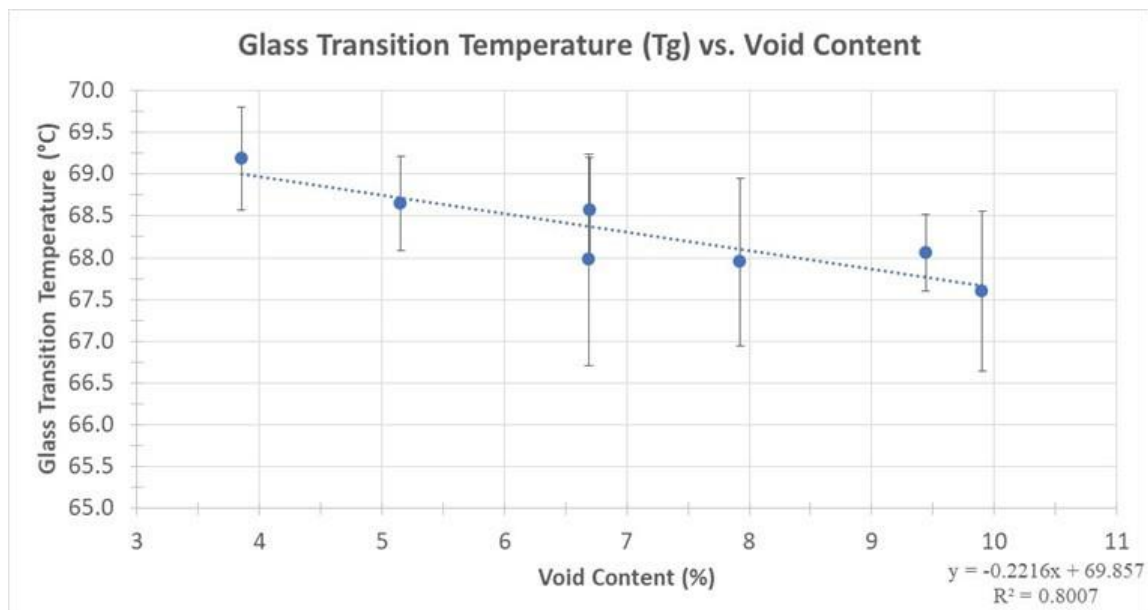
Figure 66: Nominal glass transition temperature, with sample standard deviations, as a function of void content

Table 15: Nominal glass transition temperature, with sample standard deviations, as a function of void content

Print Speed (mm/ min)	Void Content (%)	Tg from E" $_{max}$ (°C)	St.Dev (°C)
100	3.85	69.2	0.62
150	5.15	68.7	0.57
200	6.69	68.0	1.27
250	6.69	68.6	0.63
300	7.93	68.0	1.00
350	9.44	68.1	0.46
400	9.90	67.6	0.96

Despite the seemingly small range of measured glass transition temperature across the empirical data set, as well as the relatively large sample standard deviations, the negative trend shown in Figure 66 is tenable based on the first (graphically the left-most data point) and last (graphically the right-most data point) data points coupled with their associated standard deviations (graphically there is no vertical overlap). In the relevant literature, it is common to record variations in Tg as a function of small changes to the material that is subject to Dynamic Mechanical Analysis [20,34,37,38]. Furthermore, the two most relevant articles to this work have reported clear shifts in Tg, to lower temperatures, with decreased interfacial contact between the constituent reinforcement and matrix as well as increased void content (i.e. manufacturing defects) [20,37].

In consideration of the weak, negative trend observed in this work, Figure 66, a follow-up experiment was conducted with the sole purpose of further investigating measurable differences in the glass transition temperature of the printed continuous fiber reinforced thermoplastic specimen with different included void contents. Five DMA specimens were printed at each of three different print speeds, 100 mm per minute, 250 mm per minute and 400 mm per minute using the exact same hardware, continuous commingled precursor material and process parameters that were outlined in the description of the major experimental effort. Each group of five DMA specimens were subjected to DMA scans using a single sample excitation frequency

of 1 Hz, and a comparatively slower heating rate, relative to the main experimental effort, of

2 °C per minute. All other parameters of the DMA scans were held constant with respect to the

main experimental effort.

Note that constituent content determination was only performed on one DMA specimen from
each group of five specimens (three total groups), as opposed to determining constituent content
for the entire group of specimens. Constituent content determination was used to verify that
DMA specimens used for follow-up experimentation corresponded well with the nominal values
of void content that were previously determined for the printed DMA specimens at the relevant
(seven total) print speeds. The results of the follow-up experiment, specifically in terms of
measured glass transition temperature as a function of nominal void content, are presented in
Figure 67 and
Table 16. Note that nominal void content values are identical to those presented in

Figure 66. Seeing as the follow-up DMA specimens were processed identically to the specimens

from the major experimental effort, this relation was assumed valid. Results from constituent

content determination for the single tested specimens verified this assumption.

Figure 67: Follow-up experiment – nominal glass transition temperature, with associated
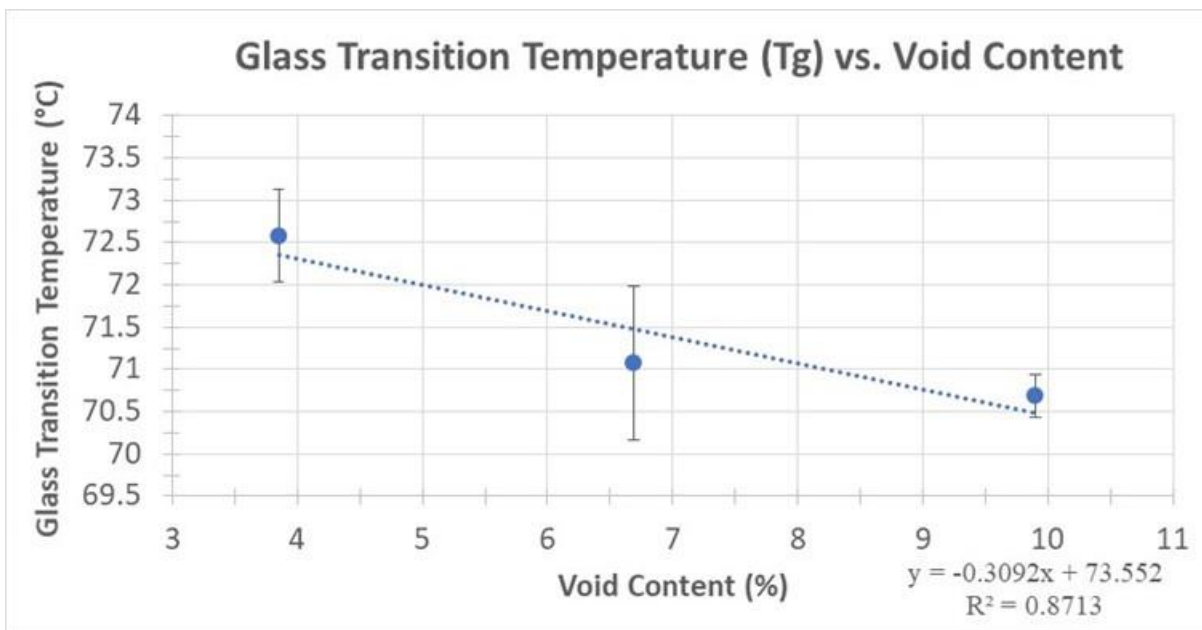sample standard deviations, as a function of void content

Table 16: Follow-up experiment – nominal glass transition temperature, with associated sample
standard deviations, as a function void content

Print Speed (mm/ min)	Void Content (%)	Tg from E" $_{max}$ (°C)	St.Dev (°C)
100	3.85	72.6	0.55

| 250 | 6.69 | 71.1 | 0.91 |
| 400 | 9.90 | 70.7 | 0.25 |

With regard to the follow-up experiment, the same weak, negative trend in measured glass transition temperature with increasing void content is observed, Figure 67. The data presented in Table 16 verifies what is graphically presented in Figure 67. Using the nominal values of Tg, the total decrease in Tg from the 100 mm per minute group to the 400 mm per minute group in the major experimental effort is approximately 1.6 °C, as compared to 1.9 °C in the current follow-up experiment. In consideration of the relevant standard deviations, this decrease in Tg is comparable and consistent. In contrast, a notable difference between the results of the follow-up and the major experimental effort is the magnitude of the measured glass transition temperatures. For example, with respect to the main experimental effort, the nominal Tg for the 100 mm per minute group is approximately 69 °C, whereas the nominal Tg for the same 100 mm per minute group in the follow-up is approximately 72 °C. The upward shift in measured Tg is consistent across the entire range of DMA specimens in the follow-up experiment.

The nominal Tg for the 100 mm per minute group, the group with the lowest void content, measured in the follow-up experiment correlates best with the value of Tg obtained by DSC for the PET thermoplastic in the commingled precursor (71.5 °C). Intuitively, this leads to the conclusion that the values of Tg measured in the main experimental effort are shifted to lower-than-expected temperatures as a result of an experimental parameter that was not controlled. It is generally accepted that moisture content has a negative effect on the general performance, both mechanically and thermally, of polymers. Literature regarding the effects of moisture content on the measured glass transition temperature for PET, albeit by means of DSC, indicates that the measured glass transition temperature can be reduced by as much as 3 °C with an 0.3 % weight sorption of water [58]. In consideration of the fact that moisture content in the DMA specimens was not controlled (in terms of recording relative humidity during specimen

fabrication/ testing or desiccation after specimen fabrication), in neither the main experimental effort nor the follow-up experiment, the discrepancy in Tg between the two experiments can be attributed to the likelihood of differing moisture contents in the different sets of DMA specimens.

4.6 Maximum Measured Damping Factor (tan δ) as a Function of Void Content

As mentioned in Chapter 3, the data measured for maximum damping factor in the printed composites was atypical in comparison to the majority of damping factor content available in the literature. It is typical for the graphical appearance of the damping factor to exhibit a clear, defined peak value within the glass transition region of the relevant polymer such that the entirety of the curve resembles something similar to a bell curve. In the current work, for all tested DMA specimens, the damping factor increases as the polymer matrix enters its glass transition region; however, the expected point of apogee does not occur in the tested temperature range and the damping factor shows a continuous increase up until the end of the respective DMA scan. In the context of the current work, typical damping factor behavior from the literature, as well as atypical damping factor behavior recorded in this work, are showed for comparative purposes in Figure 68.

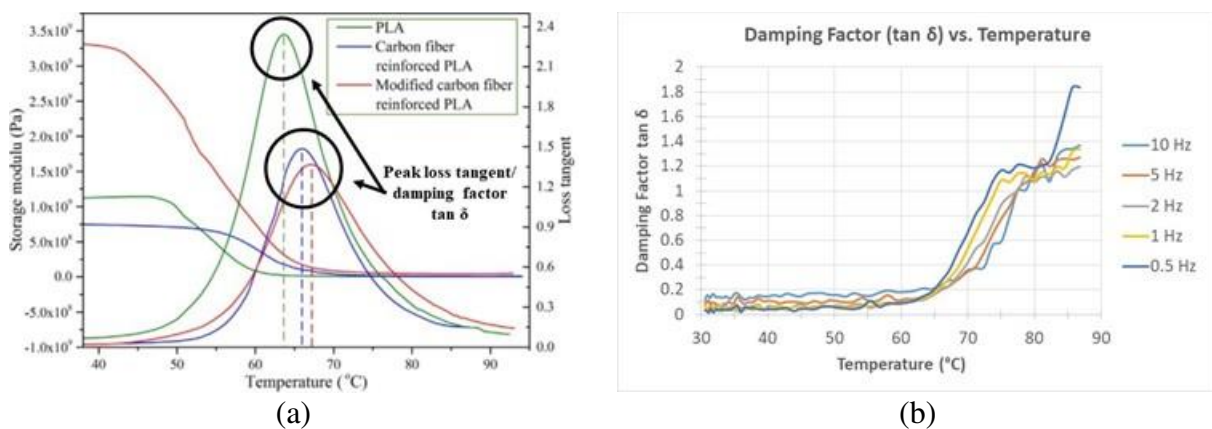(a)   (b)

Figure 68: Comparison of (a) typical damping factor appearance from the literature [20] and (b) the atypical damping factor from the current work

In examining Figure 68, it is clear that the appearance of the damping factor in (a) is different to the appearance of the damping factor in (b), where (a) shows a clear point of apogee in the glass transition region before decreasing back to some steady-state magnitude. This is the typical behavior. The atypical damping factor appearance, Figure 68 (b), does not exhibit a clear point of apogee, nor does it decrease to any steady-state magnitude as anticipated. Damping factor is, mathematically, the ratio of the loss modulus (E") to the storage modulus (E'). As such, in the temperature range immediately past the anticipated Tg for the PET matrix relevant to this work (~ 70 °C), the atypical behavior in (b) can only be explained by a disproportional increase in E" or a disproportional decrease in E'.

During experimentation, specifically during unloading of the tested DMA specimens from the DMS6100, it was noticed that the fixture clamps were consistently loose, as compared to the firm clamping pressure used upon loading of the specimens. Examination of the specimens following evaluation in the DMA showed that the specimens were often distorted at the clamped regions, such that the sample width was locally increased and sample thickness was locally decreased (albeit not significantly). This is intuitive in consideration of the fact that during the glass transition region of the PET thermoplastic, the polymer viscosity drops such that any pressure (stress) applied to the DMA specimen via the fixture can be relieved through localized polymer flow. Seeing as the specimen is constrained vertically (thickness direction) by the DCB fixture, it is logical that localized flow of the polymer would occur in the un-constrained direction relative to the DMA specimen (in the direction of specimen width).

Based on the loose fixture clamps at the end of the DMA scans, in accordance with the distorted specimen geometry at the end of the DMA scans, it is logical to conclude that the clamping pressure on the specimen was effectively lost during the glass transition region. This

implies that the mid-span DCB clamp that transfers load into the DMA specimen during the DMA scan loses intimate contact with the specimen, and as such, the specimen cannot be loaded. Further, this implies that the effective elastic stiffness (storage modulus, E') of the specimen should, from a measurement perspective, trend toward zero. In the case of E' trending toward zero during the glass transition region, as a result of lost contact with the DMA probe, the atypical damping factor behavior is explained.

The behavior described in the previous paragraph is supported by Figure 69. Figure 69 shows the graphical output of a DMA scan for a specimen from the main experimental effort. Figure 69 clearly shows that as the scan comes to an end, the damping factor continues to increase (consistent with the atypical behavior) while the storage modulus (E') trends toward zero. This is consistent across all tested specimens. These phenomena are highlighted in Figure 69. In consideration of Figure 69, it is clear that the data obtained for the maximum measured damping factor, as a function of void content, is not useful in terms of making any conclusions about how void content effects the thermomechanical performance of the printed composites. This is stated specifically in terms of the magnitude of the damping factor at the peak of the damping factor curve.
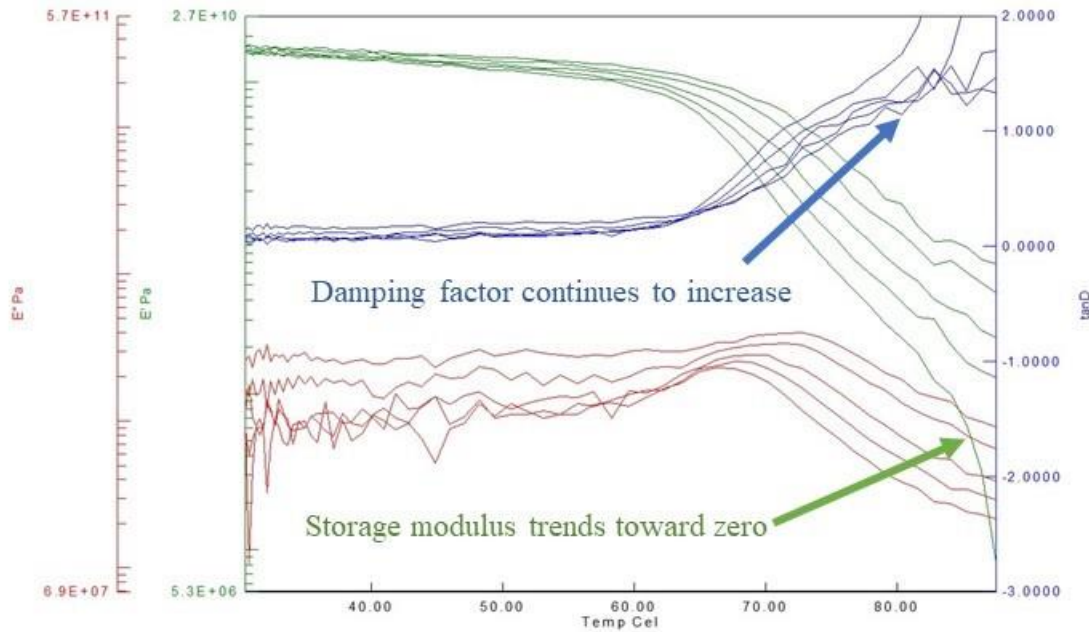
Figure 69: DMA scan showing atypical damping, coupled with atypical storage modulus behaviour after the glass transition

In further support of the claim that the atypical damping factor behavior in the region of Tg is a result of a loss of clamping pressure on the specimen, a brief follow-up experiment was conducted on a printed EG/ PET DMA specimen using a three-point bending fixture, 1 Hz frequency and a temperature sweep from 30 °C to 100 °C at 5 °C per minute. Note that the three-point bending fixture was not available at the time the main experimental effort was conducted. The graphical output of the DMA scan on the printed sample using the three-point bending fixture is shown in Figure 70. Note that a clear point of apogee is visible in the curve for damping factor, while the value of storage modulus decreases toward a horizontal asymptote in the same temperature range and does not trend toward zero. This is, relative to what is shown in Figure 69, consistent with the typical damping factor appearance/ behavior that is expected from a DMA scan. For reference, the glass transition temperature is indicated by both the maximum E" and the maximum damping factor, solely to verify the DMA specimen material is identical relative to the major experimental effort.

143
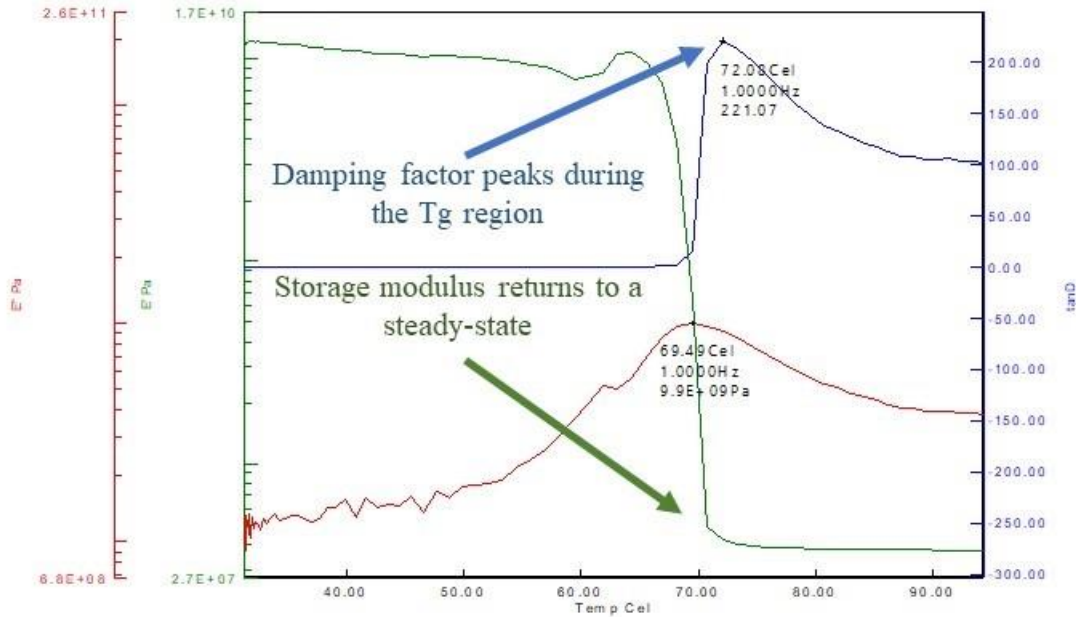
Figure 70: Follow-up experiment showing DMA output from a scan on a printed EG/ PET specimen, using three-point bending fixture

4.7 Metallographic Evaluation

The comparative metallographic information presented in Chapter 3 verifies the assumption that void content in the printed continuous fiber reinforced DMA specimens increases with increasing specimen print speed. Additionally, the images presented indicate that void content in the printed specimens is typically localized to either the periphery of the sample or to intralaminar regions, where the continuous reinforcement is effectively not wetted by the thermoplastic matrix. Using images of the representative cross-sections, the typical location of void content is identified; however, information from the cross-sections cannot be extrapolated down the length of specimen without macroscopic images of the specimens as supplementary evidence. The representative cross-section for the 250 mm per minute specimen is shown with a macroscopic view of one of the tested 250 mm per minute specimens from the main experimental effort in Figure 71 (a) and (b). In examining Figure 71 (b), it is clear that areas of opacity in the specimen tend to run length-wise (along the fibers) and are typically multiple

144

millimeters in length. This implies that intralaminar void content in the printed DMA specimens not only leaves areas of continuous reinforcement un-wetted, but that the un-wetted areas of continuous reinforcement are significant in length with respect to the total length of the DMA specimen. A consequence of this implication is that load transfer, through shear, between the PET matrix and the continuous E-Glass reinforcement is inhibited by the included void content, as the voids effectively reduce the available interfacial surface area between the constituents that is available for load transfer. This is consistent with the results of the current work, specifically in terms of the maximum measured storage modulus as a function of void content, where the elastic component of mechanical performance is clearly subject to a knock-down effect.
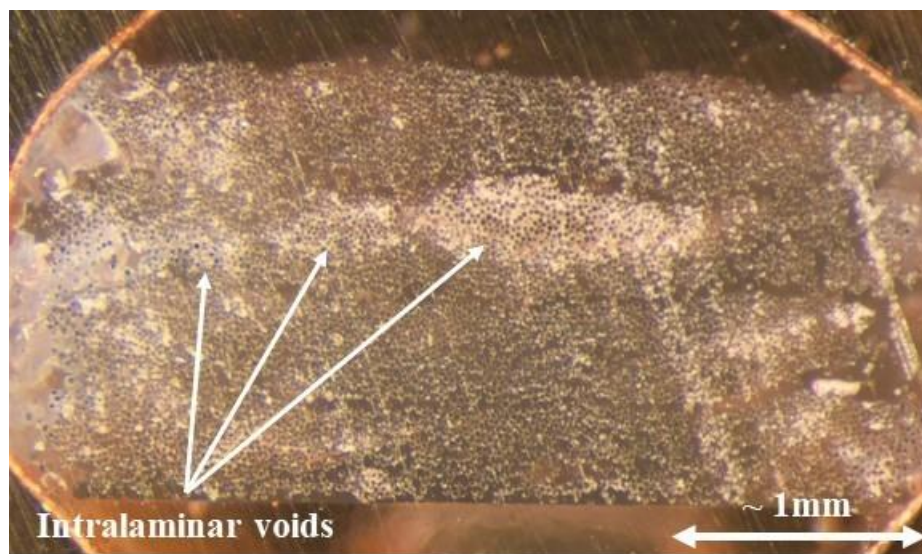
(a)
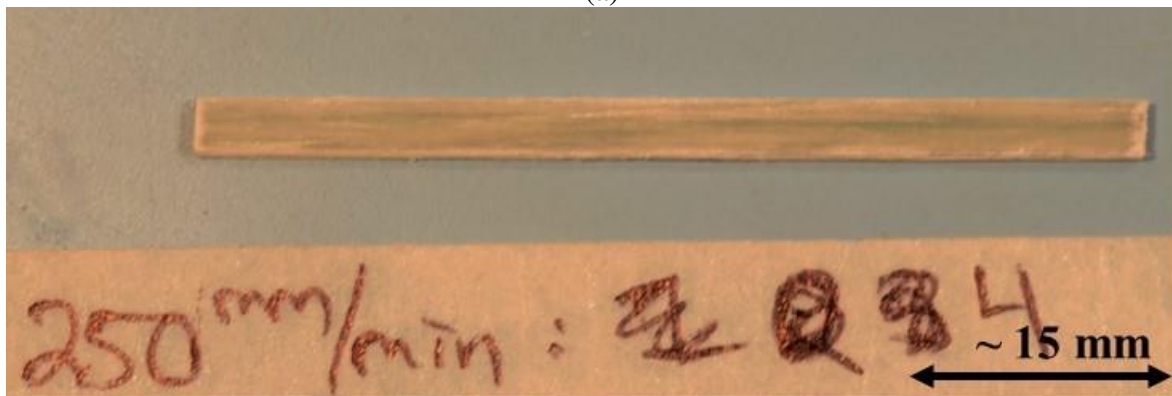
(b)

Figure 71: Comparison of 250 mm/ minute cross section and 250 mm/ minute DMA specimen

4.8 Experiment Summary

Despite idiosyncrasies in the results of the major experimental effort that have already been discussed, the current work establishes that, as compared to quasi-static quality evaluation techniques like Short-Beam Strength testing, quality evaluation by means of DMA is more sensitive to the effects of void content on the mechanical, and thermal, quality of additively manufactured continuous fiber reinforced thermoplastics. Short-Beam Strength testing is known to give good comparative information on the quality, as it relates to manufacturing defects, of carbon fiber/ epoxy laminates, on the order of a 25 % decrease in Short-Beam Strength with an approximate 6 % increase in void content (~ 4% SBS decrease per 1 % increase in void content by volume) [33]. The sensitivity in Short-Beam Strength to void content in carbon/ fiber epoxy laminates was not replicated in the current work concerned with additively manufactured continuous fiber reinforced thermoplastics. The current work found that a near 50 % increase in void content corresponded to a near 2 % decrease in Short-Beam Strength, coupled with the commonality of a destructive, inelastic failure mode. As such, an expanded study of the effects of void content on additively manufactured CFRTPs was conducted by means of Dynamic Mechanical Analysis to establish a path forward for CFRTP quality evaluation.

The expanded study of the effects of void content on the additively manufactured CFRTPs exhibited sensitivity to void content in four measured viscoelastic and thermal material properties, those being storage modulus, loss modulus, damping factor and the composite glass transition temperature. Within the relevant range of void content, non-destructive specimen evaluation by DMA resulted in a measured, frequency dependent, 5.5 – 5.8 % decrease in elastic storage modulus per 1 % increase in void content by volume. Additionally, within the relevant range of void content, a marked decrease in the maximum measured loss modulus was recorded,

on the order of 7.0 – 8.2 % per 1 % added void content. Effects of void content were also

measured in the damping factor data, although this was convoluted by the fixture/ specimen

interaction, as well as in the composite glass transition temperature, where an approximate 1.6

°C drop in Tg was recorded over the relevant void content range. These results establish both a

verification of the hypothesis made in Chapter 1, as well as a clear path to expand the current

literature, as it relates to the effects of manufacturing defects, in the additive manufacture of

CFRTP arena. Similarly, these results also establish a variety of potential paths for the work to

be continued and supplemented in the future.

4.9 Future Work

The results presented in this work serve as experimental validation of the utility of

Dynamic Mechanical Analysis as a means of evaluating the effects of manufacturing defects,

specifically void content, on the thermomechanical quality of additively manufactured

continuous fiber reinforced thermoplastics. With that in mind, the results presented in the

current work also point toward a variety of future work that could serve to clarify atypical

phenomena observed in the experimental analysis, as well as add to this work in scope. It is

clear that further analysis of the significance of the magnitude of the loss modulus, at the glass

transition temperature, is requisite to holistically understand the results presented herein.

Furthermore, it is also clear that future analyses could benefit from the use of a different test

fixture, such as a three-point bend fixture, to remove the need for specimen clamping and

provide for more useful information regarding the damping factor during the glass transition

region.

In terms of adding to the scope of this work, the use of Dynamic Mechanical Analysis,

coupled with the availability of the synthetic oscillation mode inherent to the DMS6100, opens

up possibilities in terms of generating frequency domain master curves for additively

manufactured CFRTPs. Through the use of time-temperature superposition (TTS), master

curves can be created to further characterize the effects of defects on printed continuous fiber

reinforced thermoplastics. Using TTS, viscoelastic data acquired over a variety of temperatures

and frequencies can be mathematically shifted, relative to a reference temperature, and

graphically displayed as a comprehensive representation of the viscoelasticity over timescales

that are either experimentally unattainable or prohibitively expensive to facilitate. In future

work, it may be possible that TTS could be used to create master curves for properties such as

creep compliance and stress relaxation, as a function of defect content, location, or a

combination of both. An example of the use of TTS to create master curves of storage modulus

for specimens with different void content, from the current work, is shown in Figure 72. Figure

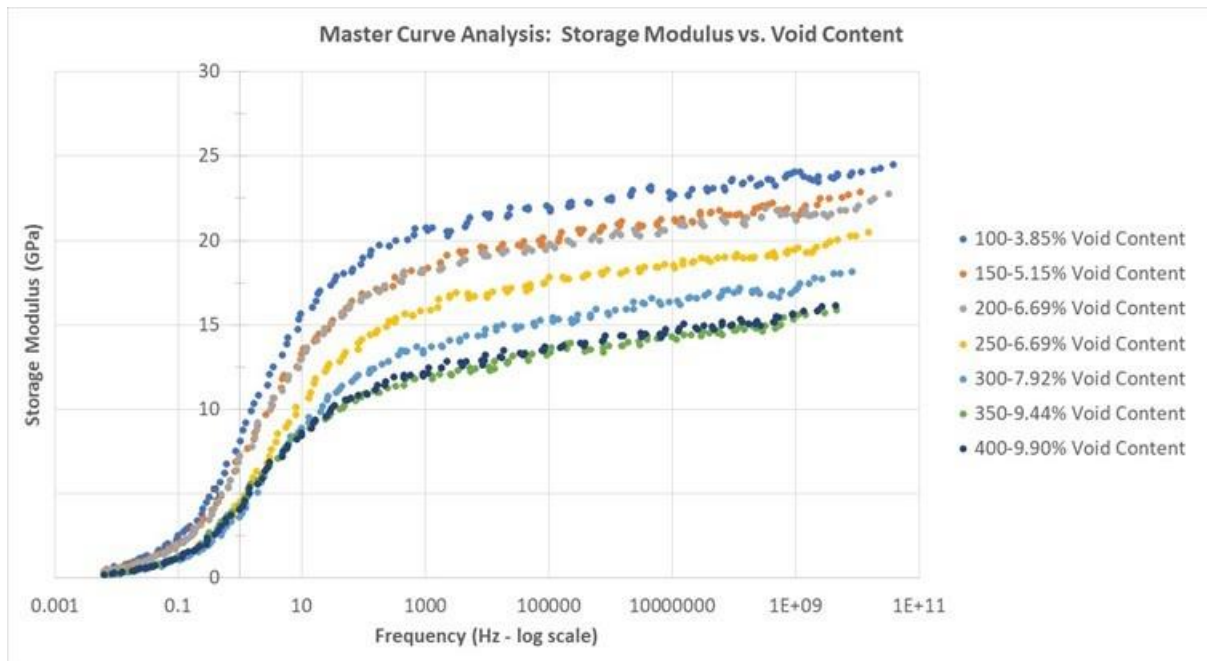72 is included solely as a proof-of-concept.

Figure 72: Example of the use of TTS to create master curves for the storage modulus of
printed DMA specimens with different amounts of void content

5 Conclusions

The current work was purposed with developing an understanding of, and expanding upon, the current state of the literature regarding additive manufacture of continuous fiber reinforced thermoplastics. Currently at the forefront of advanced continuous fiber reinforced composite manufacturing, additive manufacture of continuous fiber reinforced thermoplastics exhibits the potential to relieve many of the constraints placed on the current design and manufacturing of continuous fiber reinforced structures. At present, the additive manufacture of continuous fiber reinforced thermoplastics has been demonstrated successfully to varying extents; however, a comprehensive dialogue regarding manufacturing defects and the quality of the processed continuous fiber reinforced thermoplastics has been missing from the field.

Considering the preliminary nature of additive manufacture of continuous fiber reinforced thermoplastics, exemplary processed composites in the literature are typically subject to various manufacturing defects, most namely excessive void content. Generally, quality evaluation in the relevant literature is limited to test methods that are largely influenced by the properties of the continuous reinforcement, and as such, defects in the matrix are usually less-impactful and overlooked. In consideration of the lack of discussion regarding manufacturing defects in the matrix, it is logical to pursue a better understanding of the impact that void content has on processed continuous fiber reinforced thermoplastics.

The necessary hardware to facilitate additive manufacturing of continuous fiber reinforced thermoplastics was developed and continuous fiber reinforced specimens, with high fiber volume fractions (~ 50 %), were successfully processed. Early efforts at evaluating the processed specimens using manufacturing defect sensitive methods common to quality

evaluation of continuous fiber reinforced thermosets, specifically Short-Beam Strength (SBS), exhibited a general lack of sensitivity to void content. Within the relevant range of void content, evaluation of specimens by means of SBS resulted in destructive inelastic specimen failures, with an approximate 3.9% decrease in SBS per 1% increase in void content by volume. As such, an expanded study of the effects of void content on the thermomechanical performance of additively manufactured continuous fiber reinforced thermoplastics was conducted. Dynamic Mechanical Analysis was employed as the sole method of evaluating the thermomechanical performance of printed composite specimens, processed with varying amounts of void content. Thermomechanical performance of the printed composite specimens was evaluated specifically in terms of the measured elastic storage modulus, the viscous loss modulus, the damping factor, commonly tan δ, and the glass transition temperature (Tg) of the composite material.

In conclusion, this work has shown that DMA does yield increased sensitivity to the presence of void content in additively manufactured continuous fiber reinforced thermoplastics, as compared to conventional evaluation methods, specifically Short-Beam Strength. Within the relevant range of void content, non-destructive specimen evaluation by DMA resulted in a measured, frequency dependent, 5.47 – 5.80 % decrease in measured elastic storage modulus per 1% increase in void content by volume. Additionally, quality evaluation by DMA realized a marked decrease in the maximum measured loss modulus in the additively manufactured composites, ranging from 7.0 – 8.2 %, per 1 % increase in void content by volume. Effects of void content were also measured in both the damping factor and the glass transition temperature of the processed composite material, where an approximate 1.6 °C drop in Tg was recorded over the relevant range of void content. The results of this work indicate, firstly, that DMA is a superior evaluation method, as compared to SBS, in terms of sensitivity to void content in

additively manufactured continuous fiber reinforced thermoplastics. Additionally, the results of this work provide a clear expansion of the current state of the literature regarding processed material quality evaluation in that the effects of prominent manufacturing defects have been assessed with regard to thermomechanical material performance. Furthermore, and finally, the results of this work indicate the potential for future contributions to the literature, and the field, specifically in terms of evaluating the effects of manufacturing defects on the long-term thermomechanical performance of additively manufactured continuous fiber reinforced thermoplastics.

References

[1]   Barbero EJ. Introduction to Composite Materials Design. Second Edition. CRC Press; 2015.

[2]   Costello C. Thermoplastics for High-Temperature Composite Processes & Applications. Ticona Eng. Polym. :1–12.

[3]   August Z, Ostrander G, Michasiow J, et al. Recent Developments in Automated Fiber Placement of Thermoplastic Composites. SAMPE J. 2014;50:9.

[4]   Automated Fiber Placement Work-Cell Example Image [Internet]. Available from: http://www.automateddynamics.com/automation-equipment.

[5]   Lamontia M, Funck S, Gruber M, et al. Manufacturing flat and cylindrical laminates and built up structure using automated thermoplastic tape laying, fiber placement, and filament winding. Sampe J. 2003;39:30–38.

[6]   Khaled Y, Mehdi H. Processing of thermoplastic matrix composites through automated fiber placement and tape laying methods: A review. J. Thermoplast. Compos. Mater. 2017;089270571773830.

[7]   ASTM D2344/D2344M-16 Standard Test Method for Short-Beam Strength of Polymer Matrix Composite Materials and Their Laminates.

[8]   Ngo TD, Kashani A, Imbalzano G, et al. Additive manufacturing (3D printing): A review of materials, methods, applications and challenges. Compos. Part B Eng. 2018;143:172–196.

[9]   Sun Q, Rizvi GM, Bellehumeur CT, et al. Effect of processing conditions on the bonding quality of FDM polymer filaments. Rapid Prototyp. J. 2008;14:72–80.

[10]   Rodriguez JF, Thomas JP, Renaud JE. Maximizing the Strength of Fused-Deposition ABS Plastic Parts. 10th Solid Free. Fabr. Symp. Proc. Austin, TX; 1999. p. 335–342.

[11]   Rodríguez JF, Thomas JP, Renaud JE. Mechanical behavior of acrylonitrile butadiene styrene (ABS) fused deposition materials. Experimental investigation. Rapid Prototyp. J. 2001;7:148–158.

[12]   Prüß H, Vietor T. Design for Fiber-Reinforced Additive Manufacturing. J. Mech. Des. 2015;137:111409.

[13]   Klosterman D, Chartoff R, Graves G, et al. Interfacial characteristics of composites fabricated by laminated object manufacturing. Compos. Part Appl. Sci. Manuf. 1998;29:1165–1174.

[14]   Tekinalp HL, Kunc V, Velez-Garcia GM, et al. Highly oriented carbon fiber–polymer composites via additive manufacturing. Compos. Sci. Technol. 2014;105:144–150.

[15]   Ning F, Cong W, Qiu J, et al. Additive manufacturing of carbon fiber reinforced thermoplastic composites using fused deposition modeling. Compos. Part B Eng. 2015;80:369–378.

[16]   Der Klift FV, Koga Y, Todoroki A, et al. 3D Printing of Continuous Carbon Fibre Reinforced Thermo-Plastic (CFRTP) Tensile Test Specimens. Open J. Compos. Mater. 2016;06:18–27.

[17]   Melenka GW, Cheung BKO, Schofield JS, et al. Evaluation and prediction of the tensile properties of continuous fiber-reinforced 3D printed structures. Compos. Struct. 2016;153:866–875.

[18]   Tian X, Liu T, Yang C, et al. Interface and performance of 3D printed continuous carbon fiber reinforced PLA composites. Compos. Part Appl. Sci. Manuf. 2016;88:198–205.

[19]   Bettini P, Alitta G, Sala G, et al. Fused Deposition Technique for Continuous Fiber Reinforced Thermoplastic. J. Mater. Eng. Perform. [Internet]. 2016 [cited 2017 Jan 27]; Available from: http://link.springer.com/10.1007/s11665-016-2459-8.

[20]   Li N, Li Y, Liu S. Rapid prototyping of continuous carbon fiber reinforced polylactic acid composites by 3D printing. J. Mater. Process. Technol. 2016;238:218–225.

[21]   Radford DW, Hedin KM. Fused Deposition Technology Applied to Thermoplastic Matrix Placement and Wetout in Filament Winding. 2015;9.

[22]   Warlick KM, Radford DW, CO FC. Combining Aspects of Additive Manufacture and Filament Winding to Produce Composites with Novel Fiber Reinforcement Patterns. :14.

[23]   Vaneker THJ. Material Extrusion of Continuous Fiber Reinforced Plastics Using Commingled Yarn. Procedia CIRP. 2017;66:317–322.

[24]   Eichenhofer M, Maldonado J, Klunker F, et al. Analysis of Processing Conditions for a Novel 3D-Composite Production Technique. 2015;12.

[25]   Eichenhofer M, Wong JCH, Ermanni P. Continuous lattice fabrication of ultra-lightweight composite structures. Addit. Manuf. 2017;18:48–57.

[26]   Bourgeois ME, Radford DW. Direct Manufacture of Geometrically Complex Continuous Fiber Reinforced Composites Through the Development of a 5-Axis 3D Printing System. :14.

[27]   Qureshi Z, Swait T, Scaife R, et al. In situ consolidation of thermoplastic prepreg tape using automated tape placement technology: Potential and possibilities. Compos. Part B Eng. 2014;66:255–267.

[28]   Yang C, Tian X, Liu T, et al. 3D printing for continuous fiber reinforced thermoplastic composites: mechanism and performance. Rapid Prototyp. J. 2017;23:209–215.

[29]   Tian X, Liu T, Wang Q, et al. Recycling and remanufacturing of 3D printed continuous carbon fiber reinforced PLA composites. J. Clean. Prod. 2017;142:1609–1618.

[30]   Mori K, Maeno T, Nakagawa Y. Dieless Forming of Carbon Fibre Reinforced Plastic Parts Using 3D Printer. Procedia Eng. 2014;81:1595–1600.

[31]   Namiki M, Ueda M, Todoroki A, et al. 3D Printing of Continuous Fiber Reinforced Plastic. :6.

[32]   Goh GD, Dikshit V, Nagalingam AP, et al. Characterization of mechanical properties and fracture mode of additively manufactured carbon fiber and glass fiber reinforced thermoplastics. Mater. Des. 2018;137:79–89.

[33]   Landro LD, Montalto A, Bettini P, et al. Detection of Voids in Carbon/Epoxy Laminates and Their Influence on Mechanical Properties. Polym. Compos. 2017;25:10.

[34]   Akay M. Aspects of dynamic mechanical analysis in polymeric composites. Compos. Sci. Technol. 1993;47:419–423.

[35]   Stark W. Investigation of the curing behaviour of carbon fibre epoxy prepreg by Dynamic Mechanical Analysis DMA. Polym. Test. 2013;32:231–239.

[36]   Harris B, Braddell OG, Almond DP, et al. Study of carbon fibre surface treatments by dynamic mechanical analysis. J. Mater. Sci. 1993;28:3353–3366.

[37]   Yang Q, Shams E. Dynamic Mechanical Characterization of Manufacturing Defects In Continuous Carbon-Fiber/Epoxy Composites. :14.

[38]   Ghosh P, Bose NR, Mitra BC, et al. Dynamic mechanical analysis of FRP composites based on different fiber reinforcements and epoxy resin as the matrix material. J. Appl. Polym. Sci. 1997;64:2467–2472.

[39]   Sorrentino L, Silva de Vasconcellos D, D'Auria M, et al. Thermoplastic composites based on poly(ethylene 2,6-naphthalate) and basalt woven fabrics: Static and dynamic mechanical properties. Polym. Compos. 2016;37:2549–2556.

[40]   Bernet N, Wakeman MD, Bourban P-E, et al. An integrated cost and consolidation model for commingled yarn based composites. Compos. Part Appl. Sci. Manuf. 2002;33:495–506.

[41]   Rosselli F, Santare MH. Comparison of the short beam shear (SBS) and interlaminar shear device (ISD) tests. Compos. Part Appl. Sci. Manuf. 1997;28:587–594.

[42]   Schneider K, Lauke B, Beckert W. Compression Shear Test (CST) – A Convenient Apparatus for the Estimation of Apparent Shear Strength of Composite Materials. :20.

[43]   Berg C, Tirosh J, Israeli M. Analysis of Short Beam Bending of Fiber Reinforced Composites. In: Corten H, editor. Compos. Mater. Test. Des. Second Conf. [Internet]. 100 Barr Harbor Drive, PO Box C700, West Conshohocken, PA 19428-2959: ASTM International; 1972 [cited 2018 Jul 25]. p. 206-206–213. Available from: http://www.astm.org/doiLink.cgi?STP27748S.

[44]   Kadlec M, Nováková L, Růžek R. An Experimental Investigation of Factors Considered for the Short Beam Shear Strength Evaluation of Carbon Fiber–reinforced Thermoplastic Laminates. J. Test. Eval. 2014;42:20120043.

[45]   Ningyun W, Evans JT. Collapse of continuous fibre composite beams at elevated temperatures. Composites. 1995;26:56–61.

[46]   Bureau MN, Denault J. Fatigue resistance of continuous glass fiber/polypropylene composites: Temperature dependence. Polym. Compos. 2004;25:622–629.

[47]   Porzucek K, Coulon G, Lefebvre JM, et al. Plastic flow of polypropylene (PP) and a PP-based blend: Part 1Experimental determination of thermal activation parameters. J. Mater. Sci. 1989;24:2533–2540.

[48]   National Research Council (U.S.), editor. ASTM D3171-15 - Standard Test Methods for Constituent Content of Composite Materials. Washington, D.C: National Academy Press; 1995.

[49]   Lee D-J, Shin I-J. Effects of vacuum, mold temperature and cooling rate on mechanical properties of press consolidated glass fiber/PET composite. Compos. Part Appl. Sci. Manuf. 2002;33:1107–1114.

[50]   Yan W, Han K, Qin L, et al. Study on long fiber-reinforced thermoplastic composites prepared byin situ solid-state polycondensation. J. Appl. Polym. Sci. 2004;91:3959–3965.

[51]   Olivier R, Cottu JP, Ferret B. Effects of cure cycle pressure and voids on some mechanical properties of carbon/epoxy laminates. :7.

[52]   Menard KP. Dynamic Mechanical Analysis - A Practical Introduction. 1st Edition. CRC Press;

[53]   Swaminathan G, Shivakumar K. A Re-examination of DMA Testing of Polymer Matrix Composites. J. Reinf. Plast. Compos. 2009;28:979–994.

[54]   ASTM D4065-12 Standard Practice for Plastics: Dynamic Mechanical Properties: Determination and Report of Procedures.

[55]   Hagstrand P-O, Bonjour F, Månson J-AE. The influence of void content on the structural flexural performance of unidirectional glass fibre reinforced polypropylene composites. Compos. Part Appl. Sci. Manuf. 2005;36:705–714.

[56]   Ehrenstein GW, Riedel G, Trawiel P. Thermal Analysis of Plastics. Therm. Anal. Plast.

[Internet]. Carl Hanser Verlag GmbH & Co. KG; 2004 [cited 2018 Sep 18]. p. I–XXIX.

Available from: https://doi.org/10.3139/9783446434141.fm.

[57]   Matweb [Internet]. [cited 2018 Oct 10]. Available from: http://matweb.com/.

[58]   Bianchi R, Chiavacci P, Vosa R, et al. Effect of moisture on the crystallization behavior

of PET from the quenched amorphous phase. J. Appl. Polym. Sci. 1991;43:1087–1089.